Mobility Design and Control of Personal Mobility Aids for the Elderly

by

Haoyong Yu

B. Sc. Mechanical Engineering, Shanghai Jiao Tong University, 1988
M. Sc. Mechanical Engineering, Shanghai Jiao Tong University, 1991

Submitted to the Department of Mechanical Engineering in Partial Fulfillment of the Requirements for the Degree of

Doctor of Philosophy in Mechanical Engineering

at the

Massachusetts Institute of Technology

September 2002

Signature of Author: _____

Department of Mechanical Engineering
August 19, 2002

Certified by: _____

Steven Dubowsky
Professor of Mechanical Engineering
Thesis Supervisor

Accepted by: _____

Ain A. Sonin
Professor of Mechanical Engineering
Chairman, Departmental Graduate Committee

To my wife Xiaowen
for her love

Mobility Design and Control of Personal Mobility Aids for the Elderly

by
Haoyong Yu

Submitted to the Department of Mechanical Engineering
on August 19, 2002, in Partial Fulfillment of the Requirements for the Degree of
Doctor of Philosophy in Mechanical Engineering

ABSTRACT

Delaying the transition of the elderly to higher level of care using assistive robotic devices could have great social and economic significance. The transition, necessitated by the degradation of physical and cognitive capability of the elderly, results in drastic increase of cost and rapid decrease of quality of life. A Personal Aid for Mobility and Health Monitoring system (PAMM) has been developed at MIT Field and Space Robotics Laboratory for the elderly living independently or in senior assisted living facilities so as to delay their transition to nursing homes. This thesis research addresses the mobility design and control issues of such devices.

Eldercare environments are semi-structured, usually congested, and filled with static and/or dynamic obstacles. Developing effective mobility designs to achieve good maneuverability is a great challenge. An omni-directional mobility concept using conventional wheels has been developed independently in this research. Mobility systems based on this concept are simple, lightweight, energy efficient, and capable of operating on a range of floor surfaces.

Assistive mobility devices work in shared workspace and interact directly with their users with limited physical and cognitive capabilities. The users may not be well trained, nor fully understand system. The challenge is to design an ergonomic and intuitive human machine interaction and a control system that can properly allocate control authority between the human and the machine. For this purpose, the admittance-based control methodology is used for the human machine interaction control. An adaptive shared control framework allocates control based on metrics of the demonstrated human performance has been developed. Substantial amount of field experiments have been conducted with the actual users to validate control system design. The mobility design and control system implemented and tested on PAMM, will also be applicable to other cooperative mobile robots working in semi-structured indoor environments such as a factory or warehouse.

Thesis Supervisor: Steven Dubowsky
Title: Professor of Mechanical Engineering

Acknowledgements

I would like to thank Professor Steven Dubowsky for giving me the opportunity to work on the interesting and meaningful PAMM research project. He has given me continuous guidance and insightful advice on my research, inspired me to work towards higher standard during my time at the Field and Space Robotics Laboratory.

I would like to express my deep appreciation to Professor Asada and Professor Kuchar for their advice and guidance, and the precious time they spent meeting with me as members in my thesis committee.

I would also like to thank all the people in the Field and Space Robotics Laboratory. I learned as much from many of them as I learned from the classes. It has been a pleasure to work with them. Especially, I would like to thank Matt Spenko and Dr. Chi Zhu for their time and valuable suggestions during the field experiments in the eldercare facility. I would also like to thank Dr. Christopher Lee for his valuable suggestions in the writing of this thesis.

I would like to thank the Healthcare and Home Automation Consortium in the MIT d'Arbeloff Laboratory for Information for Information for funding the research project.

I am indebted to DSO National Laboratories, Singapore, for sponsoring my study at MIT.

Finally, I would like to thank my wife Xiaowen for her love, solid emotional support, and the many sacrifices that she made for me during the last five years at MIT.

Table of Contents

Chapter_1. Introduction 10
1.1 Motivation 10
1.2 Background Literature Review 13
1.3 Objectives of this Thesis and Summary of Results 19
1.4 Outline of this Thesis 22
Chapter_2 PAMM Experimental Systems 24
2.1 Introduction 24
2.2 PAMM System Concept 26
2.3 PAMM System Performance Goals 27
2.4 PAMM Physical Systems 27
2.5 Research Focuses of the PAMM Project 29
2.6 Summary of the Chapter 38
Chapter_3 Omni-directional Mobility Design 39
3.1 Introduction 39
3.2 Concept and Kinematics of Active Split Offset Castor 41
3.3 Omni-directional Platform with ASOC Modules 44
3.4 Analysis of Design and Control Issues 47
3.5 Test-bed Prototype and Experimental Results 56
3.6 SmartWalker Implementation and Experimental Results 59
3.7 Summary and Conclusions 65
Chapter_4 Wheel Scrubbing Analysis 66
4.1 Introduction 66
4.2 Frictional Forces on Conventional Wheels 67
4.3 Scrubbing Torque for a Single Steered Wheel 69
4.4 Scrubbing Analysis for the Dual wheel Design 71
4.5 Scrubbing Analysis of Wheels in General Motion 76
4.6 Comparison between ASOC and Active Castor 78
4.7 Summary and Conclusions 80
Chapter_5 Admittance-based Human-machine Interaction Control Design 81
5.1 Introduction 81
5.2 Force/torque Sensor as the Human Machine Interface 81
5.3 Concept of Admittance-based Control 83
5.4 PAMM Admittance Model Design 84
5.5 Experimental Study 87
5.6 Summary and conclusions 95
Chapter_6 Adaptive Shared Control Design 96
6.1 Introduction 96
6.2 An Adaptive Shared Control Framework 97
6.3 Simulation Results 102
6.4 PAMM Implementation and Field Experiments 104
6.5 Summary and Conclusions 119
Chapter_7 Conclusions and Suggustions for Future Work 120
7.1 Summary of the Thesis Contributions 120

7.2 Suggestions for Future Work 121
Appendix A 124
Appendix B 125
References 128

List of Figures

Figure 2.1 - PAMM System Concept [Dubowsky, 2000] 26
Figure 2.2 - The SmartCane Prototype PAMM System (Courtesy of Sami Kozono) 28
Figure 2.3 - The SmartWalker Prototype PAMM System 28
Figure 2.4 - PAMM System Planner 30
Figure 2.5 - Vision-based Localization System (Dubowsky, 2000) 30
Figure 2.6 - SmartCane Mobility Design 32
Figure 2.7 - Kinematic Model of SmartCane Mobility Design 32
Figure 2.8 - Posture Tracking 33
Figure 2.9 - Convergence of SmartCane Trajectory 34
Figure 2.10 - Convergence of Position Errors 34
Figure 2.11 - SmartCane Tracking Performance without Localization Control 35
Figure 2.12 - Tracking Performance with Active Localization 36
Figure 2.13 - SmartWalker Mobility Design (Courtesy of Matt Spenko) 36
Figure 3.1 - Mobility Needs of PAMM Users 40
Figure 3.2 - An Active Split Offset Castor Module (Courtesy of Matt Spenko) 41
Figure 3.3 - Coordinate System of the ASOC Module (Top View) 41
Figure 3.4 - Simulation of an ASOC Module Performing Sideward Motion 44
Figure 3.5 - A Platform with two ASOC Modules 45
Figure 3.6 - Effects of S/D on Wheel Velocities 47
Figure 3.7 - Ground Contact of ASOC Modules on Flat and Uneven Floor 48
Figure 3.8 - Added Passive Joint to the ASOC 49
Figure 3.9 - Simplest Configuration of a Vehicle with ASOC design 49
Figure 3.10 - Configuration Space of Second ASOC 51
Figure 3.11 - Kinematic Constraint and Effects of Joint Encoders 52
Figure 3.12 - Stable and Unstable Direction of the ASOC Module 55
Figure 3.13 - Direction of Orientation Change of the ASOC Module 56
Figure 3.14 - Test-bed Prototype (Built by Lani Rapp and Daniel Santos) 57
Figure 3.15 - Experimental Set-up for Test-bed Prototype 57
Figure 3.16 - Closed-loop Control Diagram Experimental System 58
Figure 3.17 - Trajectory Tracking Performance of Test-bed Prototype 59
Figure 3.18 - The PAMM SmartWalker Prototype 59
Figure 3.19 - ASOC module for the SmartWalker (Courtesy of Matt Spenko) 60
Figure 3.20 - Demonstrates Omni-directional Mobility 61
Figure 3.21 - Linear Trajectory Tracking under Open Loop Control 62
Figure 3.22 - Linear Trajectory Tracking under Closed-Loop Control 63
Figure 3.23 - Linear-arc Trajectory Tracking under Open Loop Control 64
Figure 3.24 - Linear-arc Trajectory Tracking under Closed Loop Control 64
Figure 4.1- Dual Wheel Design without Offset 67
Figure 4.2 - Resistance Forces on Conventional Wheels 68
Figure 4.3 - Wheel Contact Patch and Pressure Distribution 70
Figure 4.4 - Dual Wheel Set Scrubbing Analysis 72
Figure 4.5- Wheel Twisting Stiffness 73
Figure 4.6 - Scrubbing Torque of an Element in the Contact Patch 75
Figure 4.7 - Scrubbing Torque versus Wheel Separation 76

Figure 4.8 - A Wheel in General Motions 77
Figure 4.9 - Comparison between Active Caster and ASOC 78
Figure 4.10 - Scrubbing Analysis of the ASOC 79
Figure 4.11 - Scrubbing Analysis for the Active Castor 79
Figure 5.1 – PAMM Admittance-Based User Interaction Control 84
Figure 5.2- A mass-damper model 85
Figure 5.3 – Step Response of a Mass-damper Model 86
Figure 5.4 - Example of the PAMM Admittance Control Response 88
Figure 5.5 - User Evaluation on PAMM SmartWalker (n=8) 89
Figure 5.6 - Parameters of Test Models 90
Figure 5.7 - Example Responses of Test Models 90
Figure 5.8 - Effects of Admittance Model Parameter 91
Figure 5.9 - A Variable Damping Model 93
Figure 5.10 - User force and Speed with the Fixed Damping Model 94
Figure 5.11 - User Force and Speed with the Variable Damping Model 94
Figure 6.1 – Adaptive Shared Control Framework 97
Figure 6.2 - Effect of Parameter β on Computer Control Gain 101
Figure 6.3 – User Input in Y Direction 103
Figure 6.4 - Simulation of Adaptive Shared Control with λ=10, β=0.5 103
Figure 6.5 - Simulation of Adaptive Shared Control with λ=0.1, β=0.005 104
Figure 6.6 - Field Trial Path Design 106
Figure 6.7 - Elderly Users (94 and 85Years old) Testing PAMM SmartWalker 107
Figure 6.8 - Path and Control Gain under Adaptive Shared Control (User #1) 110
Figure 6.9 – User #1 Performance under Free-Driving 112
Figure 6.10 – User #1 Performance under Adaptive Shared Control 113
Figure 6.11 – User #1 Performance under Full Computer Control 114
Figure 6.12 - RMS Values of Deviation from Path for all three Users 115
Figure 6.13 – RMS Values of Distance to Obstacles for all three Users 115
Figure 6.14 - User Performance with Shorter Forgetting Term (λ=10) 117
Figure 6.15 - User Performance with Longer Forgetting Term (λ=0.1) 118

List of Tables

Table 2.1 - Typical Assisted Living Facility Resident's Physical and Cognitive Needs.. 25
Table 2.2 - PAMM System Level Performance Goals 27

Chapter 1

Introduction

1.1 Motivation

Assistive robotic devices offer the potential to augment human capabilities and perform many important tasks. In industry, workers are often needed to handle heavy and awkward object [Snyder and Kazerooni, 1996]. Injuries to workers due to exertion and repeated trauma, and the related down time, cost US industry close to $20 Billion a year [Akella et al., 1999; Snyder and Kazerooni, 1996]. In military services, soldiers need to handle heavy weapons and ordnance in depots, at airports, and on ship decks. In these applications, fully autonomous systems are still a research goal that will require tremendous breakthroughs in the AI, robotics and vision research communities. Factors such as the incomplete a priori knowledge of the environment, dynamic obstacles, insufficient and inaccurate sensory information, and the inherent inaccuracy of the robotic system make full automation more challenging [Sheridan, 1992]. The practical approach is to develop cooperative robotic systems that work with human operators to best use the capabilities of both the machine and the operator [Hoeniger, 1998]. Substantial research has been done to develop human machine cooperative robotic

devices to augment human capabilities and improve productivity, ergonomics and safety [Akella et al. 1996; Snyder and Kazeroni, 1996; Kosuge and Kazamura, 1997].

Elderly populations are growing rapidly in many developed countries. According to the U.S. Department of Health and Human Services [AOA, 2001], persons 65 years or older numbered 35 million in 2000 and represented 12.4% of the US population. Further more, by 2030, there will be about 70 million elderly, or 20% of the US population. This trend is also evident in countries such as Germany and Japan. As an elderly person's ability to physically and cognitively function degrades, current practice is to progressively move him or her into facilities that provide higher levels of care. The move from independent living in one's own home to an assisted-living facility and then to a nursing home is an example of this practice. With each of these moves, costs drastically increase while quality of life rapidly decreases. The largest change occurs during the transition into a nursing home. Delaying this change by using robotic assistive devices, which provide mobility aid, guidance, communication, and health monitoring functions, could have great social and economic significance. There is a growing interest in the research community in recent years to develop intelligent assistive devices for the elderly [Lacey et al., 1998; Nemoto et al., 1999; Schraft et al., 1998; Baltus et al., 2000]. At MIT Field and Space Robotics Lab, a system called PAMM has been developed to provide mobility aid and health monitoring for the elderly [Dubowsky et al., 2000]. The objective of the PAMM project is to develop the enabling technologies for assistive robotic devices for elderly living in private homes and assisted living facilities. The PAMM project is the primary focus of this thesis research, however, the approached

proposed in this thesis are also applicable to the human machine cooperative devices in industrial and military applications.

There are many technical challenges in the development of assistive robotic devices. This research addresses two particularly important challenges. The first challenge addressed in this research is the mobility design. The environments for such devices are often congested and filled with static and dynamic obstacles. Conventional wheeled robotic vehicles have limited mobility due to the non-holonomic constraints of conventional wheels, thus are not suitable for these environments. Non-holonomic systems also require complex path planning and control algorithms. Vehicles with omni-directional mobility can instantaneously move in any direction from any configuration. Therefore, omni-directional mobility is very desirable for such applications where maneuverability is important. Yet many current omni-directional mobility designs are complex and sensitive to floor irregularities. Developing a practical and low cost omni-directional mobility design that is energy efficient and robust to floor irregularities is a great challenge.

The second challenge addressed in this research is to design an effective control system for assistive robotic devices to work interactively and cooperatively with their human operators. These devices, intended to augment the strength and compensate the limitation of human operators, have to work in the same workspace and interact physically with human operators. Ergonomic, intuitive human-machine interfaces and control techniques for human machine interaction are crucial for these systems. These devices have to work with operators with different physical and cognitive capabilities or characteristics. The operators may not be well trained or do not understand the system

well. The elderly users for PAMM may have diminished physical and cognitive capabilities or have irrational behavior. In such cases, the system could exhibit dangerous behavior were it not properly controlled. The challenge is to design a shared control system that can properly allocate control authority between the human and the machine.

1.2 Background Literature Review

The related work in the literature can be broken down into four areas: a) assistive robotic devices, b) omni-directional mobility design, c) human-machine interface design, and d) shared control design for cooperative human machine systems.

1.2.1 Assistive Robotic Devices

There has been substantial research on human-machine cooperative robotic devices for industrial and field applications. Researchers have been working on devices that can be worn by humans to augment human strength to handle heavy objects, such as the extender [Snyder and Kazerooni, 1996; Kazerooni, 1998]. A system called Cabot, is developed to reduce physical and mental workload for workers in automotive assembly factories by guiding the motion along virtual surfaces defined by software [Akella et al., 1996]. Several researchers have worked on robotic systems working cooperatively with human operators to move large and/or heavy objects [Kosuge and kazamura, 1997; Fujisawa, et al., 1992; Yamamoto, 1996]. In these systems, the robotic manipulator/vehicle system supports and moves the object in the direction of the intentional force applied by the human operator.

There is a growing interest in developing intelligent assistive devices for the elderly. These devices aim to improve the elderly peoples' dignity and quality of life by improving their mobility and enabling them to perform some daily activities. The PAM-AID [Lacey and Dawson-Howe, 1998], developed at Trinity College of University of Dublin, is a robotic mobility assistance designed to provide physical support and obstacle avoidance to frail and blind elderly people. The Hitomi [Mori and Kotani, 1998] is a robotic travel aid for the blind in outdoor environments. It provides the user with orientation and map-based guidance based on information about obstacles and landmarks. The Care-O-bot [Schraft et al., 1998, Graf, 20001; Graf and Hägele, 2001] and the Nursebot [Baltus et al., 2000] are personal service robots developed for the elderly and disabled. The Care-O-bot is intended to provide mobility aid, do household jobs, and provide communication and entertainment functions. The Nursebot project has focused human machine interface methods, tele-presence via the Internet, speech interface, and face tracking. Both systems are in the very early stages of development. A device called Power-Assisted Walking Support System being developed at Hitachi to help support elderly people standing up from bed, walking around, and sitting down [Nemoto et al, 1999]. A passive device called Personal Mobility Aid is being developed at the Medical automation research center at University of Virginia Health System [Wasson et al., 2001]. It is modified from a passive three-wheeled walker by fitting a steering motor on the front wheel, adding encoders for dead reckoning, and laser and IR sensors for obstacle detection. The aim of the project is to help elderly users to steer clear of obstacles.

The mobility drives of these devices are based on skid steering or adapted from existing devices, which pose serious maneuverability limitations due to the non-holonomic constraints and make it difficult for users to handle. For all these devices, the fundamental problem of providing control to users who have varying levels of training and perhaps diminished mental and physical capabilities remains a challenge.

1.2.1 Omni-directional Mobility Design

A variety of designs for omni-directional vehicles have been developed. These designs can be broken into two categories: those with special wheel designs and those conventional wheel designs. An omni-directional vehicle is usually formed using three or more of such wheels.

Most special wheel designs are based on a concept that achieves traction in one direction and allows passive motion in another. The universal wheel is an example of the special wheel design that has a number of small passive rollers mounted on the periphery of a normal wheel. The axes of the rollers are perpendicular to that of the wheel [Fujisawa et al., 1997, Ferriere and Raucent, 1998]. When the wheel is driven forward, the passive rollers allow for a free motion in the perpendicular direction. The Mecanum wheel design [Muir and Neuman, 1987], which has angled passive rollers around the periphery of the wheel, is based on the same concept. By controlling the four wheels attached to a platform, omni-directional mobility can be achieved.

Other special wheel designs of note are the orthogonal wheel [Killough and Pin 1994] and the ball wheel mechanism [West and Asada 1997]. In the ball wheel design, power from the motor is transmitted through gears to the roller ring and then to the ball via friction between the rollers and the ball.

Such designs demonstrated good omni-directional mobility, especially the ball wheel design, but they generally have complex mechanical structures and can consequently be costly. Furthermore, vehicles based on these designs can have limited load capacity as the slender rollers support the loads, such as in the case of universal wheel design. For these designs, the height of obstacles, e.g. cables on the floor or small steps that they can pass over, is limited by the small diameter of the rollers. Designs with passive rollers can also generate unwanted vibrations as the rollers make successive contact with the ground. It is also difficult to measure all the degrees of freedom for dead reckoning in these special wheel designs, except the ball, as it is impractical to place sensors on the passive rollers [West and Asada 1997].

In contrast to special wheel designs, conventional wheels are inherently simple, have high load capacity and high tolerance to floor irregularities such as bumps and cracks, dirt and debris. Despite their non-holonomic nature, designs have been proposed to achieve near omni-directional mobility for vehicle using conventional wheels. The most common approach is to use steered wheels [Boreinstein, et al., 1996]. Vehicles based on this design have at least two active wheels, each of which has both driving and steering actuators. They can move in any direction from any configuration. However, this type of system is not truly omni-directional because it needs to stop and re-orient its wheels to the desired direction whenever it needs to travel in a trajectory with non-continuous curvatures.

A truly omni-directional vehicle can also be formed using the active castor design [West and Asada 1997]. With two or more such wheels, omni-directional mobility can be achieved for a vehicle [Wada and Mori, 1996, Holmberg and Khatib, 1999].

One major drawback of the above conventional wheel designs is the wheel scrubbing during steering as the wheel is twisted around its vertical axis [Killough and Pin, 1994]. Wheel scrubbing reduces positioning accuracy and increases energy consumption and tire wear, especially for heavy vehicles. One solution to this problem is to use the dual wheel design, which is commonly found in the aircraft landing gears. Vehicles using the dual wheel design for steering are still not omni-directional, as they need to stop and reorient the wheels on paths with non-continuous curvatures [Hashimoto et al, 1999; Betourne and Fournier, 1993]. However, the frictional forces experienced in dual wheel design are substantially smaller compared with the single steered wheels and the active castors. Although this is widely recognized in the literature, there is no sufficient analytical analysis on the fundamental mechanics for the reduced scrubbing.

1.2.3 Human-Machine Interface Designs

The Human-machine interfaces for crucial for systems designed to work cooperatively with humans. The interface is the means via which the user controls and communicates with the system. The users of mobility aids generally have direct physical interaction with the system for support. A key requirement is that the interface should be able to adapt to users with different levels of physical and mental functionality. The interface should provide reliable bilateral communication between the user and the machine to ensure safety. It should also provide a natural feel for the user and be easy for the user to learn to use. Researchers have studied various forms of interfaces. The joystick is widely used for robotic wheelchairs [Levine, 1999; Lankenau and Rofer, 2001]. However, for the mobility aids concerned in this paper, where the user and the machine are two dynamic entities, the joystick tends to cause oscillatory motion when

users walk with the device [Lacey and MacNamara, 2000]. Switches and buttons can be used to select directions or control modes, but they are limited by their discrete nature [Lacey and MacNamara, 2000]. They could also increase the mental workload and cause confusion and frustration for the elderly users. Touch screens have also been implemented as an interface for the elderly [Baltus et al., 2000; Schraft et al., 1998]. Using voice communication as human machine interface is another area of active research. These can become effective high-level command and bilateral communication tools, but they cannot serve as continuous control interface.

For cooperative robotic devices in industrial applications, where the human operator and the machine have direct physical interaction, force sensing and the related force control strategies are widely used [Al-Jarrah and Zheng, 1997]. However, a force sensor itself can not guarantee a good interface. Using force signals directly to generate motion can result in unstable motion due to the fluctuation of the signals. This problem has been encountered in the Care-O-bot project [Graf, 20001; Graf and. Hägele, 2001]. This thesis developed an admittance-based control method that uses the force/torque sensor to provide a natural and intuitive interface for elderly users.

1.2.4 Shared Control Design for Cooperative Human Machine Systems.

A major challenge of the control system development is how to allocate the control between the user and the machine. A shared control system integrates the best capabilities of both the human and the machine. Humans are best at high level cognitive tasks such as object identification, error handling and recovery, use of heuristics and common sense in the presence of uncertainty. On the other hand, machines have high mechanical and computational power, and good accuracy. A substantial amount of work

has been done in the shared autonomy and cooperative control for tele-operations, space, and aviation systems [Sheridan, 1992]. Many researchers are developing shared control strategies for assistive devices. Various methods of shared control design of power wheelchairs are reviewed in [Cooper, 1995]. In these control strategies, there are a few preset discrete behavior modes using fuzzy logic or probabilistic models, such wall following, passing doorways, obstacle avoidance. The shared control methods are used to select from one of them based on the obstacle sensor information and user input. Methods have also been developed to make the shared control system adaptive to different tasks and situations for a wheelchair [Levine et al., 1999; Simpson and Levine, 1999]. Obviously, these few behavior modes can limit the freedom of the user.

In summary, substantial research with significant progress has been done on the control of robotic and telerobotic systems and vehicles. However, the important problem of identifying the capabilities of the operator, particularly when the user may have diminished mental and physical capabilities, and then adjusting his authority to ensure safe system operation based on those capabilities remains unsolved. This problem is addressed in this thesis in the context of the PAMM systems.

1.3 Objectives of this Thesis and Summary of Results

The first objective of this thesis research is to develop an omni-directional mobility concept for mobile systems working in congested and dynamic environments. The design should be lightweight, energy efficient and be able to operate on a wide range of floor surfaces.

A concept for omni-directional mobility design has been developed independently using active split offset castors (ASOC) [Yu et al., 2000]. A similar design concept has also been proposed by Wada [Wada, 1999]. An ASOC module consists of a pair of independently driven coaxial wheels that are separated by a short distance along the axial direction and connected to the platform with an offset link. By controlling the velocities of the two wheels, arbitrary velocities can be achieved at the joint of the offset link. The three-degree of freedom motion of a planar mobility platform can be fully defined by the velocities at any two distinctive points on the platform. Therefore with a minimum of two ASOC modules, an omni-directional mobility platform can be constructed. Compared with the existing omni-directional mobility designs, the ASOC design is simpler in structure, has higher loading capacity, and is more robust to floor irregularities. Its dual-wheel construction effectively alleviates wheel scrubbing and increases system power efficiency, while increasing the traction and disturbance force rejection capability of the platform.

Substantial study and analysis has been done on the important design and control issues for implementing the design, such as parameter selection, suspension design for even floor. A method has been developed using fundamental principles of mechanics for the analysis of wheel scrubbing, an important problem in wheeled mobile robot design that has not been addressed in the literature. The ASOC design has been implemented on the PAMM SmartWalker, which demonstrates excellent omni-directional mobility and tracking performance.

The second objective of this research is to develop control methodologies for such systems to work interactively and cooperatively with human operators. This objective is

two fold. First, an ergonomic, natural, and intuitive interface along needs to be developed with a control method to allow the user to interact with the system. Second, a shared control methodology to allocate appropriate control between the human and the machine to ensure the safety of the operator, the system, and the environment, is to be developed.

Using the force/torque sensor as the human machine interface, an admittance-based control method for human machine interaction has been developed for the PAMM test-bed. The admittance model emulates a dynamic system and makes the user "feel" as if he is interacting with a system described by the model [Durfee et al., 1991].

An adaptive shared control framework is proposed in this research. The goal is to develop a control scheme that can dynamically allocate the control between the human and the machine according to the task situation, the capabilities of the human and the physical system. This approach has a structure similar to a classical adaptive controller [Narendra and Annaswamy, 1989]. The system has a planner to plan an ideal path through the environment based on the task and its knowledge of the environment. It has a computer controller to guide the user back to the preplanned trajectory. The human operator interacts with the system through the force/torque sensor and the admittance based controller. The core of this approach is the adaptive shared controller. There are two control inputs to the shared controller, the computer and the human, both of which have an associated gain, $K_{computer}$ and K_{human}, respectively. The shared controller combines the two inputs using the gains calculated by the adaptation law. The adaptive law controller adjusts the gains, $K_{computer}$ and K_{human}. The adaptation law first computes a perfomance index, which will be a measure of how well the user is performing. It then

adjusts the two gains to minimize the performance index. The adaptive shared control has also been implemented on PAMM.

Substantial field trials have been conducted at an assisted living facility. Clinical trials provide a means to assess system performance and to gather user feedback. It is also critical for the development of effective human-machine interface and control system.

Although implemented and tested on PAMM, the proposed approaches in thesis are applicable to other cooperative mobile robots working in semi-structured indoor environment such as a factory or a warehouse.

1.4 Outline of this Thesis

This thesis consists of seven chapters. This chapter describes the motivation and the technical challenges of the research. A survey on the background literature on the thesis topic is given. It also outlines the objectives of the thesis research and summarizes the contributions of the thesis.

Chapter 2 introduces the PAMM system, which is experimental system of this research. It presents the PAMM system concept, user needs and PAMM functions, and the design requirements. It also describes the physical system design of the two PAMM configurations and gives an overview of the research focus of the PAMM project.

Chapter 3 describes an omni-directional mobility concept based on the ASOC design. It also investigates several important issues for effective implementation of the design, and presents some experimental results of mobility system implemented on the PAMM SmartWalker.

Chapter 4 is an analytical study of the wheel scrubbing of conventional wheels, which is an important issue for heavy loading and/or battery powered mobile systems. The fundamental causes and the contributing factors to wheel scrubbing are identified. This analysis provides a means to estimate the scrubbing torque of wheel in general planar motion, which is meaningful for design of all wheeled systems.

Chapter 5 presents admittance based human-machine interaction control. It describes the concept of the admittance-based control, the admittance model design for PAMM and approaches for experimental evaluation. It also presents results of the field experiments with PAMM.

Chapter 6 presents the development of the adaptive shared control approach. It starts with discussion on the various aspects of the adaptive shared control framework. It then introduces the implementation of the control on PAMM SmartWalker and the experimental results the PAMM system with users in an assisted living facility.

Chapter 7 summarizes the contributions of this thesis and suggests some issues for future work related to this thesis research.

Chapter

2

PAMM Experimental Systems

2.1 Introduction

The elderly populations in many countries are growing rapidly according to the U.S. Department of Health and Human Services [AOA, 2001]. For example, persons 65 years or older numbered 35 million in 2000 and represented 12.4% of the US population [AOA, 2001]. As people grow older, their physical and cognitive functions degrade. Current practice is to move such an elderly individual into facilities that provide higher levels of care.

Assisted living facilities are generally the first alternative to independent living. These facilities aid their residents with daily activities such as bathing and meal preparation; however, most such facilities cannot provide labor-intensive support, such as guidance for the residents that become disoriented frequently. Approximately 30 to 40 percent of assisted living facility residents suffer from some level of senile dementia [ALFA Advisor, 1995]. These residents often require assistance with guidance, medication regulation, health-condition monitoring, and scheduling daily activities, see Table 2.1. When these disabilities progress to the point that the elderly require the

constant attention of a caregiver, the transition to a skilled nursing facility is traditionally the only solution. In these facilities, costs are higher and quality of life is often reduced [Burton, 1997]. The cost of staying in a skilled nursing facility (often called a nursing home) in major city in the US can easily exceed $90,000 to $100,000 per year compared to less than $40,000 per year for an assisted living facility. Clearly it is cost-effective to keep the elderly out of nursing homes if possible. It is also well known that the transition to a nursing home is a very traumatic experience for many elderly people. Hence there are great social and economical benefits delaying the transition using robotic technology. Smart assistive technology offers the potential solutions to delay the need for individuals to enter nursing homes..

Table 2.1 - Typical Assisted Living Facility Resident's Physical and Cognitive Needs.

Need	Physical Deficiency	Cause
Guidance	Failing memory, disorientation.	Senile dementia, Alzheimer's.
Physical Support	Muscular- skeletal frailty, instability.	Osteoporosis, Diabetes, Parkinson's, Arthritis, etc.
Health Monitoring	Poor cardiovascular potential strokes and heart attacks.	Age, lack of exercise, illness (e.g., flu or pneumonia).
Medicine and Other Scheduling	Need for a variety of medicines coupled with failing memory.	Senile dementia, general frailty.

A series of robotic aids, called PAMMs (Personal Aids for Mobility and Monitoring), have been developed in the Field and Space Robotics Laboratory at MIT to assist the elderly in assisted living facilities and delay their transition to nursing homes [Dubowsky et.al., 1997, Godding, 1999, Spenko, 2001, D'Arrigo, 2001].

The development of PAMM is the work of a group of graduate students and research engineers, who spent various amounts of time on this project, under the

supervision of Professor Dubowsky. With overlapping efforts and collaboration, each member of the group was responsible for a specific area. My main contributions to PAMM project are the mobility system design, the control system development, control software development, sensor integration, and field experiments.

2.2 PAMM System Concept

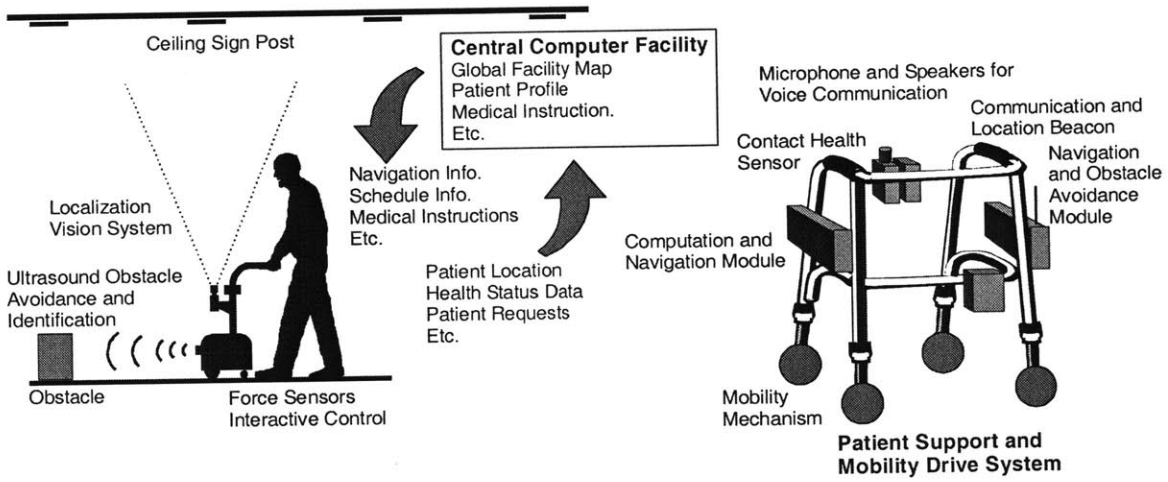

Figure 2.1 - PAMM System Concept [Dubowsky, 2000]

Figure 2.1 shows the PAMM concept. The PAMM can be either a cane or a walker. It has a six-axis force-torque sensor mounted under the user's handle to serve as the main user interface. An admittance-based controller integrates the user input signals with the instruction of the schedule based planner, the facility map information, and signals from the obstacle avoidance sensor in order to control the system. On-board sensors monitor the user's basic vital signs. The system communicates via a wireless link with a central computer in order to receive up-dated planning information and to provide information on the health and location of the user. The location of PAMM is determined from a CCD camera which reads passive signposts placed on the ceiling of the facility.

2.3 PAMM System Performance Goals

Working with several Assisted Living Facilities in the Boston Area, a set of performance goals for the PAMM concept were established based on the user needs and environment conditions, see Table 2.2.

Table 2.2 - PAMM System Level Performance Goals

Potential Users	Elderly with mobility difficulty due to physical frailty and/or disorientation due to aging and sickness.
Environment	Assisted living facilities. Known structured indoor environment with random obstacles such as furniture and people. Flat and relatively hard floor or ramps less than 5 degrees.
Physical Stability	Provide equal or better stability than that of a standard four-point cane.
Guidance and Obstacle Avoidance	Provide guidance to destinations via pre-programmed maps, schedules, user commands, and sensed obstacles.
Health Monitoring	Provide continuous health monitoring.
Communication	Provide two-way communication with centralized computer.

2.4 PAMM Physical Systems

Canes and walkers are the two common mobility aids for residents in assisted living facilities. PAMM configurations have been developed to meet the needs of both cane and walker users. The cane configuration is called SmartCane and is shown in Figure 2.2. The walker configuration is called SmartWalker and is shown in Figure 2.3. It has basically the same electronic and sensor system as the SmartCane. A walker gives the user substantially more physical support than a cane. It has basically the same computer, electronic and sensor systems as the SmartCane. The mobility design of the SmartCane uses skid steering. While this is acceptable for the SmartCane as it is relatively small in size, the nonholonomic constraint of such a system is not suitable for the SmartWalker.

The SmartWalker uses the omni-directional mobility drive developed in this thesis research [Yu et. al, 2000, Spenko et. al. 2002].

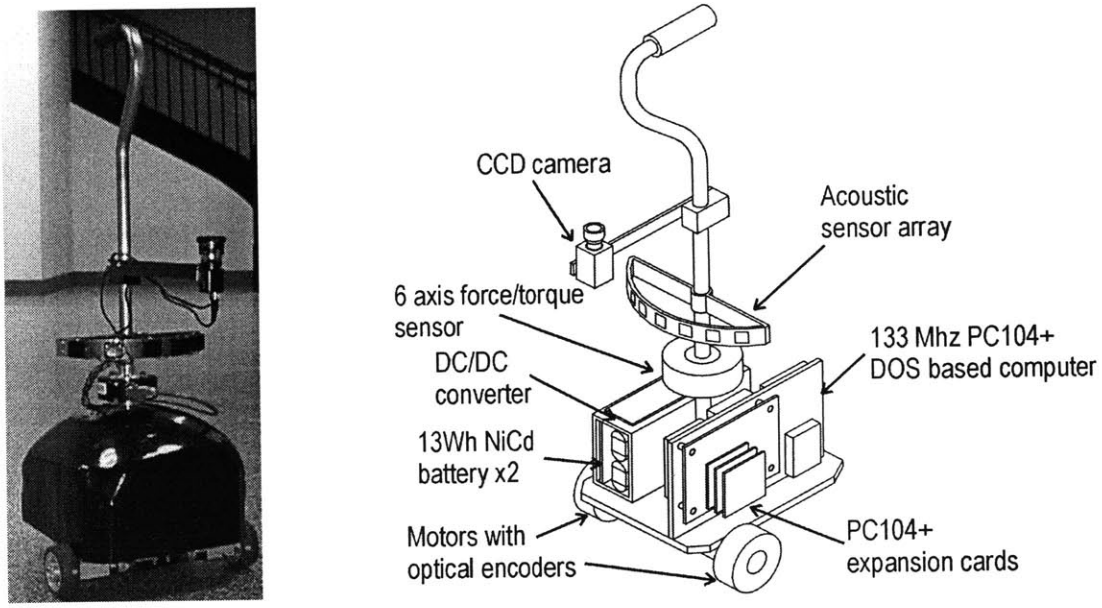

Figure 2.2 - The SmartCane Prototype PAMM System (Courtesy of Sami Kozono)

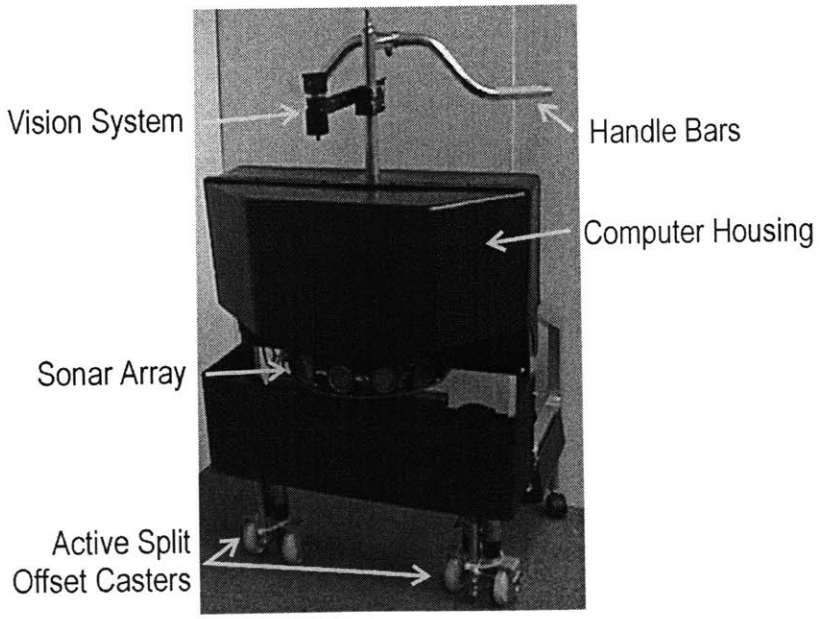

Figure 2.3 - The SmartWalker Prototype PAMM System

The construction of the PAMM systems is the work of several members working on the project. Sami Kozono and Xiaowen Lin designed and built the electronics and the developed the interface codes. Dr. Long Seng Yu designed and built the mechanical system for the SmartCane. Matt Spenko designed and built the mechanical system for the SmartWalker.

2.5 Research Focuses of the PAMM Project

There are many technical challenges for developing assistive devices like PAMM. In addition to the development of the system concept, the PAMM project has four areas of research focus. The first is planning in dynamic environment. The second is mobility design and motion control. The third is control system development. The fourth is health monitoring sensor development. This thesis research addresses the mobility design and control system development.

2.5.1 Planning

To provide guidance to the user, PAMM needs to plan the best path based on a facility map while avoiding obstacles and accepting user-inputs, see Figure 2.4. The planner needs to determine where the system is located in the assisted living facility at all times. For this purpose, a vision-based localization system has been developed. The planner also needs to identify objects in the environment so that it can dynamically re-plan its trajectory. The path planning, mapping, obstacle avoidance and object identification are described in [Dubowsky et. al. 2000].

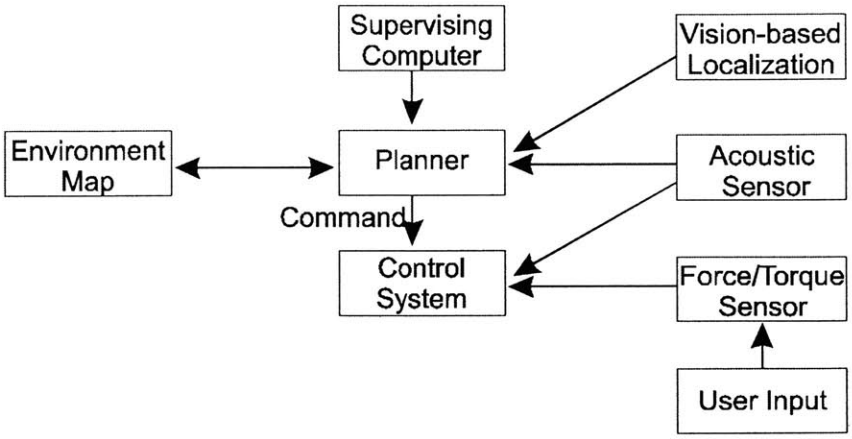

Figure 2.4 - PAMM System Planner

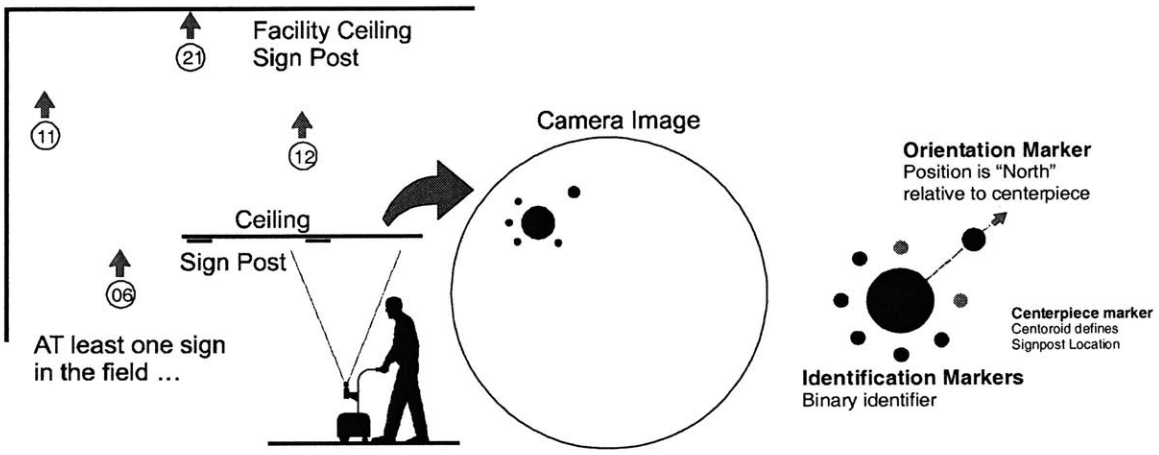

Figure 2.5 - Vision-based Localization System (Dubowsky, 2000)

A brief introduction of the vision based localization system is given here, as it is an essential tool for the experimental study of this research. The localization system for the SmartCane was developed by Adam Skwersky and was improved and ported to the SmartWalker. It uses a single CCD camera, which looks at signposts placed periodically on the ceiling of the facility (see Figure 2.5). The signpost has a binary design and can be printed on standard office paper. Each signpost has a unique pattern of identification

markers with three elements (see Figure 2.5). The first two, the "Orientation Marker" and "Centerpiece Marker" are self-explanatory. The presence or absence of individual markers represents a binary number. A design with **N** placeholders for identification markers allows 2^N-1 separate signposts. At least one signpost must be visible to the onboard camera at all times. This allows PAMM to continually determine its absolute position and orientation within the facility.

The main challenge for development of the localization system is to make it robust. An adaptive threshold setting method has been developed to make the system robust to varying lighting conditions within the eldercare facility. An error-tolerant search algorithm has also been developed to cope with the image blurring caused by the motion of the system. The localization system achieved a success rate of more than 90% with position accuracy of 1 inch and orientation accuracy of 1 degree, when PAMM was driven by elderly persons at a speed of about 0.3 m/s in the natural setting of an assisted living facility.

2.5.2 Mobility Design and Motion Control

2.5.2.1 SmartCane Mobility Design and Control

The SmartCane employs a relatively simple skid steering drive with two driving wheels and a rear-mounted caster, see Figure 2.6. Each drive motor has an incremental optical encoder for motion control and odometry. This configuration has relatively good maneuverability in congested environments as it allows an on-the-spot rotation. The mobility base is modular, so caster and motor assemblies can be rearranged to study different configurations.

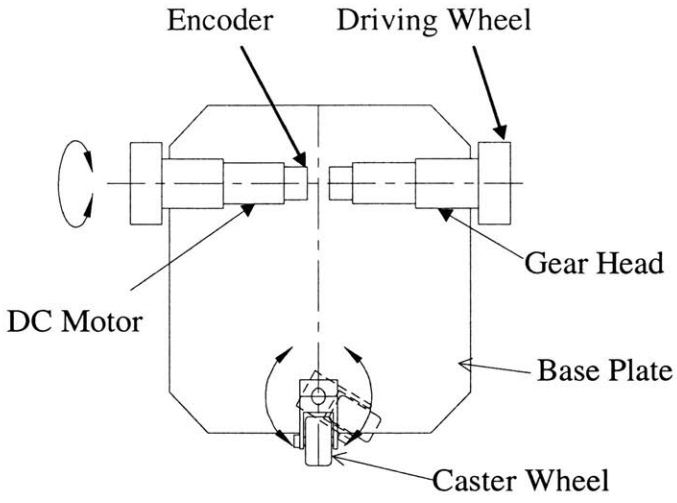

Figure 2.6 - SmartCane Mobility Design

The skid steering is a non-holonomic system. For the coordinate system defined in Figure 2.7, the kinematic model of the system is given by:

$$\begin{aligned} \dot{x} &= \cos\theta(v_1 + v_2)/2 = \cos\theta v \\ \dot{y} &= \sin\theta(v_1 + v_2)/2 = \sin\theta v \\ \dot{\theta} &= (v_1 - v_2)/(2c_r) = \omega \end{aligned} \tag{2.1}$$

The non-holonomic constraint due to the non-sliding condition is given by:

$$[\sin\theta, -\cos\theta, 0]\dot{\mathbf{q}} = 0 \tag{2.2}$$

where $\mathbf{q} = [x, y, \theta]^T$ is the generalized coordinates of the system.

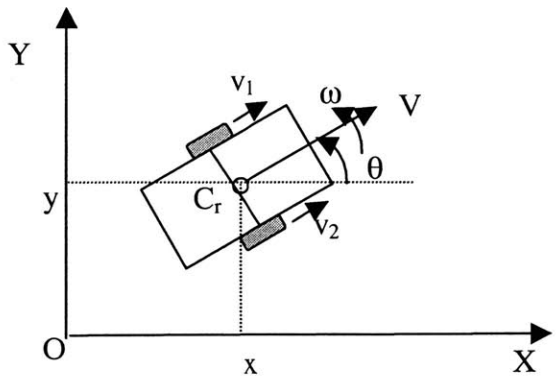

Figure 2.7 - Kinematic Model of SmartCane Mobility Design

To control the SmartCane, a trajectory-tracking algorithm using non-holonomic feedback control has been implemented and tested. It is based on the nonlinear feedback posture-tracking algorithm developed by [Samson and Ait-Abderrahim, 1991]. The controller follows the trajectory by tracking the desired velocities v_r and ω_r, as shown in Figure 2.8. The control law is given by:

$$\begin{aligned} v &= k_1 e_1 + v_r \cos e_3 \\ \omega &= k_2 v_r \frac{\sin e_3}{e_3} e_2 + k_1 e_3 + \omega_r \end{aligned} \tag{2.3}$$

where e_1, e_1, e_3, are the errors in x, y and θ respectively, and k_1 and k_2 are the gain defined by:

$$\begin{aligned} k_1 &= 2\xi(\omega_r^2 + b v_r^2)^{1/2} \\ k_2 &= b = \omega_n^2 \end{aligned} \tag{2.4}$$

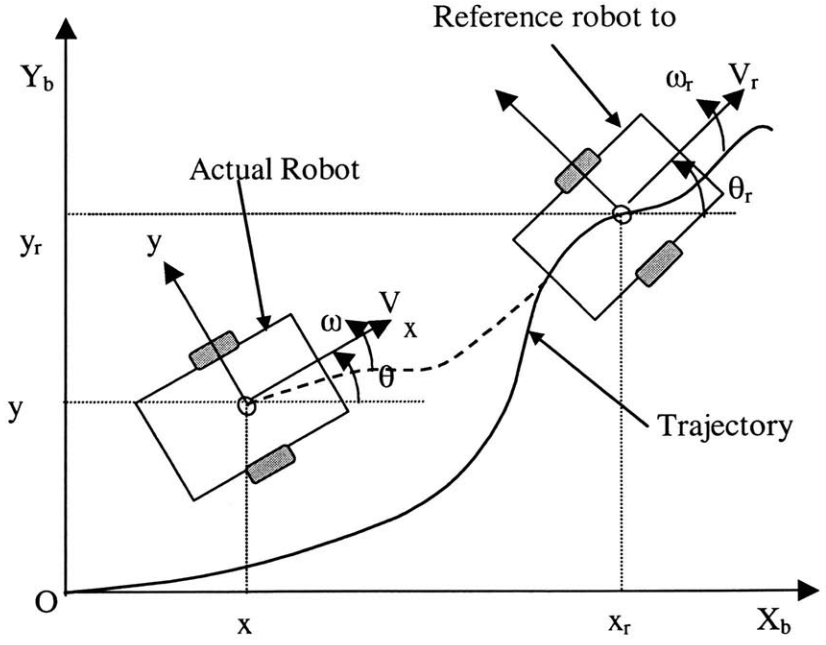

Figure 2.8 - Posture Tracking

Figure 2.9 and Figure 2.10 show the simulation results of the cane starting from an initial position at $\mathbf{X_0}$=[0, 0.3, 5°], with reference velocities V_r=0.3 and ω_r=0.0.

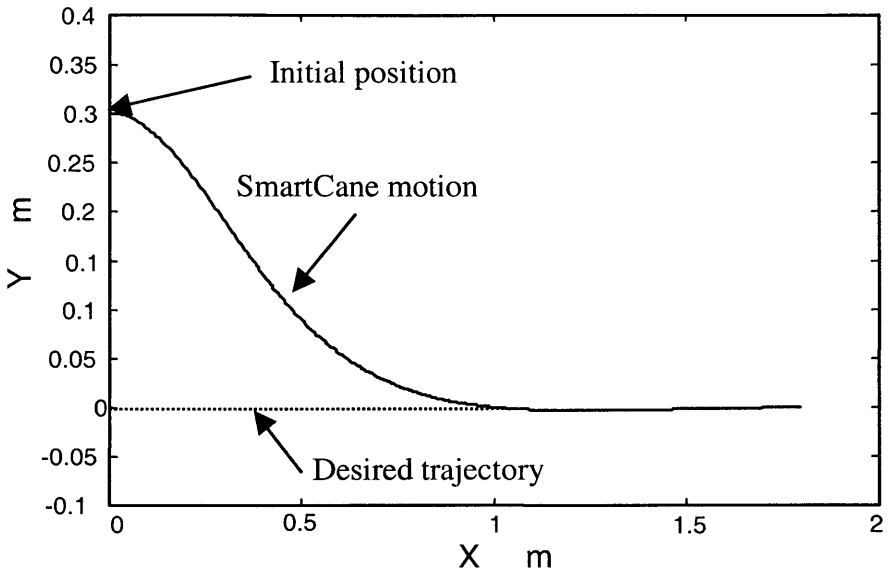

Figure 2.9 - Convergence of SmartCane Trajectory

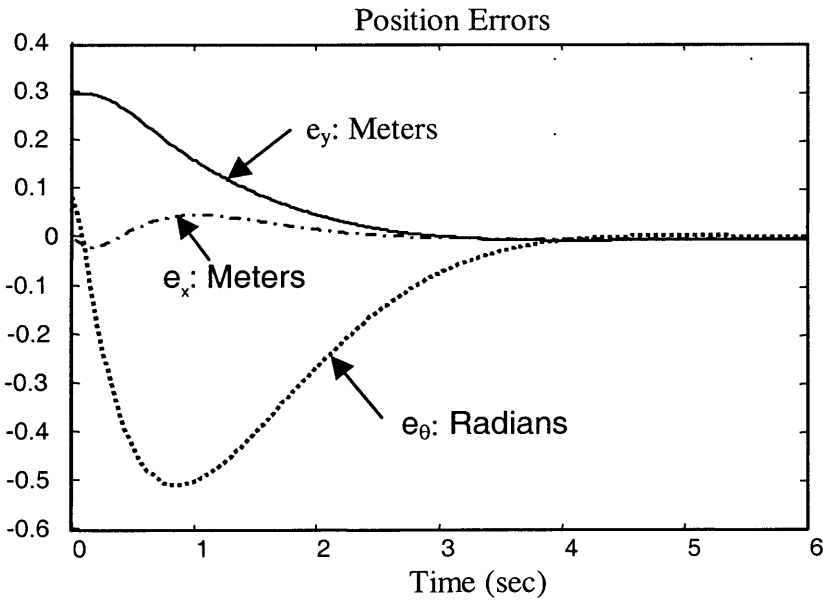

Figure 2.10 - Convergence of Position Errors

It can be seen that the SmartCane converges to the trajectory asymptotically and the position errors go to zero. An advantage of this algorithm over many other non-holonomic control methods is that it has no control action when the desired speed is zero, even when position errors exist. It is most suitable for this application since it allows the user to stop and will not force the user to the intended trajectory.

Figure 2.11 and Figure 2.12 shows the laboratory performance of the SmartCane with and without the signpost localization control. In each case PAMM is commanded to follow an elliptical-like path approximately 15 meters long. There are signposts on the ceiling in the neighborhood of the path. Figure 2.11 shows the system that depends entirely upon odometry using the wheel encoders for location. The errors grow during the motion and by the second turn the cane is essentially "lost." The small circles in the figure show where on the path the cane's actual position is measured by the CCD camera. However these values are not used by the system to correct its location. In Figure 2.12.10 the localization information from the camera and signposts is used by the non-holonomic controller to correct the path of the cane. The figure shows that the cane is able to complete the route successfully.

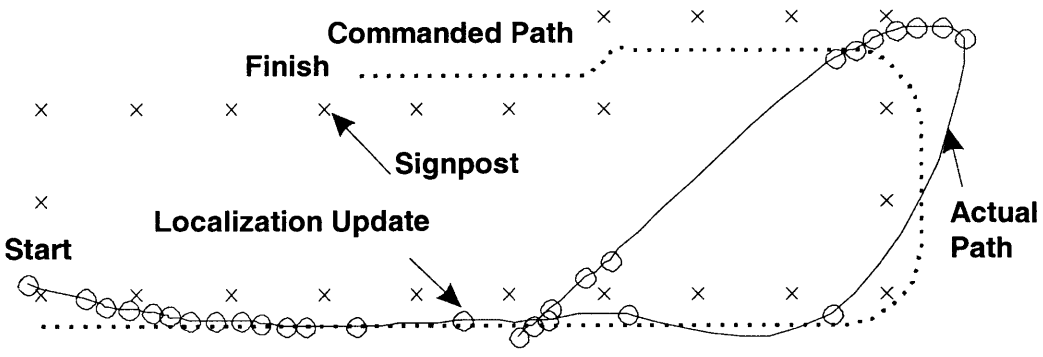

Figure 2.11 - SmartCane Tracking Performance without Localization Control

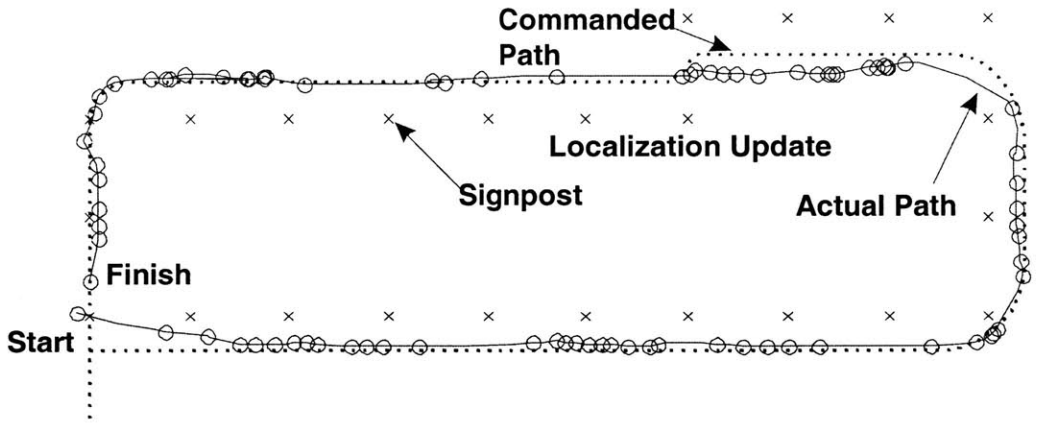

Figure 2.12 - Tracking Performance with Active Localization

2.5.2.2 SmartWalker Mobility Design

While skid steering is acceptable for the SmartCane as the cane is relatively small, it would not be acceptable for the SmartWalker as the walker has much bigger size. The PAMM SmartWalker thus implements the omni-directional mobility concept based on the active split offset castor (ASOC) design, see Figure 2.13. The SmartWalker has two ASOC modules and two passive castors. Chapter 3 has the details of the technical development of the mobility design and the implementation results on the SmartWalker.

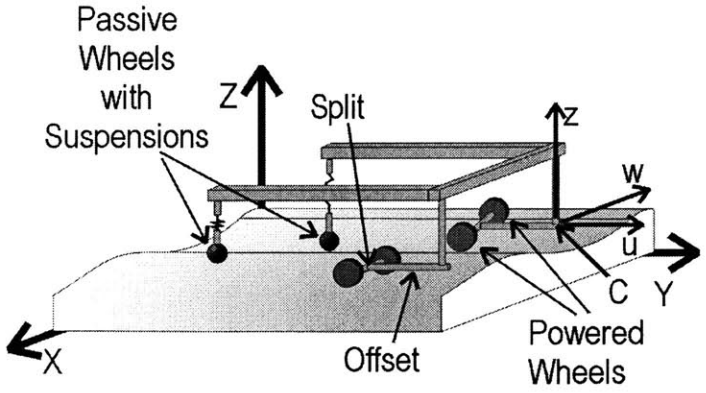

Figure 2.13 - SmartWalker Mobility Design (Courtesy of Matt Spenko)

2.5.3 Control System Design

The goal of the control system is to ensure that PAMM works interactively and cooperatively with the elderly. First, a natural and intuitive interface and a control

method for the human machine interaction need to be developed. Second, a shared control method needs to be developed to allocate appropriate control between the user and PAMM. An admittance-based control method is developed for the human-machine interaction for PAMM, which responds to the forces and torques of the user. The admittance model is defined by software and can be tuned to create a desired feel for the user. An adaptive shared control framework has been developed for the control allocation based on the demonstrated performance of the user. The development of control systems for human-machine systems is less analytical and precise than traditional control for completely determined systems and autonomous control, because humans are very difficult to model. Hence its development and evaluation depends largely on experimental work carried out with the elderly in the eldercare facilities. Extensive field trials were conducted at an eldercare facility to evaluate both the admittance based human-machine interaction control and the adaptive shared control. The details of the control system design and the field experiment are presented in Chapter 5 and Chapter 6.

2.5.4 Health Monitoring

PAMM provides an excellent platform for health monitoring sensors because it allows for continuous monitoring [Dubowsky, 2000; D'Arrigo, 2001]. Due to the limited mobility capabilities of the user, PAMM is always with the user in their daily activities. The vital signs of users of can be recorded every time the user comes in contact with the walker. The resulting volume of data provides physicians with a clearer idea of the users' health. Using the person's medical history also simplifies the diagnostic process—only a *change* in a health signal is necessary to indicate the presence of an illness. Since the data is collected while the walker is in motion, the user's speed and applied forces are

known. Thus, the person's activity level can be correlated with their health parameters, providing medical professions with further assessment capabilities. A noninvasive, robust, ECG-based pulse sensor was developed and tested. A method of assessing the hydration change of the elderly using Impedance Analysis (BIA), a diagnostic tool that relates an individual's hydration level to their body's electrical impedance, has also been investigated for this application. This part of the research has been done by Christina Joy D'Arrigo. Another valuable sign to monitor using PAMM is the user's gait characteristics and its change [Dubowsky, 2000]. Because it is highly dependent upon sound neurological and motor functioning, gait indicate a person's health. With information from the force/torque sensor and the wheel encoders, certain gait parameters of the user such as stride frequency, stride length, and gait asymmetry could be detected from examining force and acceleration power spectra. A system that monitors gait characteristics on a long-term basis might be useful for clinical detection and evaluation of a person's condition. Experimental study of the gait of elderly users was conducted with a special walker test-bed by Shane McNamara.

2.6 Summary of the Chapter

This chapter presents an overview of PAMM research project. PAMM is experimental system for this thesis research. The objective of the project is to develop a concept and the enabling technologies for a robotic aid to provide mobility assistance and heath monitoring for the elderly. PAMM is intended to assist the elderly living independently or in senior assisted living facilities. It provides physical support and guidance, and it monitors the user's basic vital signs.

Chapter

3

Omni-directional Mobility Design

3.1 Introduction

Service mobile robots have to work in environments congested with static and/or dynamic obstacles, such as those commonly found in nuclear plants, offices, factory workshops and warehouses, eldercare facilities, and hospitals. Current wheeled vehicle designs based on skid steering can be a liability in these environments, because their mobility is limited by the non-holonomic constraints of their wheels. While they can generally reach any position and orientation in a plane, skid-steered vehicles commonly require complex maneuvers and complicated path planning algorithms and control strategies to operate in constrained environments [Laumond, 1998]. Systems with omni-directional mobility are highly maneuverable, as they can move in any direction instantaneously from any configuration. Therefore, omni-directional mobility is desirable for above-mentioned the applications.

The main considerations in the design of the mobility drive for a mobile system are maneuverability, controllability, traction and stability, navigation, environment impact, and simplicity. The PAMM SmartCane uses two-wheel skid-steering drive

because of its simplicity in construction. It has two individually controlled driving wheels and up to two passive casters, as shown in Figure 2.6. Each drive motor has an incremental optical encoder for motion control and dead reckoning. This configuration also has relatively good maneuverability in congested environments as it allows an in-place spin. The user can easily maneuver the cane despite its non-holonomic design.

While this is acceptable for the SmartCane as the cane is relatively small, it would not be acceptable for the SmartWalker as the walker has much bigger size. Users of the walker always need to move between chairs and tables, as illustrated in Figure 3.1. It would be frustrating for an elderly person to do several back and forth maneuvering before she could sit down in a chair at the dinner table. Omni-directional mobility should thus be required for the walker. However, the design should also meet the requirements of being simple, lightweight, robust to floor irregularities, and most of all, suitable for the walker configuration. The omni-directional mobility design based on the Active Split Offset Castor (ASOC) developed in this thesis meets these requirements.

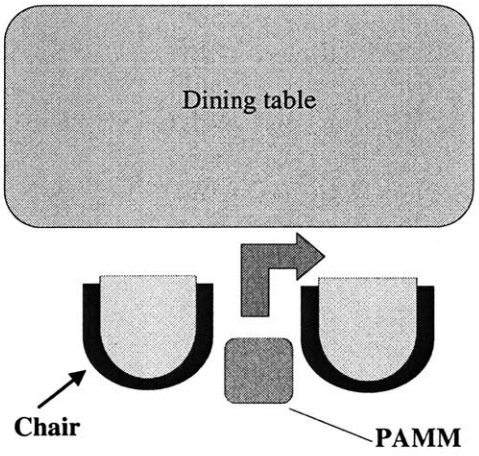

Figure 3.1 - Mobility Needs of PAMM Users

In the following sections, the concept of using the ASOC design to achieve omni-directional mobility is presented. The design and control issues, such as the parameter

selection for the ASOC module, the suspension design, and error sources and compensation are discussed. Finally, the effectiveness of the ASOC design is demonstrated with the experimental results of the SmartWalker.

3.2 Concept and Kinematics of Active Split Offset Castor

An active split offset castor (ASOC) module consists of two independently driven coaxial conventional wheels, which are separated at a distance D and connected via an offset link S to the platform at the joint, as shown in Figure 3.2.

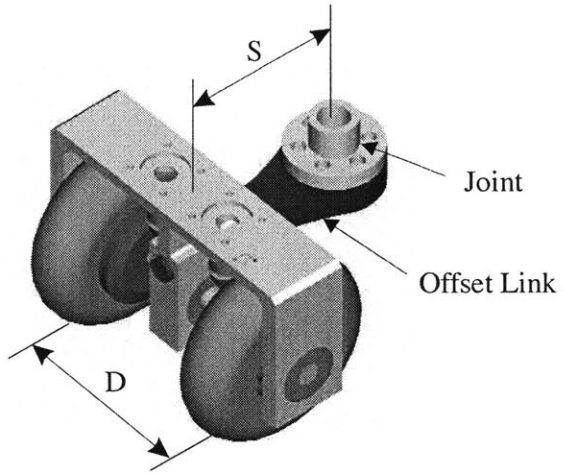

Figure 3.2 - An Active Split Offset Castor Module (Courtesy of Matt Spenko)

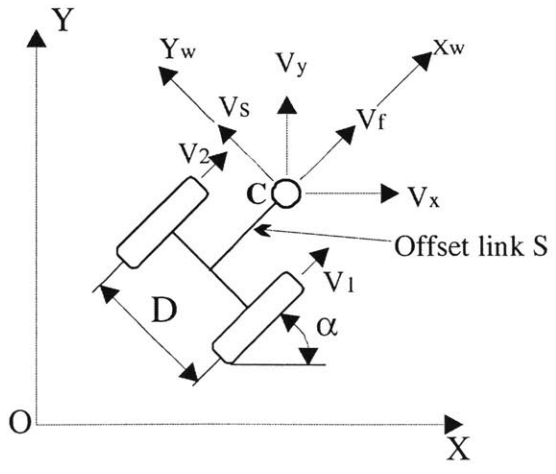

Figure 3.3 - Coordinate System of the ASOC Module (Top View)

In the coordinate systems defined in Figure 3.3, XOY is the inertial coordinate frame and X_wCY_w is the moving coordinate frame attached to the wheel module at the offset link joint. The wheel and joint (point C in Figure 3.3) linear velocities with respect to ground are V_1, V_2, V_f and V_s respectively. The two vectors $\mathbf{u}$ and $\dot{\mathbf{q}}_w$ are defined by:

$$\begin{aligned} \mathbf{u} &= [v_1 \quad v_2]^T \\ \dot{\mathbf{q}}_w &= [v_f \quad v_s]^T \end{aligned} \tag{3.1}$$

The relation between the vectors $\dot{\mathbf{q}}_w$ and $\mathbf{u}$ can be written as:

$$\dot{\mathbf{q}}_w = \mathbf{J}_w \mathbf{u} \tag{3.2}$$

where $\mathbf{J}_w$ is the Jacobian matrix of the ASOC module in the moving coordinate X_wCY_w and is given as :

$$\mathbf{J}_w = \begin{bmatrix} 1/2 & 1/2 \\ S/D & -S/D \end{bmatrix} \tag{3.3}$$

The velocity of point C in the inertial frame is defined as $\dot{\mathbf{q}}$ and is given by:

$$\dot{\mathbf{q}} = [v_x \quad v_y]^T = \mathbf{R}\dot{\mathbf{q}}_w \tag{3.4}$$

where:

$$\mathbf{R} = \begin{bmatrix} \cos\alpha & -\sin\alpha \\ \sin\alpha & \cos\alpha \end{bmatrix} \tag{3.5}$$

and α is the orientation of the ASOC module with respect to the X axis in the inertial frame.

The kinematic relationship between the inertial velocity of the offset link joint C and the two wheel velocities is simply:

$$\dot{\mathbf{q}} = \mathbf{R}\mathbf{J}_w\mathbf{u} = \mathbf{J}\mathbf{u} \tag{3.6}$$

where **J** is the Jacobian matrix for the ASOC module in the inertial coordinate frame XOY, which is given as:

$$\mathbf{J} = \begin{bmatrix} \frac{1}{2}\cos\alpha + \frac{S}{D}\sin\alpha & \frac{1}{2}\cos\alpha - \frac{S}{D}\sin\alpha \\ \frac{1}{2}\sin\alpha + \frac{S}{D}\cos\alpha & \frac{1}{2}\sin\alpha - \frac{S}{D}\cos\alpha \end{bmatrix} \tag{3.7}$$

The determinant of **J** is:

$$\det \mathbf{J} = -\frac{S}{D} \tag{3.8}$$

This means that the ASOC module has no singularity, as long as S is nonzero. For a dual-wheel design without the offset link, where S is zero, the Jacobian matrix is degraded to:

$$\mathbf{J}_n = \begin{bmatrix} \frac{1}{2}\cos\alpha & \frac{1}{2}\cos\alpha \\ \frac{1}{2}\sin\alpha & \frac{1}{2}\sin\alpha \end{bmatrix} \tag{3.9}$$

Obviously, the determinant is always zero and the system has the following non-holonmic constraint:

$$v_y = v_x \tan\alpha \tag{3.10}$$

Which means the velocities in X and Y direction at the center are not independent.

By controlling the velocities of the two wheels of the ASOC module, arbitrary and unique velocities at the joint C of the offset link can be achieved. Figure 3.4 shows the simulation results for an ASOC wheel module producing a velocity of 0.3m/s at X direction at the point C. The figure shows the starting configuration, the trajectory of the wheel module at the point O, and the velocities of the two wheels. The parameters for the simulation are D = 0.12m and S = 0.06m. It can be seen that the wheels follow a

smooth trajectory while point C moves perpendicular to the connecting offset link. At first the two wheels move in opposite directions, then they converge to the same velocity. Although the wheels themselves cannot move perpendicular to their original orientations, the joint of the offset link can move in any direction instantaneously from any configuration. This is the fundamental feature of the ASOC design that enables it to achieve omni-directional mobility.

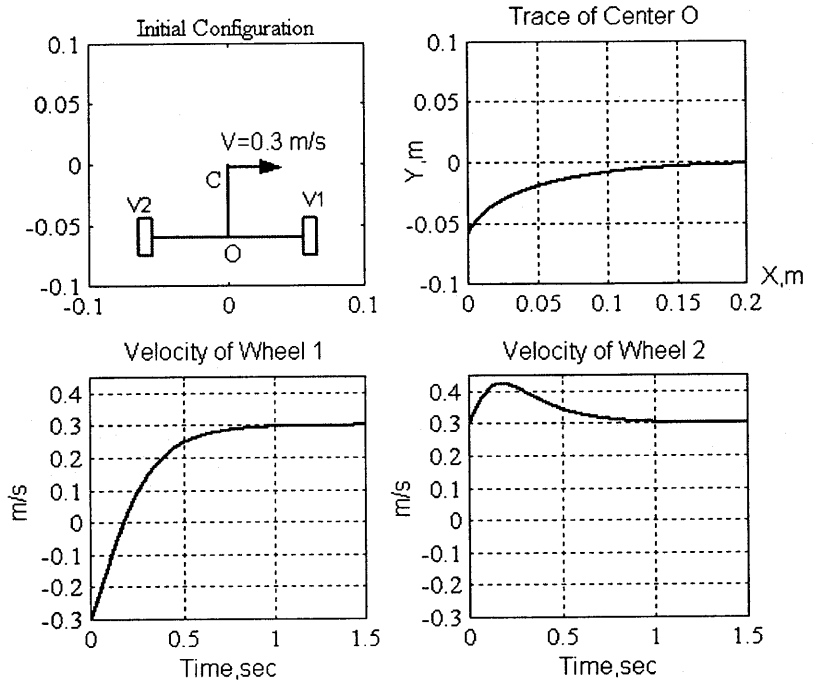

Figure 3.4 - Simulation of an ASOC Module Performing Sideward Motion

3.3 Omni-directional Platform with ASOC Modules

If a platform or a vehicle is considered as a rigid body moving on a plane, its motion in the three degrees of freedom, namely x, y, and ϕ, can be fully defined by the velocities at any two distinct points (see Figure 3.5). If the velocities at these two points can be

controlled arbitrarily, arbitrary motions in three degrees of freedom can be achieved, which also means omni-directional mobility can be achieved.

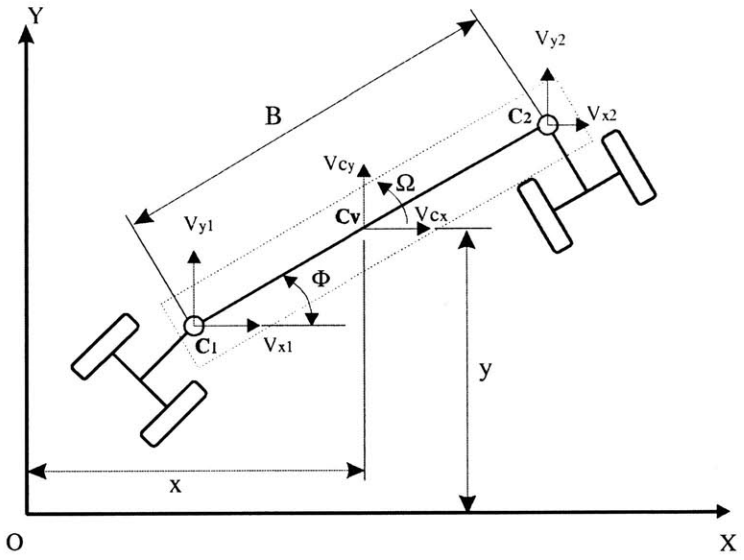

Figure 3.5 - A Platform with two ASOC Modules

As shown in the previous section, the ASOC module can achieve an arbitrary velocity at the joint of the offset link (point C) by independent control of its two wheels. Therefore, with a minimum of two ASOC modules, an omni-directional mobility platform can be constructed as illustrated in Figure 3.5. In the inertial coordinate frame, the velocities V_{cx}, V_{cy}, Ω of the platform at its center C_v and the velocities V_{x1}, V_{y1}, V_{x2}, V_{y2} of the two ASOC modules at their joints C_1, C_2 can be defined as the following vectors:

$$\begin{aligned} \dot{\mathbf{p}}_v &= \begin{bmatrix} V_{cx} & V_{cy} & \Omega \end{bmatrix}^T \\ \dot{\mathbf{q}}_v &= \begin{bmatrix} V_{x1} & V_{y1} & V_{x2} & V_{y2} \end{bmatrix}^T \end{aligned} \tag{3.11}$$

where Ω is $d\phi/dt$. The velocities of the platform can be expressed in terms of the velocities at the offset link joints as:

$$\dot{\mathbf{p}}_v = \mathbf{J}_v \dot{\mathbf{q}}_v \tag{3.12}$$

where:

$$\mathbf{J}_v = \begin{bmatrix} \frac{1}{2} & 0 & \frac{1}{2} & 0 \\ 0 & \frac{1}{2} & 0 & \frac{1}{2} \\ \frac{1}{B}\sin\phi & -\frac{1}{B}\cos\phi & -\frac{1}{B}\sin\phi & \frac{1}{B}\cos\phi \end{bmatrix} \tag{3.13}$$

Given the desired platform velocities, the joint velocities obtained with the inverse kinematics, which is given as:

$$\dot{\mathbf{q}}_v = \mathbf{N}_v \dot{\mathbf{p}}_v \tag{3.14}$$

where $\mathbf{N}_v$ is a 4x3 matrix given as:

$$\mathbf{N}_v = \begin{bmatrix} 1 & 0 & \frac{B}{2}\sin\phi \\ 0 & 1 & -\frac{B}{2}\cos\phi \\ 1 & 0 & -\frac{B}{2}\sin\phi \\ 0 & 1 & \frac{B}{2}\cos\phi \end{bmatrix} \tag{3.15}$$

It should be noted that $\mathbf{N}_v$ is not the inverse matrix of $\mathbf{J}_v$ as $\mathbf{J}_v$ is not invertible. Rather, Nv is derived directly from the kinematic relations. The system has four inputs and three outputs, creating an over-constrained system. This issue is further dealt with in section 3.4.3. Once the joint velocities are determined based on the above relation, the wheel velocities for the two wheels of each ASOC module can be determined based on the kinematic Equation (3.6).

Clearly a vehicle needs at least one additional passive castor wheel for static stability. To achieve better traction, three or four ASOC modules can be used. However, the velocity control must be coordinated since there will be more actuators than the three degrees of freedom of the system.

3.4 Analysis of Design and Control Issues

3.4.1 Selection of Parameters for ASOC Module Design

It can be seen from the ASOC module's kinematics Equation (3.6) that the velocities of the two wheels depend not only on the joint velocity and its orientation α, but also on the ratio between the wheel distance, D, and the offset, S. To illustrate this relationship, a simulation for an ASOC module with different S/D ratios under the same motion as shown in Figure 3.4 is performed. The commanded velocity at the joint is 0.3 m/s at the X direction. Figure 3.6 shows the velocities of the two wheels for different ratios of S/D.

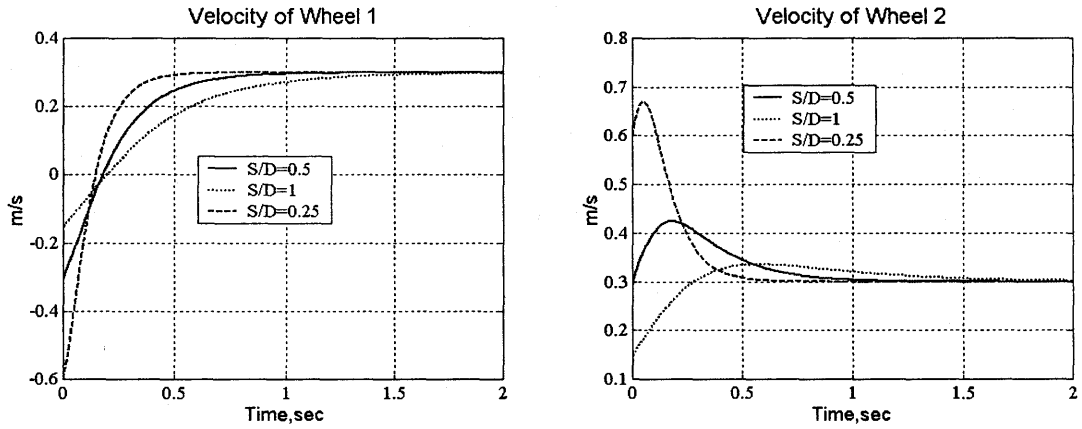

Figure 3.6 - Effects of S/D on Wheel Velocities

It can be seen that the bigger the ratio of S/D, the smaller the velocity change or acceleration is. Excessive velocity changes can present difficulties for the wheel velocity control and can lead to actuator saturation and wheel slippage. Thus a large ratio of S/D is generally advantageous. However, large S/D ratios lead to large physical size of the ASOC module. As S/D increases, the footprint of the vehicle will vary over a greater range as the ASOC module rotates around the joint. For the case of the SmartWalker for the elderly, large S/D ratio could increase the size of the walker and may make it difficult

to maneuver through doorways and between obstacles. Clearly the selection of S/D for a specific application requires careful trade-off design studies. The overall size constraint of the walker, the user's foot positions, the size of the wheels, and the velocity requirement of the walker were carefully studied in deciding the proper S/D ratio.

3.4.2 Mobility Analysis and Suspension Design

The simplest configuration of an omni-directional vehicle using this approach will have two ASOC modules and one conventional passive castor. This vehicle will have five wheels. For the vehicle to maintain control, all four driving wheels must contact the floor at all times. All of the five wheels must maintain contact with the floor to maintain stability. This would require the floor to be perfectly flat. In practice, floor irregularities are unavoidable. This is evident by examining Figure 3.7, where one of the diving wheels loses contact with the floor on uneven floor.

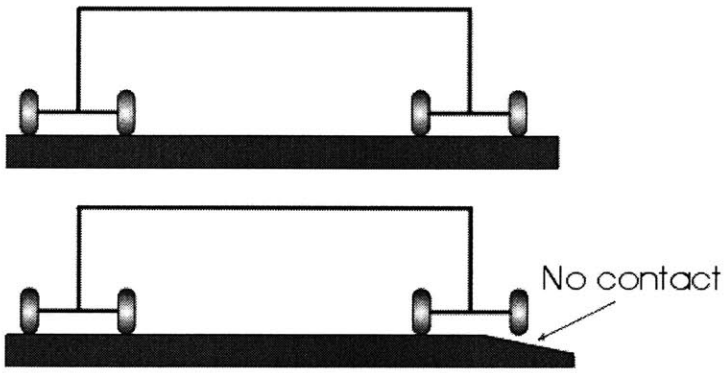

Figure 3.7 - Ground Contact of ASOC Modules on Flat and Uneven Floor

Although some compliance in the wheel and the mechanical structure will alleviate this problem to some degree, it is often not sufficient. To accommodate the floor unevenness, suspensions must be built into the system. Adding independent suspensions can make the system complex, especially when more than two ASOC modules are used. The simple and effective solution proposed in this thesis is to add one

passive joint to each ASOC module at point C in the direction perpendicular to the wheel axis, see Figure 3.8. It allows the shaft to rotate freely about the **u**-axis. As shown in the following analysis, with the added passive joints, the simplest configuration with two ASOC modules and a castor will not need any additional suspension for all the five wheels to be in contact with the uneven floor. This passive joint design is necessary for any vehicle using the ASOC design or normal dual wheel design and helps reduce the number of suspensions needed for the vehicle.

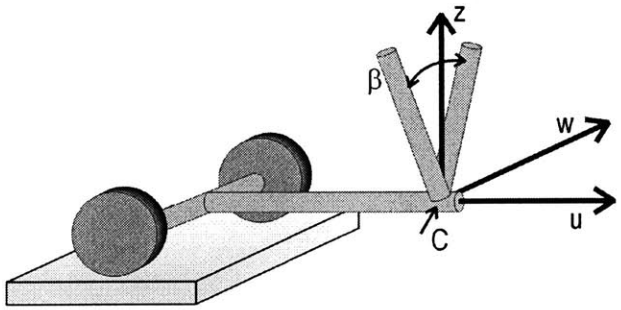

Figure 3.8 - Added Passive Joint to the ASOC

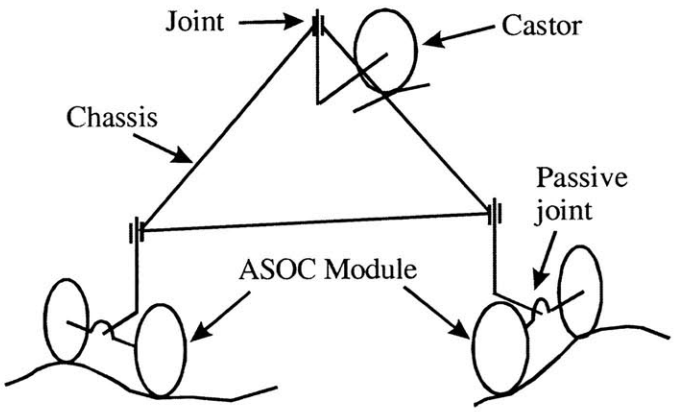

Figure 3.9 - Simplest Configuration of a Vehicle with ASOC design

To demonstrate the effectiveness of the joint, the platform with the simplest configuration (see Figure 3.9) must be proven to maintain wheel contact all the times

with the ground on an uneven terrain during its movement. When the two wheels of one ASOC module and the passive castor are in touch the ground, the two wheels of the other ASOC module must be able to maintain contact with the ground on uneven terrain.

One approach to show that all the four driving wheels can maintain contact with uneven floor is to use workspace analysis. This is done by Matt Spenko and presented here for completeness of the topic [Spenko, 2001]. The study assumes a platform with two active ASOC modules and two addition passive castors for support, which is the mobility configuration for the PAMM SmartWalker, see Figure 2.13. The approach is to first assume that the two wheels of the first ASOC module contact the floor, then to find the configuration space of the wheels for the second ASOC module using geometric equations. As one can see from Figure 3.10, the configuration space for the ASOC design without the added joint lies in a plane (a), while the configuration space for the design with the joint lies within a sphere (b). As long as the terrain exists inside of the configuration space, all the four wheels will maintain contact with the floor. The passive casters will also contact the ground as long as they have a suspension that allows them to elongate linearly downward and the ground lies within the allowable travel of the suspension. Thus, all of the wheels touch the ground at all times. This study further shows that the addition of the passive joint does not significantly affect the dead reckoning accuracy of the platform on non-ideal uneven floors. Therefore, the planning and control algorithms developed for an ideally flat floor perform adequately for a realistic uneven floor.

Experimental results of the SmartWalker proved the effectiveness of the suspension design. The walker can run over bumps, wires, and transitions of carpets

without losing control. The walker also demonstrated good tracking accuracy on rough surfaces.

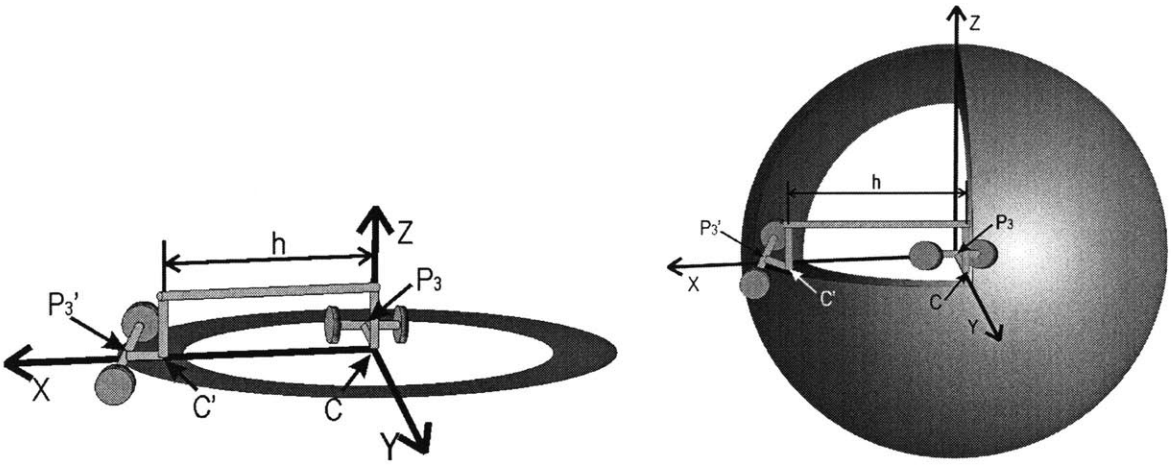

(a) (b)

Figure 3.10 - Configuration Space of Second ASOC

3.4.3 Reducing Wheel Slippage Using Joint Encoder

An omni-directional vehicle has only three degrees of freedom X, Y and ϕ. However, vehicles with the ASOC design need at least two ASOC modules with a total of four actuators, which results in an over-constrained system (see Figure 3.11). This is due to the physical constraint from the constant distance between the two offset link joints C_1 and C_2. This physical constraint leads to the following velocity constraint:

$$V_1 \cos\gamma_1 = V_2 \cos\gamma_2 \tag{3.16}$$

where V_1 and V_2 are the resultant joint velocity, γ_1 and γ_2 are the angles between the line connecting C_1 and C_2, see Figure 3.11.

Violating this constraint will result in wheel slippage and degrade the tracking performance of the system. There are many sources of errors that can contribute to the violation of this constraint. Mechanical inaccuracy, such as errors in wheel diameter, parameters S, D and B, could be eliminated through measurement and calibration. In

general, however, there are many errors that are unavoidable. These include wheel and structure deformation under loads, floor irregularities such as debris, bumps, cracks, slippery area, and wheel velocity control errors due to limited bandwidth and saturation. Effective methods have to be found for the design and control to reduce the slippage and improve the system performance in the presence of these errors.

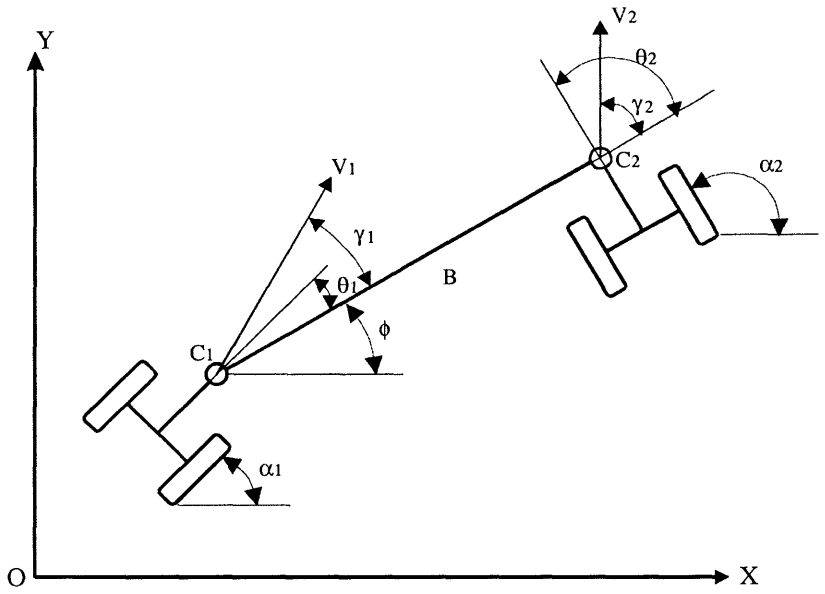

Figure 3.11 - Kinematic Constraint and Effects of Joint Encoders

Recall the kinematics of a platform with two ASOC modules. For the platform to move at velocity (V_{cx}, V_{cy}, Ω), the joint velocities (V_{x1}, V_{y1}, V_{x2}, V_{y2}) are first obtained from the inverse kinematics based on the orientation ϕ. Wheel velocities for each ASOC module are then resolved based on its orientation α. That means accurate knowledge of both α and ϕ is necessary for generating velocity commands that will not violate the constraint.

In theory, the values of α for each module could be obtained via dead reckoning calculation using the wheel encoder signal. Further, the orientation ϕ of the vehicle could be estimated based the dead reckoning results from the two ASOC modules. However,

dead reckoning is not reliable because any error due to wheel slippage will become unbounded.

For closed-loop control, the absolute position and orientation of the vehicle must often be obtained from localization sensors. For example, the SmartWalker has a vision based localization system [Dubowsky et al, 2000]. If the system is under manual control, no absolute information is needed. However, accurate information about the orientation of the ASOC module relative to the vehicle is still important to ensure that the velocity commands do not violate the constraint.

One important feature of the ASOC design is that an encoder is placed on each joint of the offset link. These encoders measure the angles θ_1 and θ_2 between the vehicle chassis and ASOC modules at every sampling time of the control loop. From Figure 3.11, for each ASOC module, the following relation is observed between θ, α and ϕ:

$$\alpha = \theta + \phi \tag{3.17}$$

When ϕ is known, α can be known from the measurement of θ at every sample time and correct velocity commands can be generated to satisfy the constraint given by Equation (3.16).

Therefore, with the joint encoders, errors within each sampling time do not propagate. This greatly improves the accuracy of the system, as shown in the experimental results later in this chapter. In the case of manual control, where it is necessary to know the absolute orientation of the platform, the joint encoders are sufficient to ensure smooth motion of the platform.

3.4.4 Elimination of Slip Rings

To control the motors of the ASOC module, power and signals need to be transmitted between the chassis and the wheels. When an omni-directional platform moves arbitrarily on a plane, the ASOC modules will generally rotate continuously around their joints. This would cause wires to wrap around the shaft, so slip rings have to be used for the transmission in order for the platform to achieve arbitrary motions. For example, the SmartWalker uses a slip ring with ten channels for each of the two ASOC modules.

However, in applications where the platform is commanded to move along preplanned trajectory, the slip rings can be eliminated by proper motion planning based on the characteristics of the ASOC wheels. For an ASOC module as shown in Figure 3.2, the rate of change of its orientation α can be expressed as:

$$\dot{\alpha} = \frac{V_1 - V_2}{D} \tag{3.18}$$

Based on Equation (3.6), this can be expressed in terms of the joint velocities as:

$$\dot{\alpha} = -\frac{v_x}{S}\sin\alpha + \frac{v_y}{S}\cos\alpha \tag{3.19}$$

Assuming the ASOC module is moving at a velocity V along the direction α_0, the joint velocity is given as:

$$\begin{aligned} v_x &= V\cos\alpha_0 \\ v_y &= V\sin\alpha_0 \end{aligned} \tag{2.20}$$

If there is a small disturbance ε to the orientation α_0 such that $\alpha = \alpha_0 + \varepsilon$, the rate of change of ε will be:

$$\dot{\varepsilon} = \dot{\alpha} = -\frac{V\cos\alpha_0}{S}\sin(\alpha_0 + \varepsilon) + \frac{V\sin\alpha_0}{S}\cos(\alpha_0 + \varepsilon) \tag{3.21}$$

When $|\varepsilon| << 1$, under the following approximations:

$$\begin{aligned} \cos(\alpha_0 + \varepsilon) &= \cos\alpha_0 - \varepsilon \sin\alpha_0 \\ \sin(\alpha_0 + \varepsilon) &= \sin\alpha_0 + \varepsilon \cos\alpha_0 \end{aligned} \tag{3.22}$$

the dynamics of ε become:

$$\dot{\varepsilon} = -\frac{V}{S}\varepsilon \tag{3.23}$$

and

$$\varepsilon(t) = e^{-\frac{V}{S}t} \tag{3.24}$$

When V is positive, $\varepsilon(t) \to 0$, which means that the direction along the offset link is stable, see Figure 3.12 (a). The ASOC module can maintain its orientation in the presence of disturbance. However, When V is negative, $\varepsilon(t) \to \infty$, meaning the direction opposite to the offset link is an unstable direction, see Figure 3.12 (b). Any small disturbance will lead to the change of the orientation of the ASOC module until it flips to the stable direction.

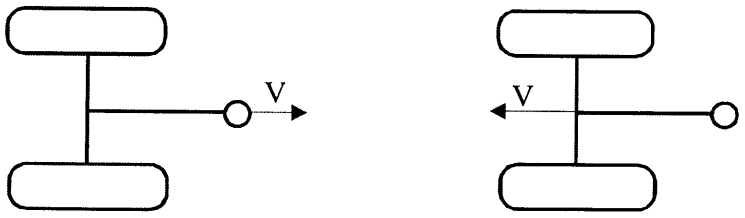

(a).Stable Direction (b).Unstable Direction

Figure 3.12 - Stable and Unstable Direction of the ASOC Module

In the unstable direction, there are two possible directions for the evolution for the ASOC module's orientation, as shown in Figure 3.13. This characteristics can be used to avoid wrap-around of the wheel module.

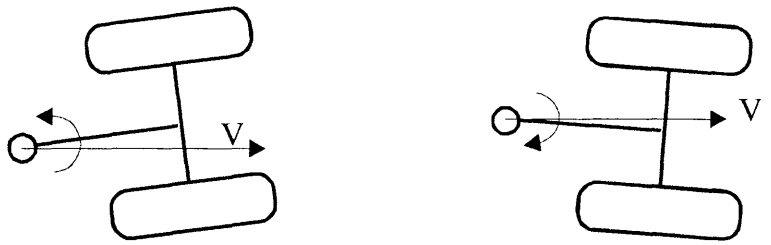

Figure 3.13 - Direction of Orientation Change of the ASOC Module

When it needs to unwrap the wheel module, the ASOC module can be commanded to moves in the unstable direction. By introducing a small disturbance error ε to the orientation α, the direction in which the ASOC module will rotate can be selected. Trajectories could be planned using this property so that the ASOC module never rotates continually in the same direction around its shaft and the slip rings can be eliminated. However, the PAMM SmartWalker needs slips for its ASOC modules as it will perform random motions under its user's command.

3.5 Test-bed Prototype and Experimental Results

To demonstrate the omni-directional mobility design concept and evaluate its performance, a simple experimental test-bed has been built, as shown in Figure 3.14.

The experimental system has two ASOC units and one passive split offset castor unit. Each active unit is driven by a gear-head DC motor with an optical encoder. Each offset link joint has an optical encoder. The control system is implemented using a PC equipped with D/A converters, encoder interface boards, and power amplifiers. The platform can be can be controlled manually using velocity commands or operate in an autonomous mode along preplanned trajectories.

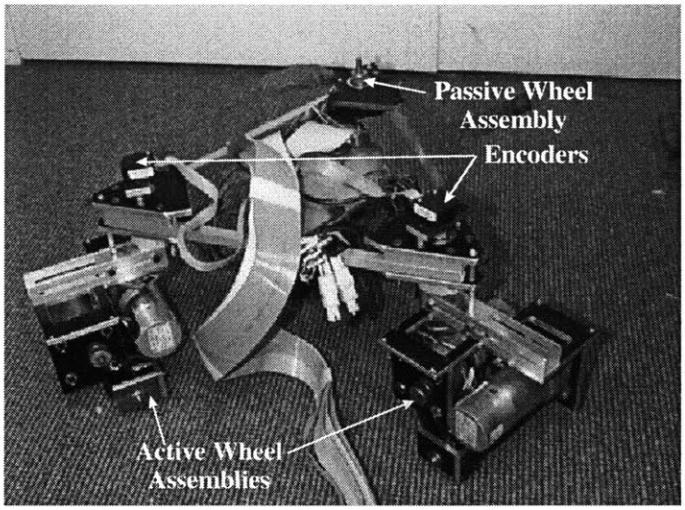

Figure 3.14 - Test-bed Prototype (Built by Lani Rapp and Daniel Santos)

The autonomous trajectory tracking implements closed-loop control using the absolute position and orientation of the platform in the inertial coordinates as feedback. The information is obtained using a vision-based localization system. During the experiments, the localization is done on a second PC, which communicates with the control PC via wireless modem as shown in Figure 3.15. Figure 3.16 shows the block diagram of the control of the experimental system.

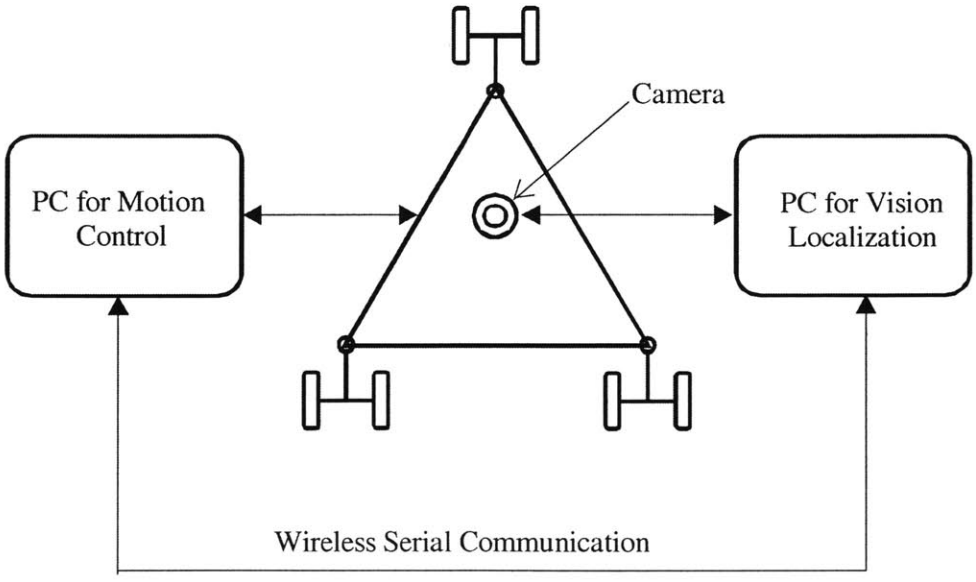

Figure 3.15 - Experimental Set-up for Test-bed Prototype

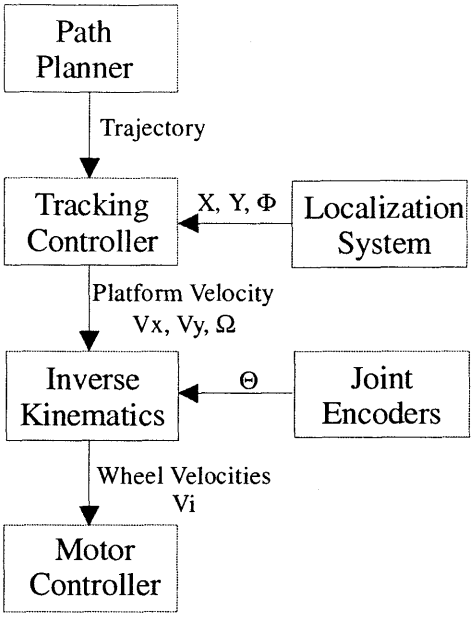

Figure 3.16 - Closed-loop Control Diagram Experimental System

To simplify the design, no slip rings were used. There is no special passive pivot joint built into the ASOC module. The test-bed demonstrated quite smooth motion even for complex trajectories. As expected, there are tracking errors for complex trajectories under open loop control, but the system achieved very good tracking accuracy under closed-loop control. Figure 3.17 shows a tracking result for a square trajectory of 1.2 m by 1.2 m at a constant speed of 0.05m/s. The system does not stop at the corners of the target path. Figure 3.17 (a) shows that the error is about 35 cm at the end of the trajectory for the open loop control. Figure 3.17 (b) shows that with close-loop, the maximum error along the trajectory is reduced to less than 6 cm. These errors are caused mainly by the wheel slippage due to wire tangling and occasional loss of contact between the wheels and the floor.

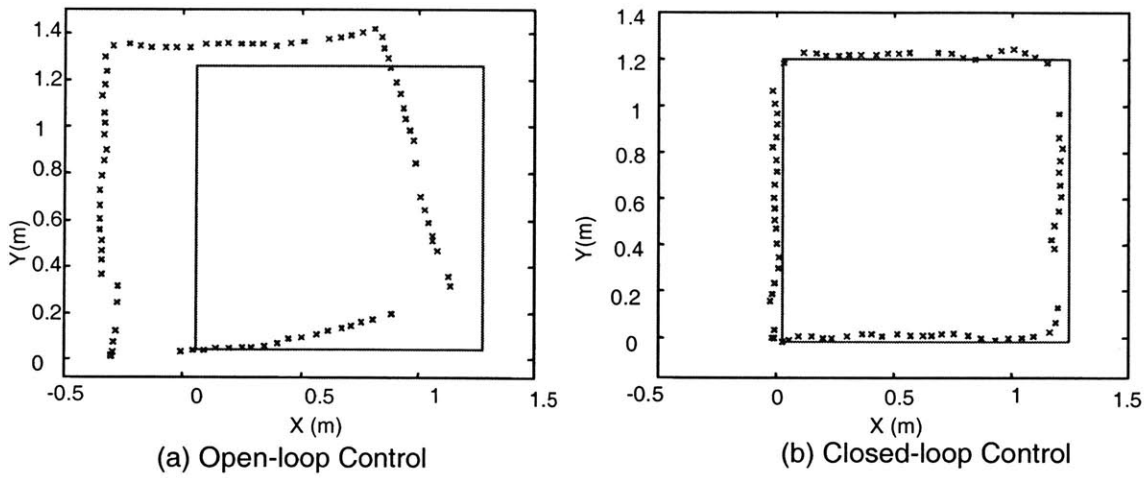

Figure 3.17 - Trajectory Tracking Performance of Test-bed Prototype

3.6 SmartWalker Implementation and Experimental Results

3.6.1 SmartWalker Mobility Design

The ASOC design has been implemented as the mobility drive for the PAMM SmartWalker (see Figure 3.18).

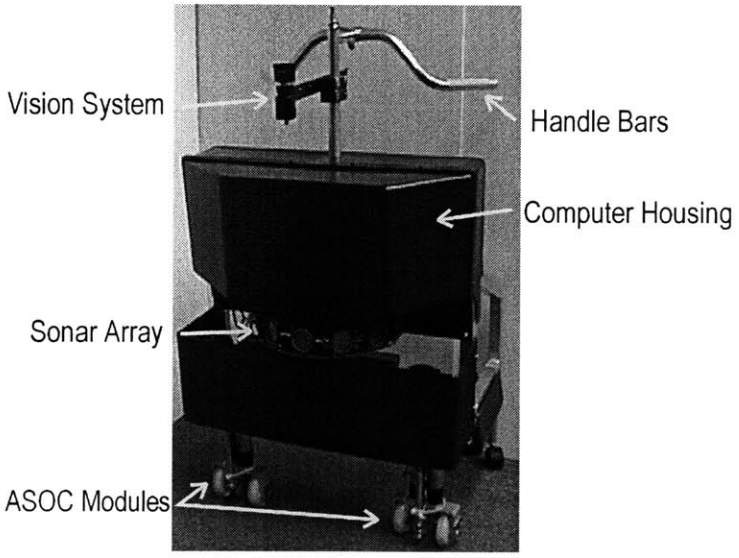

Figure 3.18 - The PAMM SmartWalker Prototype

The SmartWalker mobility system has two ASOC modules and two passive castors for static stability. Figure 3.19 shows the detail of the ASOC module design used for the SmartWalker [Dubowsky, 2000]. Slip rings are used to transmit power to the motor and signals to and from the encoders. To demonstrate the omni-directional mobility and evaluate the effectiveness of the design, a series of experiments were performed. For example, the SmartWalker was commanded to traverse a circular path, and follow a square path without stopping at the sharp corner when changing direction. The walker has also been tested to various floor conditions, such as carpeted floor, concrete floor and tiled floor. The walker has also been commanded to run over bumps at doorframes and to run over network cables in the lab. The SmartWalker demonstrated smooth motions in all these tests.

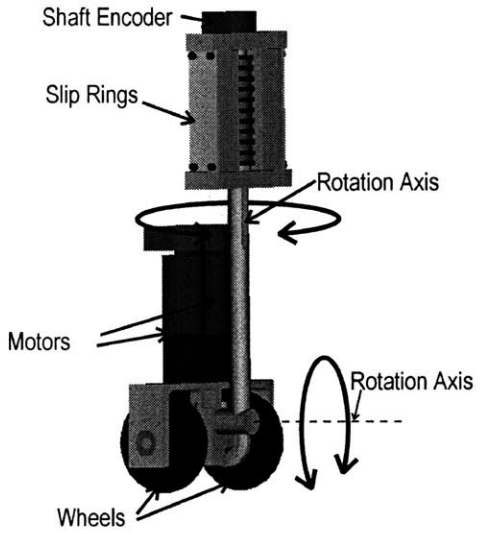

Figure 3.19 - ASOC module for the SmartWalker (Courtesy of Matt Spenko)

3.6.2 Omni-directional Mobility Demonstration

One of the most distinctive features of the mobility system is that it can simultaneously perform translational and rotational motions. Figure 3.20 demonstrates the SmartWalker moving forward in a straight line in the Y direction while rotating

around its center counterclockwise. During the experiments, the actual position and orientation of the system are obtained using the SmartWalker's vision based localization system. The localization system continually determines the position and orientation of the platform in the inertial coordinate frame. The trajectory shown in the figure is the position of the camera, which is mounted at a distance of 0.18m from the center. The omni-directional mobility is clearly demonstrated by the good cycloid trajectory of the camera. The small deviations from the perfect cycloid path are due to the movement of the walker, uneven floor, and errors of the vision localization itself.

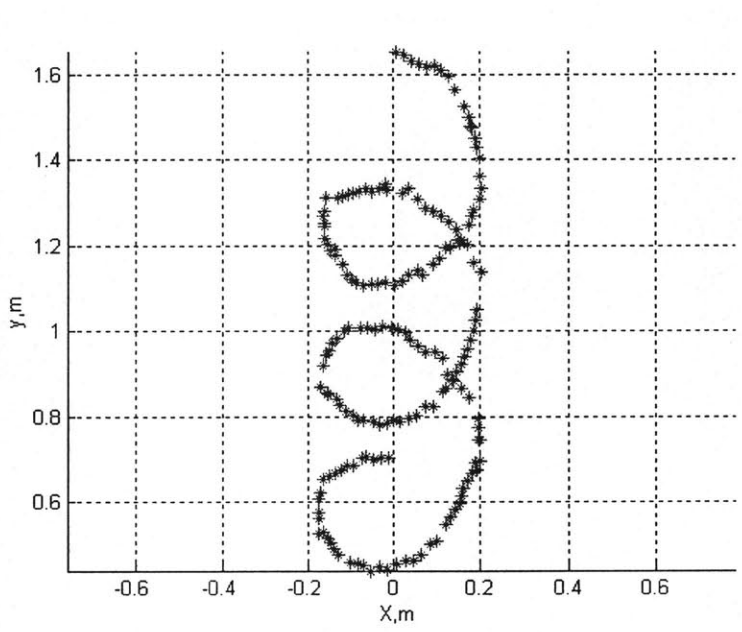

Figure 3.20 - Demonstrates Omni-directional Mobility

3.6.3 Trajectory Tracking Performance Evaluation

To further evaluate the effectiveness of the design, experiments were conducted to asses the trajectory tracking performance of the mobility system. The SmartWalker were commanded to track complex trajectories under both open loop and closed-loop control. Good trajectory tracking performance under the open loop control can reduce the

frequency of the vision localization, which is relatively computation intensive. The experiments were carried out in the corridor in front of the FSRL lab, where the concrete floor is not tiled. The test paths were planed to go through a waffle iron plate to test the performance on uneven floor. The omni-directional mobility system can sideways without the need the stop and change its orientation, so the first path consists of straight light segments with 90-degree sharp turns (Figure 3.21). The omni-directional mobility system can also move like a non-holonomic system, so the second path consists of both line and arc segments (Figure 3.23).

In Figure 3.21, the walker is commanded to follow a trajectory that is about 15 meters long with five sharp turns. It travels at a constant speed of 5 cm/s. The walker does not stop at the sharp turns and does change its orientation. It moves sideways and maintains it orientation. The maximum deviation from the path is less than 30 cm. It can be seen that the error results from the angular error when the walker makes sharp turn.

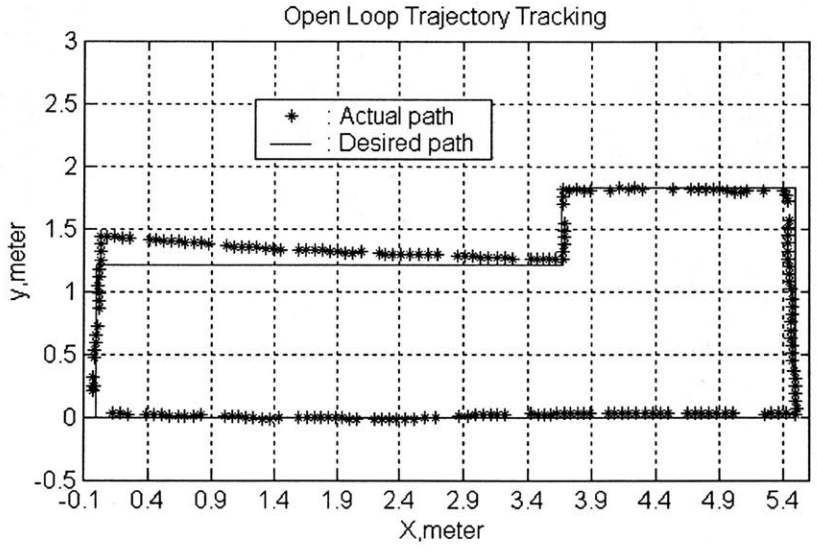

Figure 3.21 - Linear Trajectory Tracking under Open Loop Control

As expected, there will be some errors when maneuvering along complex trajectories under open loop control, but the system achieved much better tracking accuracy under close-loop. Figure 3.22 shows that under closed-loop control, the error along the trajectory is reduced to within 0.1 meter.

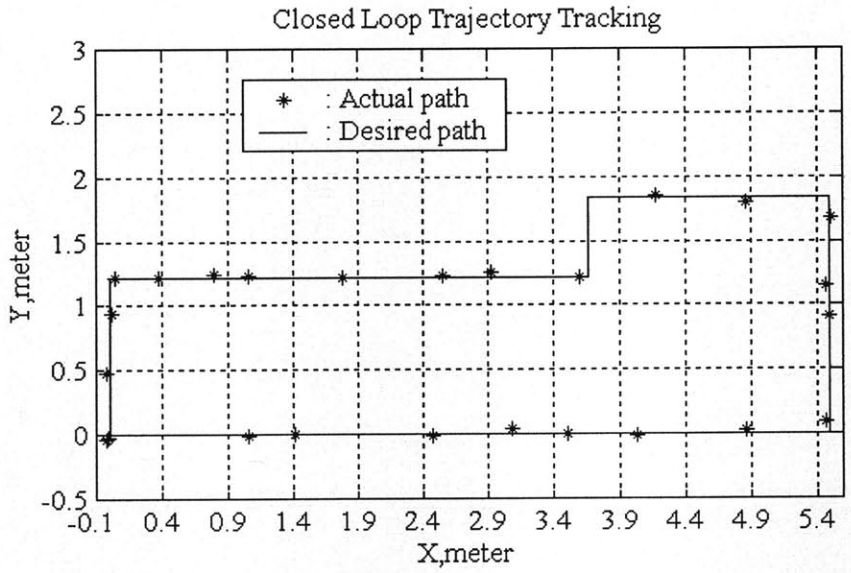

Figure 3.22 - Linear Trajectory Tracking under Closed-Loop Control

Figure 3.23 shows the tracking performance of the walker going along the linear-arc path. The walk also travels at a constant speed at 5 cm/s. During the course of tracking, the orientation of the walker is always tangential to the path. The error is about 0.3 meter. The error is resulted from the two close turns. Again the error is less than 0.1m under the close loop control, as shown in Figure 3.24.

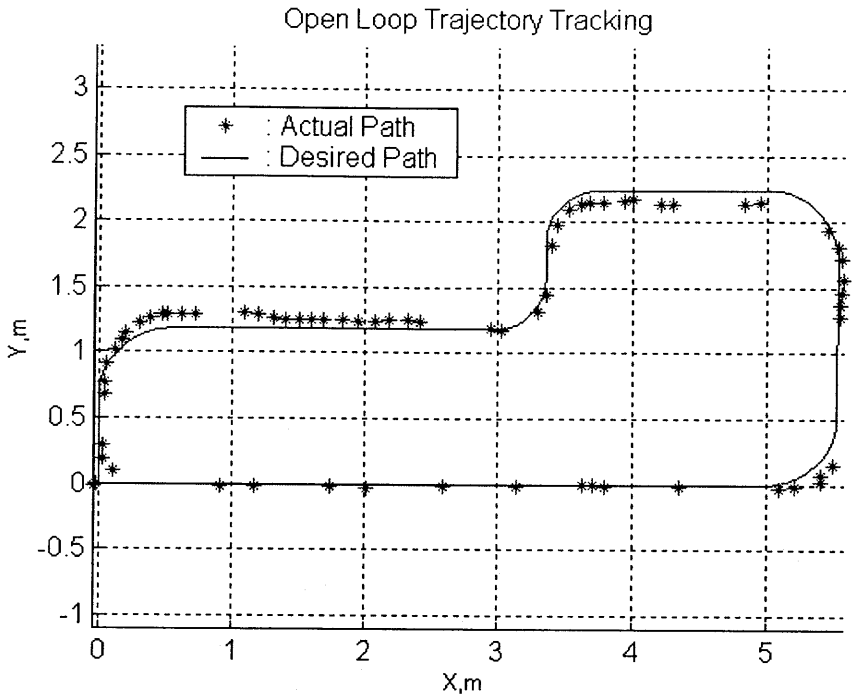

Figure 3.23 - Linear-arc Trajectory Tracking under Open Loop Control

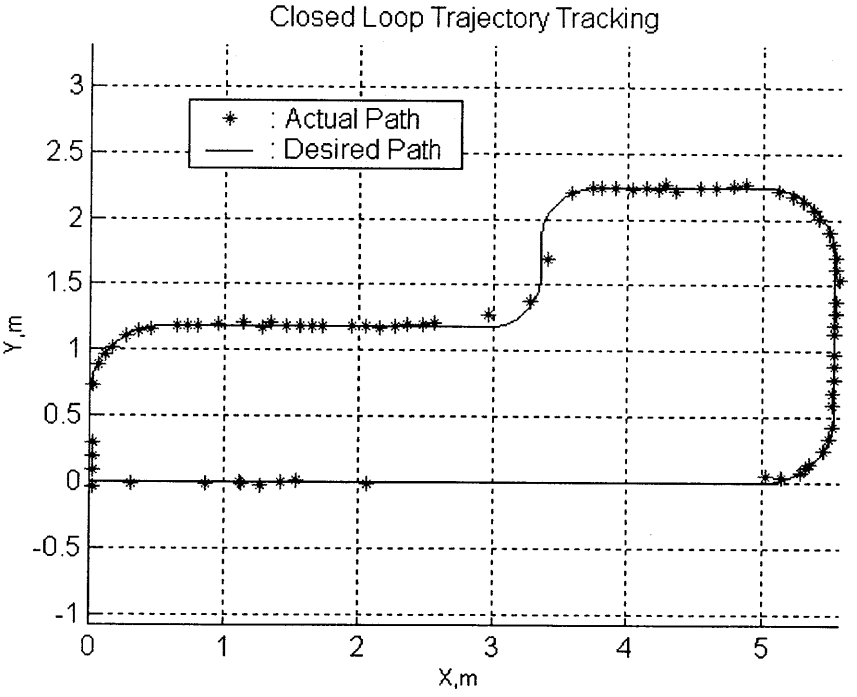

Figure 3.24 - Linear-arc Trajectory Tracking under Closed Loop Control

3.7 Summary and Conclusions

In this chapter, the concept for omni-directional mobility platform design is presented. It is based on the active split offset castor (ASOC) design. Each ASOC module has two coaxial and independently driven wheels and is connected to the platform via an offset link. An omni-directional platform can be constructed with a minimum of two ASOC modules and one passive castor. This design offers advantages over existing omni-directional platforms based on special wheel designs. These advantages include a simple mechanical structure, high loading capacity, vibration free and smooth motion, and robustness to floor conditions. The next chapter will also show that this design has significantly lower wheel scrubbing compared with conventional active castor designs and is thus more energy efficient. This concept has been used as the mobility design for PAMM SmartWalker. The experimental results of the SmartWalker demonstrated omni-directional mobility and excellent tracking performance flowing complex trajectories on uneven floors.

Chapter 4

Wheel Scrubbing Analysis

4.1 Introduction

Vehicles with conventional wheel designs experience high resistance forces during steering (Killough and Pin, 1994). The resistance torque experienced by a wheel when twisted around its vertical axis is called "scrubbing torque". This wheel scrubbing reduces vehicle positioning accuracy and increases power consumption and tire wear, especially for heavy vehicles. It is known that dual-wheel design, which has two wheels on the same axis (see Figure 4.1), has substantially smaller scrubbing torque compared with the single design. The dual-wheel design is commonly found in aircraft landing gears and has also been used to replace steered wheel design for robotic systems [Hashimoto et al, 1999, Betourne and Fournier, 1993]. For the same reason, the ASOC design described in Chapter 3 also has reduced wheel scrubbing. Although this effect has been recognized in the literature, the fundamental mechanics for the reduced wheel scrubbing have not been well studied. A common experience to people driving a car is that the steering is much heavier when the car is still than when it is moving. The fundamental mechanics behind this remains to be investigated.

During the study of the scrubbing of the ASOC design, some important findings have been made. Because the wheel scrubbing is an interesting and important issue for wheeled systems in general, its study is presented here as a separate chapter.

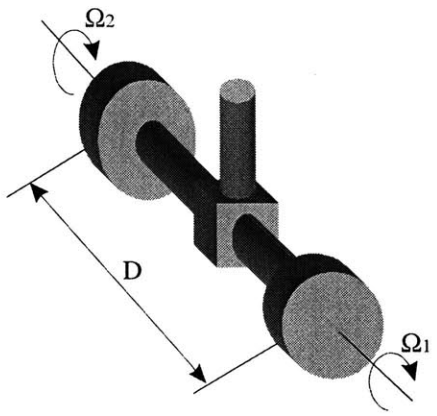

Figure 4.1- Dual Wheel Design without Offset

First, the frictional forces on a conventional wheel in general planar motion are defined and the wheel scrubbing torque is analyzed for a single wheel twisted around its vertical axis on the spot. Then the wheel scrubbing torque for a dual wheel and the fundamental reason for reduced scrubbing are analyzed. The scrubbing analysis is then generalized to wheels in general planar motions. Finally, the scrubbing torque, power and energy consumption for the active castor wheel design and the ASOC design are compared. For simplicity and without losing generality, the analysis in this chapter is based on the assumption of cylindrical solid rubber wheels.

4.2 Frictional Forces on Conventional Wheels

Conventional wheels in general planar motion on hard surfaces experience three major resistance forces, the contact friction f, the rolling resistance moment M_r, and the scrubbing torque M_s, as illustrated in Figure 4.2.

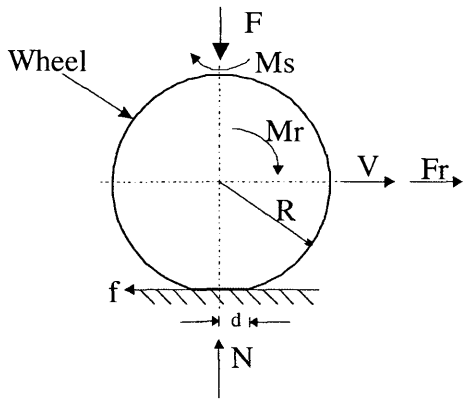

Figure 4.2 - Resistance Forces on Conventional Wheels

The contact frictional force f that prevents the wheel from slipping is related to the normal force N acting on the wheel and the coefficient of friction μ by:

$$f \leq \mu N \tag{4.1}$$

The coefficient of friction depends on the material properties of both the wheel and the floor. For a solid rubber wheel and a concrete floor, μ is about 0.8. This frictional force determines the traction of the wheel on the floor.

The rolling resistance moment M_r is often represented with a force F_r, which is defined as the force needed to roll the wheel forward. The coefficient of rolling resistance μ_r is defined as the ratio of F_r to the normal force N as:

$$\mu_r = F_r / F \tag{4.2}$$

μ_r is in the range of 0.001 to 0.01, depending on the type of wheels and the speed of the wheels [Wong, 1993]. For a wheel of diameter R, the rolling resistance moment M_r can thus be expressed as:

$$M_r = \mu_r NR \tag{4.3}$$

The scrubbing torque M_s is the torque required to twist the wheel around its vertical axis. M_s is the friction force generated as the wheel material slips on the floor during the

twisting. It is proportional to the frictional coefficient μ and the load F applied on the wheel. M_s is generally high because of the high value of μ, especially for heavily loaded vehicles. While M_s can be estimated when a wheel is twisted on the spot, it is not straightforward to analyze when a wheel is undergoing general motion.

4.3 Scrubbing Torque for a Single Steered Wheel

The contact between a solid rubber wheel and a rigid concrete floor can be approximated as a Hertzian contact problem [Hertz, 1895]. The shape of the contact patch and the pressure distribution depend on the load on the wheel, the material properties, and the geometry of the wheel and floor. When the contact pressure distribution is known, M_s can be calculated by integrating the frictional force elements over the entire contact patch between the wheel and the floor.

In general, the equations for contact pressure and deformation for two deformable bodies given in many reference books are complicated and sometimes need graphical interpretation and thus are not suitable for numerical analysis [Slocum, 1993]. However, there exist exact solutions for cylindrical bodies in contact. For a cylinder of length B and diameter d_1 loaded with a force F/B along its length and in contact with a cylinder of diameter d_2, the contact area between the cylinders is a rectangle of width 2b [Slocum, 1993], b is given by:

$$b = \left(\frac{2Fd_1d_2}{\pi BE_e(d_1+d_2)}\right)^{1/2} \tag{4.5}$$

where E_e is the equivalent modulus of elasticity determined based on the elastic modulii and Poisson ratios of the two materials in contact:

$$E_e = \frac{1}{\frac{1-\eta_1^2}{E_1} + \frac{1-\eta_2^2}{E_2}} \tag{4.6}$$

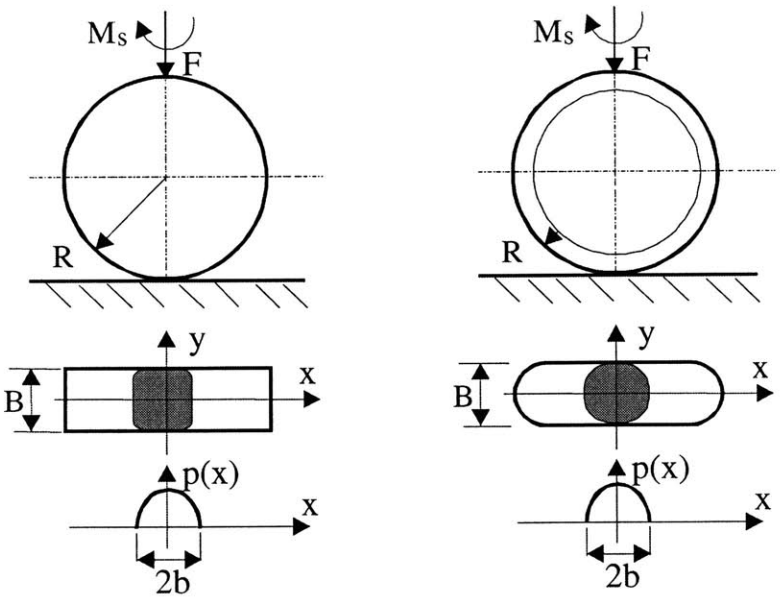

(a) Cylindrical Wheel (b) Wheel with Arc Profile

Figure 4.3 - Wheel Contact Patch and Pressure Distribution

Most wheels can be treated as cylindrical as shown in Figure 4.3 (a). For a cylindrical wheel on a rigid planar floor, d_2 and E_2 are infinity. The Hertzian pressure distribution [Barber, 1992] in this case is

$$p(x) = -\frac{2F\sqrt{b^2 - x^2}}{B\pi b^2} \tag{4.7}$$

There are also wheels with arc profile. When the radius of the arc is close to that of the wheel, the problem can be treated as a spherical body in contact with a rigid planar floor as shown in Figure 4.3 (b), where the contact patch is a circle with radius a

$$a = (\frac{3FR_e}{2E_e})^{1/3} \tag{4.8}$$

where R_e is the equivalent radius based on the gap bending hypothesis [Slocum, 1993] and is given by:

$$R_e = \frac{1}{\frac{1}{R_{1major}} + \frac{1}{R_{1minor}} + \frac{1}{R_{2major}} + \frac{1}{R_{1minor}}} \tag{4.9}$$

where R_{2major} and R_{2minor} are infinity for the floor.

The scrubbing torque M_s can be obtained by integrating the torque elements over the contact area. For the cylindrical wheel, the scrubbing torque is

$$M_s = 4\mu \int_0^{B/2} \int_0^b \sqrt{x^2 + y^2}\, p(x) dx dy \tag{4.10}$$

For the wheel with spherical profile, the integration is

$$M_s = \mu \int_0^a 2\pi x^2 p(x) dx dy \tag{4.11}$$

These equations can be easily solved with numerical methods.

Taking the wheels of SmartWalker for the elderly as an example, the radius of the wheel R is 40 mm, the width of the wheel b is 10 mm. Assuming μ is 0.8, the wheel material has a modulus of elasticity E of 8 Mpa, a Poisson ration η of 0.47, and a vertical load F of 100 N. The scrubbing torque for a cylindrical wheel is 0.34 Nm and that for a spherical wheel is 0.31Nm. Assuming μ_r is 0.005, for the same normal force F of 100N, the rolling resistance based on Equation (4.3) is 0.019Nm. The scrubbing torque is about 15 times bigger than the rolling resistance.

4.4 Scrubbing Analysis for the Dual wheel Design

While it is easy to understand and estimate the scrubbing torque for a single wheel twisted around its vertical axis, it is not so obvious for the dual wheel case. Now

consider a wheel set consisting of two wheels separated at a distance D as shown in Figure 4.4, where the wheels are the same as that considered in the single wheel case.

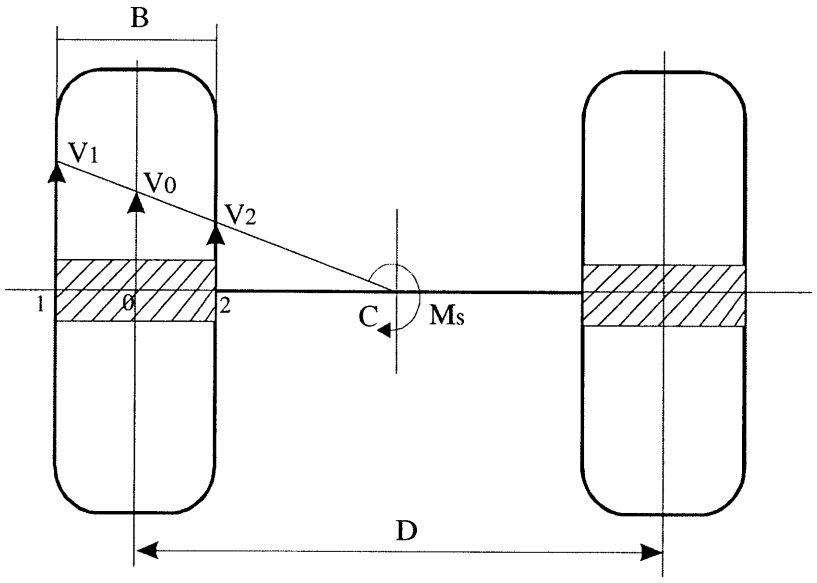

Figure 4.4 - Dual Wheel Set Scrubbing Analysis

Under the same total load F, each of the two wheels has a contact area similar in shape but smaller in size to the single wheel case. When the wheel pair is twisted around its center C for a full turn, the contact patches of the two wheels also undergo a full rotation. The question arises is that does wheel scrubbing occur for these two wheels? If it does, how does the total scrubbing torque compare with that of a single wheel? To answer these questions, one needs to look more closely at the scrubbing of a single wheel, examine the case of the dual wheel pair in detail, and find the fundamental difference between the two cases.

For a single wheel twisted about its vertical axis under the twisting moment T, there is no initial relative motion between the wheel material and the floor. This is due to the deformation of the wheel material in the tangential direction. As T increases, this deformation reaches a limit and slippage occurs. That is when the scrubbing happens and

T becomes the scrubbing torque. The relation between the twisting moment and the angle can be represented in a curve, as shown in Figure 4.5. The slope of the curve reflects the twisting stiffness of the wheel. This curve can be obtained with experimental methods [Moore, 1975]. One must also remember that during the twisting of a single wheel, it is always the same part of the wheel material in the contact area that is rubbing against the floor. Each element of material in the contact area undergoes tangential deformation and experiences slippage.

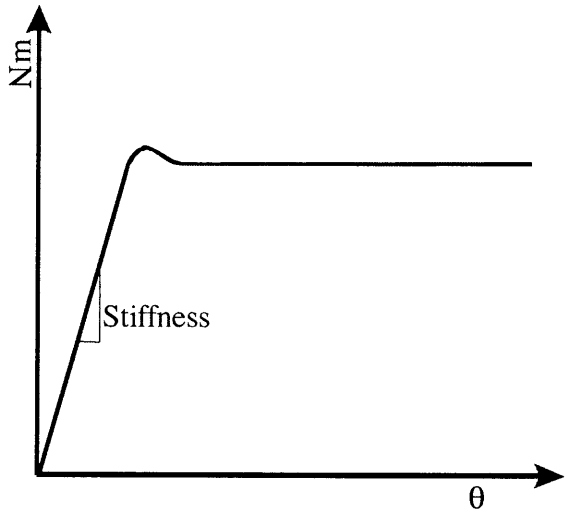

Figure 4.5- Wheel Twisting Stiffness

For the dual wheel case, when the wheel set is twisted around its center at an angular velocity ω_s, both of its wheels are rolling at a speed

$$V_0 = R\omega_s \tag{4.12}$$

where R is D/2. That means at any instantaneous moment, different elements of the wheel material are in contact with the floor as the wheel rolls. The wheel material elements are impinging on the floor at the speed V_0. However, the actual velocities at various points in the contact area are different. For example, the velocities at the three points (0, 1, 2) in Figure 4.4 along the wheel axis are

$$V_0 = R\omega_s$$
$$V_1 = (R + \frac{B}{2})\omega_s \tag{4.13}$$
$$V_2 = (R - \frac{B}{2})\omega_s$$

Therefore, at every point in the contact area, except at point O, there exists a difference between the velocity at which the material tends to move and the actual speed at which it moves. For point 1 and 2, the velocity differences are

$$\Delta V_1 = \frac{B}{2}\omega_s$$
$$\Delta V_2 = -\frac{B}{2}\omega_s \tag{4.14}$$

That means on the outer edge of the wheel, the wheel material is being stretched and on the inner edge of the wheel, the material is being compressed.

At those points with velocity difference, deformation happens as the material elements make contact with the floor. The tangential deformation of an element $p_i(x,y)$ within the contact patch (see Figure 4.6) can be expressed as the ratio of the velocity difference over the wheel's rolling velocity V_0, which is given by:

$$\varepsilon_i = \frac{\|\Delta \mathbf{V}_i\|}{\|\mathbf{V}_0\|} = \frac{\|\bar{\mathbf{d}}_i - \bar{\mathbf{R}}\|}{R} \tag{4.15}$$

where d_i is the distance from the center of rotation, C. If ε_i at the element reaches a limit ε_0, which depends on the material property and can be determined experimentally, that element will contribute to the scrubbing torque. The contribution of that element is given as:

$$\delta M_s = \mu p(x,y)(x\sin\beta - y\cos\beta)\delta x\delta y \tag{4.16}$$

By integrating the contributing elements over the contact patch, the total scrubbing torque is obtained.

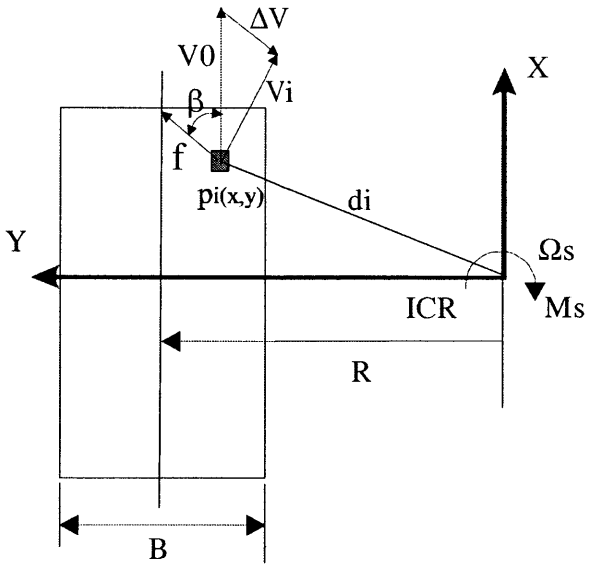

Figure 4.6 - Scrubbing Torque of an Element in the Contact Patch

In the single wheel case, ε_i at every point in the contact patch will eventually reaches a limit ε_0, and slippage will occur, so every material element contributes the scrubbing torque. In the dual wheel case, however, at those points where ε_i is small, no slippage will occur before the elements move out of contact. Those material elements have no contribution to the scrubbing torque. Therefore, the total scrubbing torque can be smaller than when a single wheel is twisted on a spot. However, wheel scrubbing does exit in the dual wheel design.

It is obvious that the limit ε_0 is a function of the wheel material. From Equation (4.15), it also can be seen that ε_i does not depends on ω_s, it depends on D only. Therefore, the total scrubbing torque depends on both wheel material and the wheel separation.

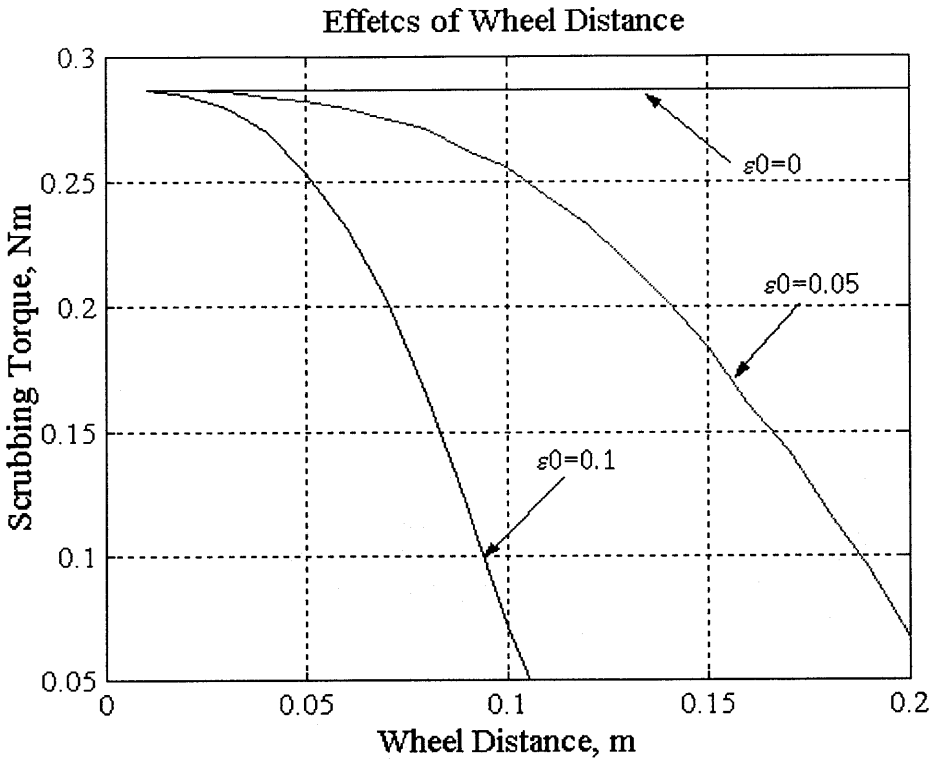

Figure 4.7 - Scrubbing Torque versus Wheel Separation

Figure 4.7 shows the simulation result of the total scrubbing torque of a dual wheel set as a function of the wheel separation distance. The wheels in the calculation are the same as those used in the single wheel analysis. It shows that for elastic material, the wheel scrubbing decreases as D increases. Moreover, as ε_0 increases, or as the elasticity of the wheel material increase, the wheel distance will have a bigger effect. In contrast, for rigid material where ε_0 is zero, the scrubbing torque will be the same as for the single wheel twisted on the spot and does not depend on the wheel distance.

4.5 Scrubbing Analysis of Wheels in General Motion

The discussion on the scrubbing of the dual wheel set shows that the scrubbing torque depends on the wheel separation distance. A wheel in general planar motion has two

velocities, rolling velocity V and turning velocity ω. Under the assumption of rolling without slipping in the tangential direction, the motion of the wheel can always be treated as if it is being twisted around a point along the line perpendicular to its rolling velocity (Figure 4.8). This point is called the instantaneous center of rotation (ICR). The distance from the ICR to its vertical axis R is given by

$$R = V / \omega \tag{4.17}$$

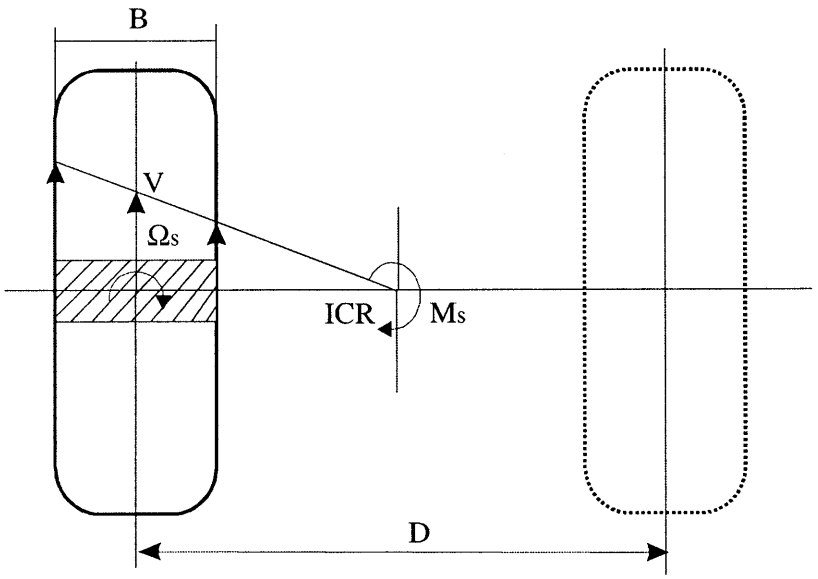

Figure 4.8 - A Wheel in General Motions

Therefore, at any instantaneous time, a single wheel in general motion can be treated as one of the two wheels in a dual wheel set with a wheel distance of D and the scrubbing torque can be calculated. When the wheel is twisted without moving forward, the scrubbing torque is higher than when the wheel is moving at the same time. That explains why it is lighter to steer the car when it is moving.

With this extension, the scrubbing torque, power and energy consumption can be calculated for any vehicle with conventional wheels. Energy consumption is one of the

key issues for self-contained systems, such as a robotic walker for the elderly or automatic transport vehicles in factories.

4.6 Comparison between ASOC and Active Castor

For an example, we can compute the power consumption due to wheel scrubbing for a vehicle built with the ASOC design and compare it with that of a vehicle with the active castor wheel design. For simplicity, we can just consider one mobility module as shown in Figure 4.9. In each case, the mobility module is commanded to drive the chassis in a straight line to the sideward direction. It is assumed in the simulation that all the wheels are the same and the total vertical load is the same for the two cases. The results of the simulation are shown in Figure 4.10 and Figure 4.11. The velocities of the two wheels, the individual and the total torque, the total power and energy consumed due to wheel scrubbing are calculated. The simulation results shows that the active castor has a higher wheel scrubbing torque and a higher total power consumption than the ASOC.

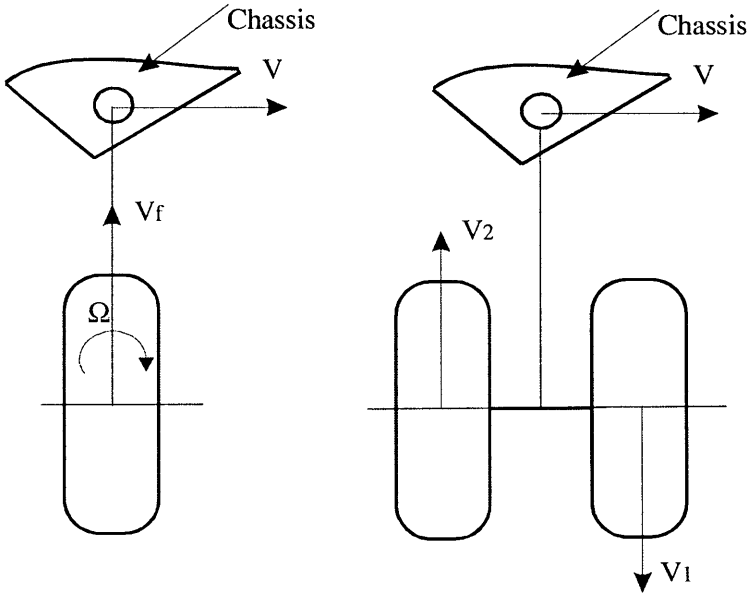

Figure 4.9 - Comparison between Active Caster and ASOC

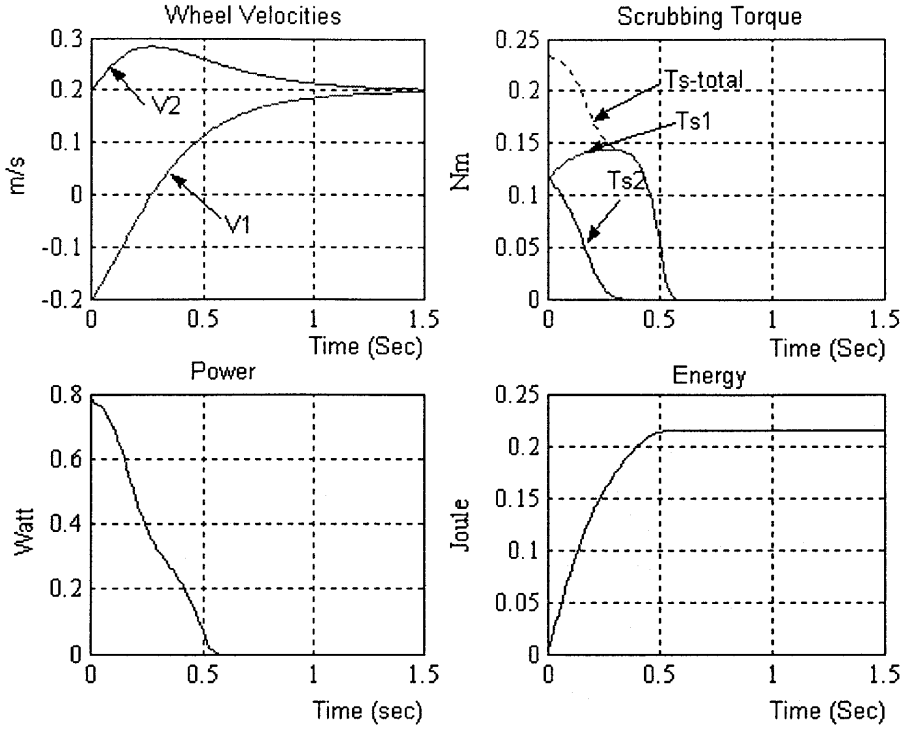

Figure 4.10 - Scrubbing Analysis of the ASOC

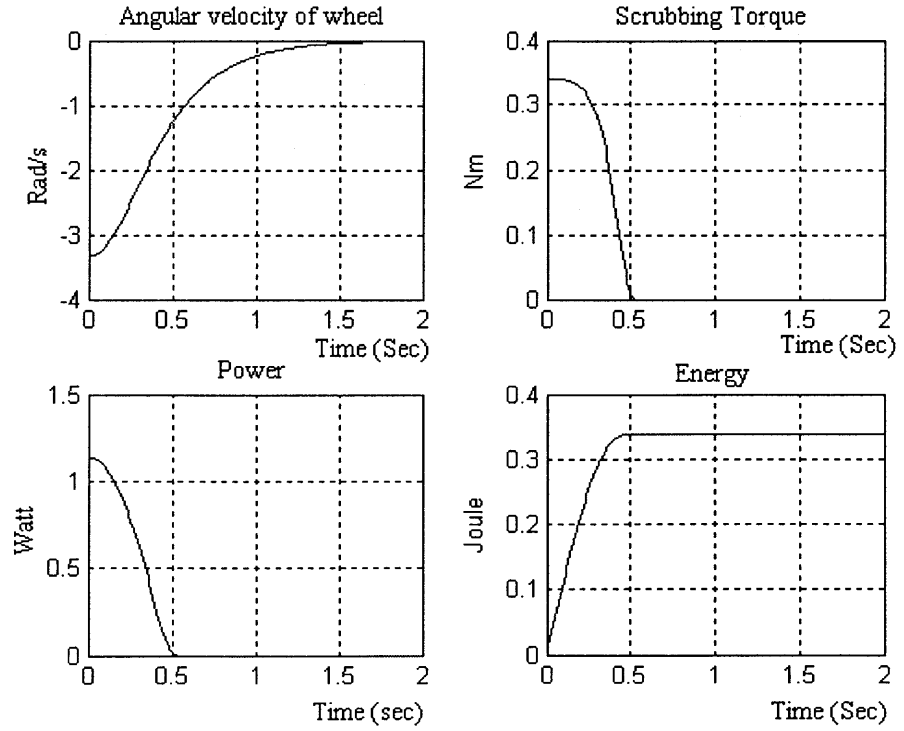

Figure 4.11 - Scrubbing Analysis for the Active Castor

4.7 Summary and Conclusions

Wheel scrubbing is an important issue for vehicles with conventional wheel design. Wheel scrubbing can lead to low tracking accuracy, require large actuators, and cause high power consumption, especially for heavily loaded systems. This chapter presents an analytical study of the problem, identifies the fundamental causes, and contributing factors to wheel scrubbing for both single wheel design and double wheel design. The analysis is then generalized to wheels in general planar motions, which provides a means to estimate the wheel scrubbing torque and actuator size for all wheeled systems.

Chapter

5

Admittance-Based Human-Machine Interaction Control Design

5.1 Introduction

The second objective of this thesis research is to develop control methodologies for assistive devices to work interactively and cooperatively with human operators. The control of PAMM has two levels. The lower level is the user interaction control based on the admittance-based control methodology. The higher level is the adaptive shared controller for the control allocation between the user and the machine, which is addressed in Chapter 6. This chapter presents an admittance based control methodology for the human-machine interaction control for PAMM. The use of force/torque senor as human-machine interface and the concept of admittance-based control are presented first, followed by the admittance model design and evaluation. Experimental results from field trials with elderly users are presented.

5.2 Force/torque Sensor as the Human Machine Interface

User interface design is critical for the performance of human-machine systems. A well-designed user interface can reduce errors and needs for training and improve user

acceptance. The design must address both the user characteristics and the nature of the user-machine interaction. The users of mobility aids such as PAMM have direct and physical interaction with the system. Moreover, they are typically elderly people with physical and/or cognitive deficiencies. The human-machine interface should provide reliable bilateral communication between the user and the machine to ensure safety, while reducing mental and physical workload. It should also improve the comfort and quality of use and facilitate learning how to use the device. The joystick, which is commonly used in electric wheelchairs, is not suitable for this application as the relative motion between the user and the machine can cause oscillation [Lacey and McNamara, 2000]. Switches and buttons can cause confusions and errors. Voice communication can provide only simple discrete commands and not all users like other people to think that they are talking to themselves. Visual tough screen offers unilateral information from the user to the machine and can only be used as high-level command.

Due to fact that the user has to have direct physical interaction with the system in order to get physical support, the user interface for PAMM should not just be a device to send command but also be a means for physical interaction control. A six-axis force/torque sensor is used as the main user machine interface for PAMM. Through the force/torque sensor, the user has continuous control of the system and gets physical support in the same time. The signals form the force/torque sensor contains not only user's intention but also the support and stability information of the user.

More importantly, the use of force/torque sensor allows for the admittance control based technique to be used for the interaction control, which is the presented in the following sections.

5.3 Concept of Admittance-based Control

The admittance of the modeled dynamic system is defined as a transfer function with the user's forces and torques, **F(s)**, as input and the PAMM's velocities, **V(s)**, as the output [Stelman, 1988]. It is expressed as:

$$\mathbf{G(s)} = \frac{\mathbf{V(s)}}{\mathbf{F(s)}} \tag{5.1}$$

The reciprocal transfer function is called impedance, which is the basis for the widely used concept of impedance control. The response of the PAMM is obtained by solving the dynamic equations in real time, and solving the inverse kinematics of the physical system to get the desired actuator velocity. The admittance control approach allows the PAMM dynamics to be set like a linear or nonlinear system, subject to limitations of actuator power, servo control bandwidth, and computation limitations. Models with fast dynamics require higher bandwidth and fast sampling time for the control system. Complex models obviously require more computation power. However, these do not appear to be significant issues for devices for slow moving elderly people.

The admittance-based interaction control for PAMM is shown in Figure 5.1. Users of PAMM interact with PAMM through the force/torque sensor. Signals from the force/torque sensor contain not only the user's intention but also the support, stability, and gait information of the user. The signals from the force sensor first go through a transformation so that the driving forces and the support force at the handle are extracted. The support force, which points downward, is not used to generate motion directly, but is used for stability analysis and as a condition to start or stop the motion. It was found in field experiments that a few users generated unintended forces, which are coupled with

the driving forces. For example, some users of the SmartCane initially generated an unintentional twisting torque at the handle. However, with some practice they developed good control of the cane. Driving forces are also filtered before the admittance model to eliminate high frequency noise. The admittance model can be changed for each individual user. The states of the system, such as velocities, are monitored and used to change the dynamic model so that the control is variable.

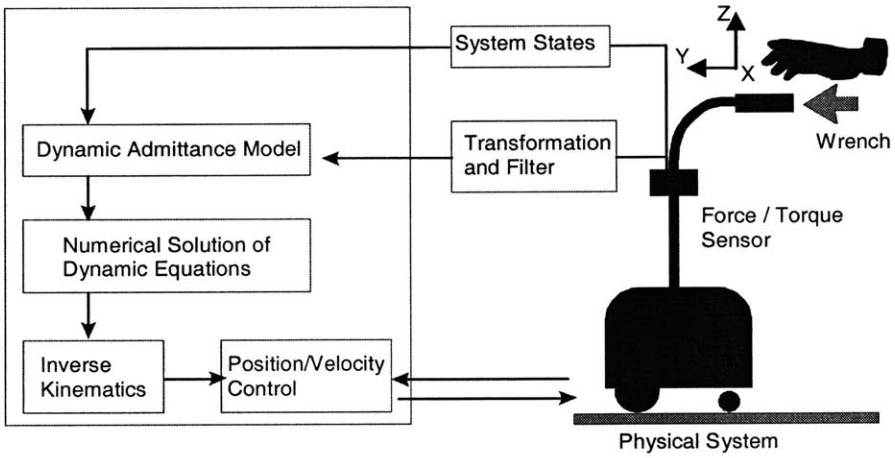

Figure 5.1 – PAMM Admittance-Based User Interaction Control

5.4 PAMM Admittance Model Design

While conceptually easy, the design of admittance-based interaction control presents many challenges, which include determining the appropriate model, choosing a measure to evaluate the performance of the model, and optimizing the dynamics to minimize operator effort. The PAMM SmartCane has two degrees of freedom, one for forward motion in the Y direction, and the other for rotation around the Z direction. The PAMM SmartWalker is omni-directional and has 3 degrees of freedom. Hence admittance models with two and three DOF mass-damper systems have been implemented on the

SmartCane and SmartWalker respectively. A linear 2 DOF mass-damper model for the SmartCane is defined as:

$$\begin{bmatrix} M_y & 0 \\ 0 & I_z \end{bmatrix} \begin{bmatrix} \dot{v}_y \\ \dot{\omega}_z \end{bmatrix} + \begin{bmatrix} B_y & 0 \\ 0 & B_z \end{bmatrix} = \begin{bmatrix} F_y \\ T_z \end{bmatrix} \tag{5.2}$$

where M_y, v_y, B_y, and F_y are the mass, velocity, damping, and the force in the forward direction Y, and I_z, ω_z, B_z, and T_z are the moment of inertia, damping, and torque in the rotational direction around Z.

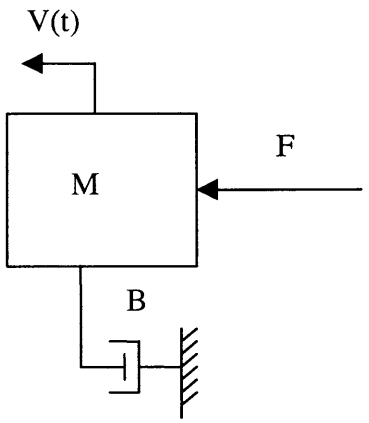

Figure 5.2- A mass-damper model

In the forward direction, the system emulates a plant of a mass M and damping B, as illustrated by Figure 5.2. With F as the user input force in the forward direction and V as the system response in the same direction, the transfer function of the system is:

$$G(s) = \frac{V(s)}{F(s)} = \frac{1}{Ms + B} \tag{5.3}$$

The time response of the system for a step input is:

$$v(t) = \frac{F}{B}(1 - e^{-t/\tau}) \tag{5.4}$$

where τ is the time constant defined by τ is *M/B*. The steady state velocity of the system is V_{ss} is *F/B*.

Figure 5.3 shows the step response of a model with a mass of 14 Kg and damping of 40 Ns/m with an input of 15 N. It shows that the mass-damper model allows the system to start gently. In the same way, it will allow the system to stop gently.

The exact values of model parameters depend on the human input frequency and the servo control bandwidth. The input of elderly people is from 0.5 to 1 Hz based on their walking pace. Therefore, the corner frequency of the model should be more than 2 Hz or the time constant of the model should be less than 0.5s second so that the model can respond to the user input. The physical system bandwidth should again be at least 4 Hz so that the system can respond to the output of the admittance model. When implementing the model in real time, the sampling time should be at least 10 times that of the admittance model.

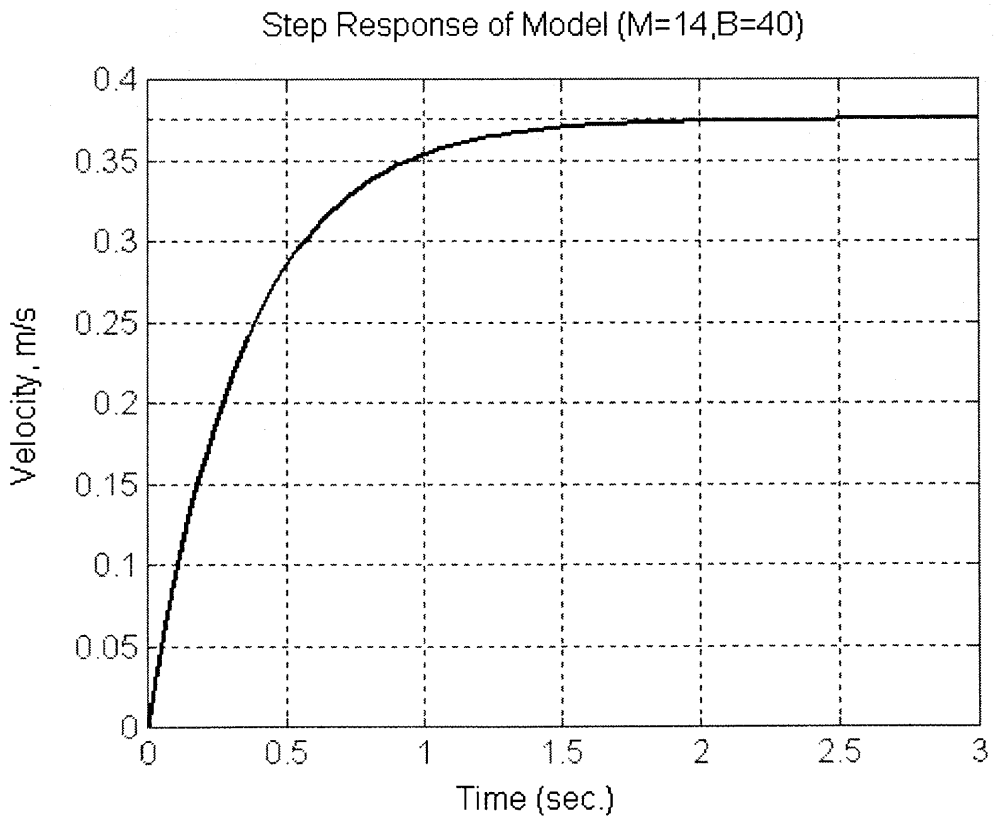

Figure 5.3 – Step Response of a Mass-damper Model

5.5 Experimental Study

The challenge in the design of admittance controller was found in determining the appropriate model (M and B), choosing a metric to evaluate the performance of the model, and optimizing the dynamics to minimize operator effort. This question can only be answered with experiments with the actual users through field trials. In the process of PAMM development, extensive experiments have been conducted for both the SmartCane and SmartWalker with elderly residents at an assisted living facility in Cambridge, Massachusetts. Appendix A shows the floor plan of the first floor of eldercare facility, where most of the field experiments were conducted. The result of the initial field experiments with the PAMM SmartCane has been presented in [Godding, 1999].

5.5.1 General Evaluation Tests

First, a series of tests were conducted to evaluate the general usability of PAMM with the admittance control. Figure 5.4 shows typical response of the PAMM SmartWalker driven by an elderly user. The admittance model has M and B as 14 Kg and 40 Ns/m respectively. The model has a time constant of 0.35 seconds. These values were determined based on the time constant consideration discussed above and the user feedback in the field trials. It shows that the user walks at an average speed of about 0.25 m/s. The average driving force (F_y in the forward direction) is about 12 N. Because the mass-damper model also acts as a low pass filter, high frequency noise due to shock and vibration from the floor and the tremor of the user are removed. The driving force signal has some high frequency noise, but PAMM's speed is quite smooth with a lower frequency variation that corresponds to the user's gait. Figure 5.4 also shows that the

forward driving force and the downward support force are in concert, meaning the user gets good support walking with the SmartWalker. The support force for the user is in the range of 40N to 70N. This is very close the forces measured on a conventional wheeled-walker by the researchers of the Care-O-bot [Graf 2001].

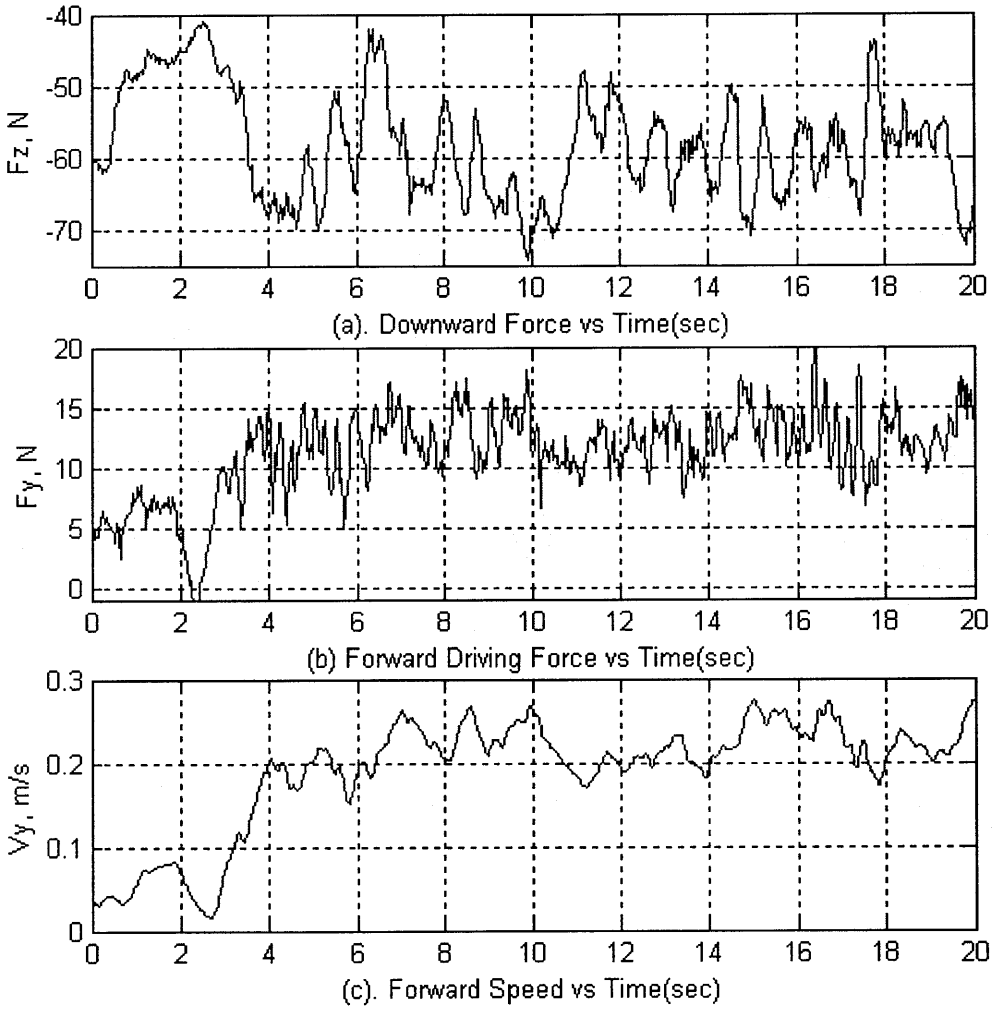

Figure 5.4 - Example of the PAMM Admittance Control Response

To study the acceptance of PAMM and to help select the values of the admittance model (M and B), questionnaire surveys were used in the field experiments as a qualitative measure. Users were asked to drive the SmartWalker freely in the facility and

compare it with their conventional mobility aids. Issues on ease of control, heaviness of drive, ease of learning, physical support, and overall acceptance of PAMM as a mobility aid were evaluated using a five point scale rating. The questionnaire used in the evaluation is on Appendix B. Figure 5.5 shows the result of the tests of PAMM SmartWalker by a group of eight users with an average age of 89. The model used for these tests has a mass M of 14 Kg and a Damping B of 40 Ns/m. The figure shows the highest, average, and lowest ratings given by the users on each issue. Although the average ratings are relatively high on every issue, the variations suggested that different users require different system parameters.

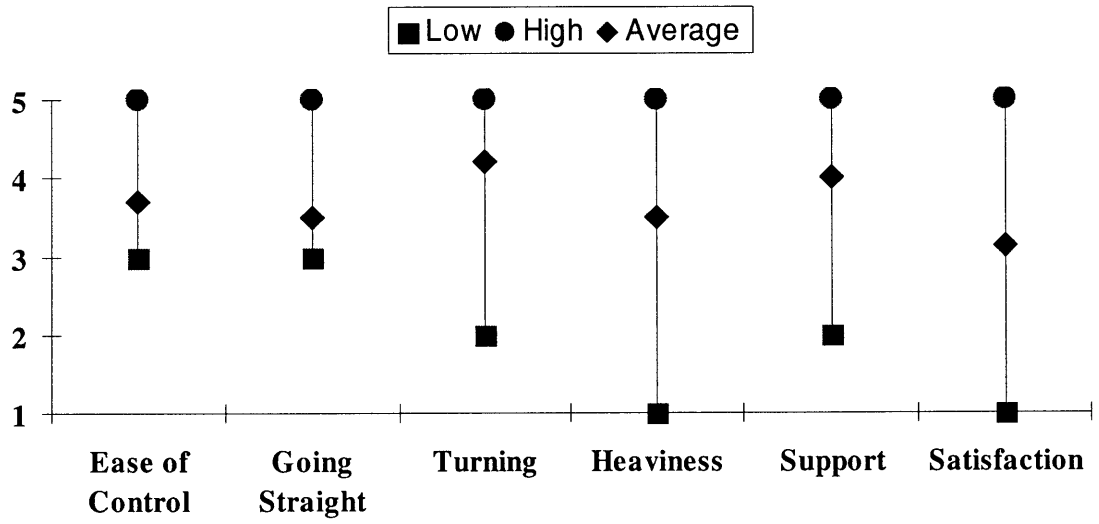

Figure 5.5 - User Evaluation on PAMM SmartWalker (n=8)

5.5.2 Study of Model Parameters

The experiments revealed that different users require different system responsiveness. It is important to understand the effects of parameters if the model on the response of the system when operated by the users. To this end, nine models with

different mass and damping combinations were tested with the SmartCane. The values of M used are 2.5, 5, and 10 Kg, and the values of B are 10, 20, 30 Ns/m, see Figure 5.6.

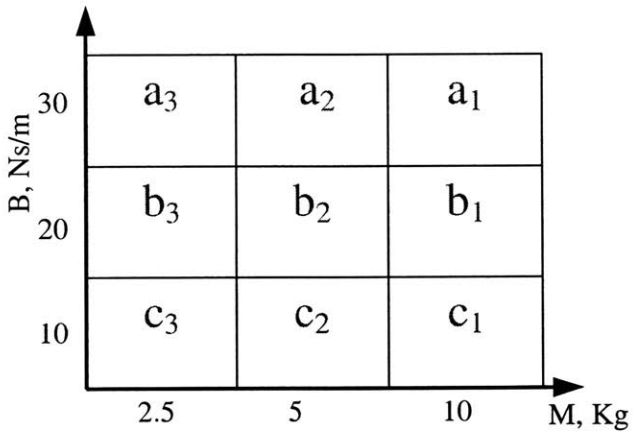

Figure 5.6 - Parameters of Test Models

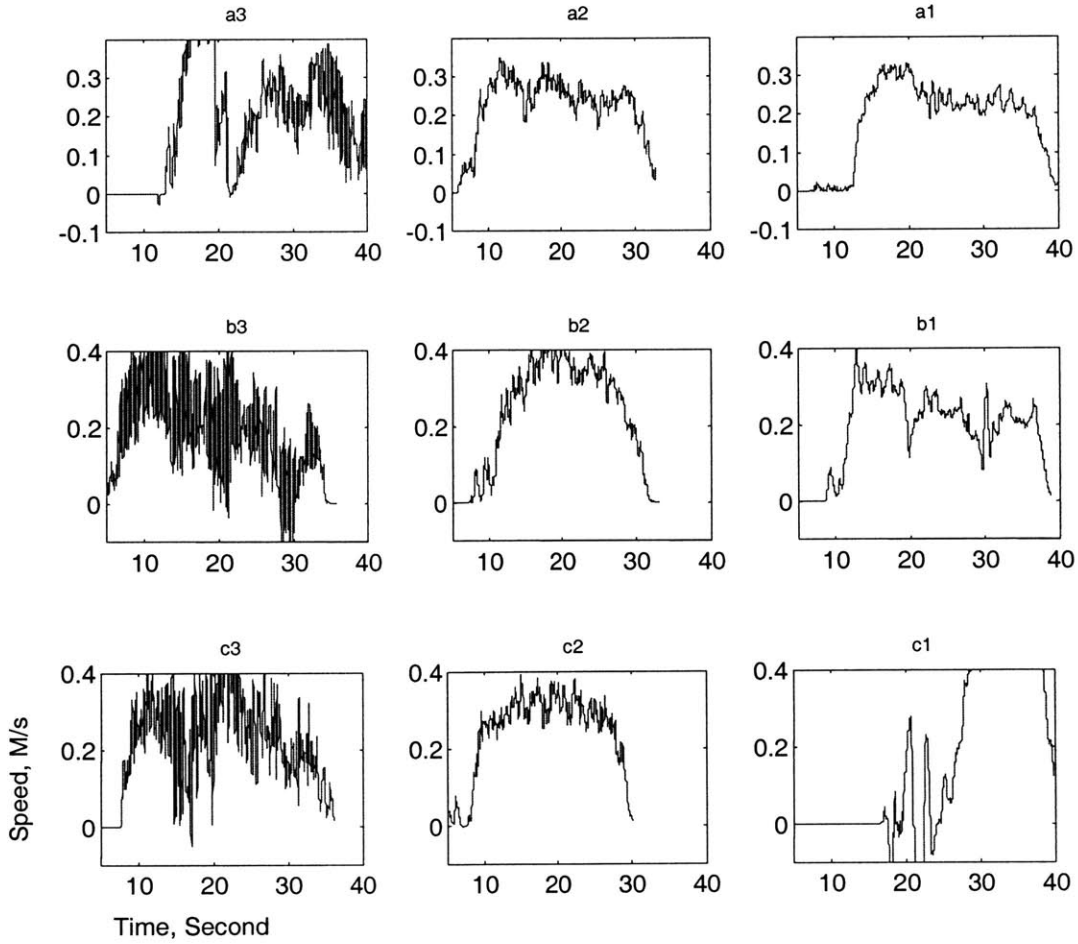

Figure 5.7 - Example Responses of Test Models

Figure 5.7 shows the velocity response of the different models for the same user driving the SmartCane to start from a standing position, walk, and then stop again. From these test results, the effects of different mass and damping combination have been identified, as shown in Figure 5.8. For models with small mass and damping, the motion is oscillatory. For models with small mass and high damping, which have small time constant, the motion is also oscillatory due to high frequency noise. For models with large mass and small damping, the motion is difficult to control as the inertia is too large; users felt that they were dragged along when they wanted to stop. When both mass and damping are too large, the system is too heavy. There exists a range for both B and M that is acceptable; but the exact value should to be tuned to each individual's needs.

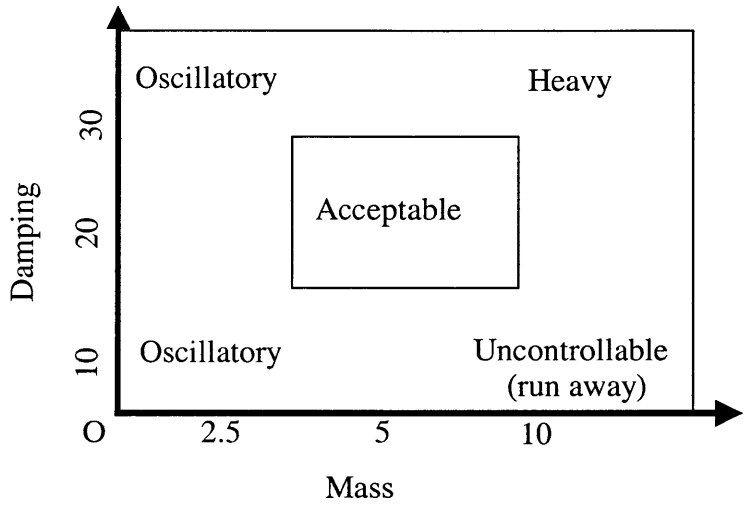

Figure 5.8 - Effects of Admittance Model Parameter

5.5.3 Variable Damping Model Design

It was also found that users have different requirements during different phases of motion. Elderly people feel less assured when they walk from a standstill with PAMM when M and B make PAMM feel light (or responsive) as they are afraid of falling.

Therefore, the model should be less responsive at the start, with higher mass and damping.

When an elderly wants to stop or slow down, PAMM should be able to stop immediately to avoid dragging the user forward. A model with bigger mass would require bigger damping to slow down. It might also need the user to apply backward force to slow down; causing oscillatory motion that is uncomfortable and dangerous for the user. That means it is necessary for the model to have higher damping and smaller mass.

Users always want PAMM to be light (meaning small driving forces) when they are walking at a certain speed. From the steady state response of the model, it is known that the force required to achieve a certain steady state velocity depends on the damping alone. Although it is necessary to let the user to feel some force so that she feels that she is in control, the force should be kept small to prevent the user from fatigue. That means the damping should be kept smaller.

Obviously, the fixed parameter model cannot satisfy the seemingly contradictory requirements for different phases of motion of the system. It can be seen that the damping has a more important role to play. An admittance model with velocity-dependent damping has been designed. The damping of the model is given by:

$$b = b_m - \frac{b_m - b_0}{V_m}|V| \tag{5.5}$$

Where b_m and b_0 are the maximum and minimum damping respectively and V_m is the maximum speed, see Figure 5.9. With the variable damping, the model can have a relatively high mass.

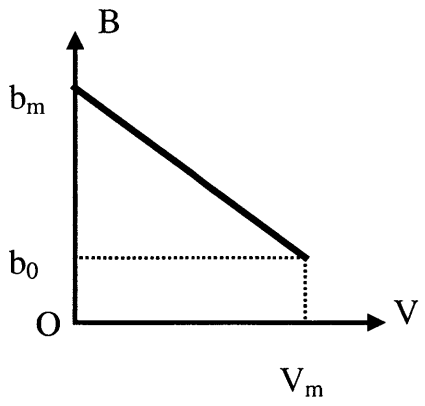

Figure 5.9 - A Variable Damping Model

With the variable model, PAMM will initially respond to user input slowly due to the high mass and damping at low speed. However, when the user is walking steadily at a relatively high speed, the user will need less driving force due to the reduced damping and the speed will not fluctuate too much because of the high mass. When the user needs to stop, PAMM stops quickly as the damping increases, so that the user does not feel the drag. This model has been implemented on both the SmartCane and SmartWalker and was tested by more than 10 users.

Figure 5.10 shows force and speed of a user driving the SmartCane with the fixed damping model with a mass of 10 Kg and damping of 30 Ns/m. Figure 5.11 shows the force and speed of the same user with the variable model, with the damping in the range of 40 to 15 Ns/m. It can be seen that, with the variable damping model, the average force the user needs to push is about 40% lower than what is needed with the damping model when the user walks at the about same speed. This can reduce the fatigue of the user and improve the user satisfaction. The users tested PAMM with the variable model all said that it was much easier to drive.

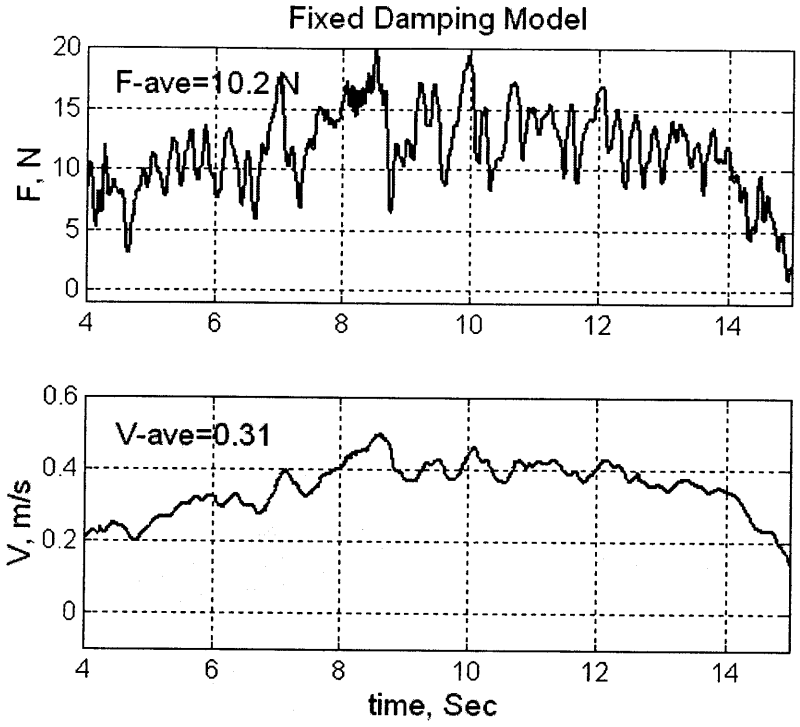

Figure 5.10 - User force and Speed with the Fixed Damping Model

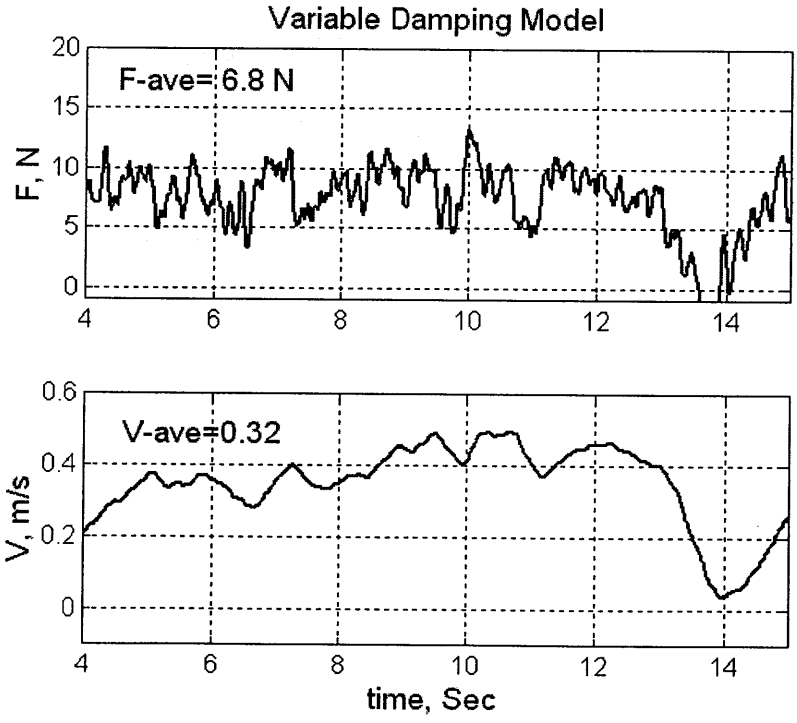

Figure 5.11 - User Force and Speed with the Variable Damping Model

5.6 Summary and conclusions

This chapter presents the development of user interface and the admittance-based control for PAMM. PAMM uses the force/torque sensor as a natural and intuitive user interface. The admittance model, which is define in software, emulates a dynamic system and makes the user "feel" as if he is interacting with system specified by the model. A mass-damper model has been proposed as the dynamic model for PAMM. Field experiments with actual elderly users are the only effective means for developing the admittance-based control for PAMM. Extensive field trials have been carried out to evaluate user acceptance of PAMM with the admittance control, to identify the effects of the parameters of model. A variable damping model has been derived from the experiments, which can improve user acceptance by reducing user fatigue.

Chapter

6

Adaptive Shared Control Design

6.1 Introduction

This chapter addresses the second aspect of the control system, which is the shared control design. The goal is to develop a control scheme that can dynamically allocate control between the human and the machine according to the task situation, and the capabilities of both the human and the physical system. For assistive devices like PAMM, the controller is used to assist the user rather than replace the user in performing his or her task. The user should be given as much control while still ensuring adequate performance. However, elderly users of PAMM could have limited psychical and cognitive capability or irrational behavior. When the user demonstrates that he or she cannot operate PAMM safely, for example when the user tends to deviate too much from the trajectory leading to the destination or runs too close to obstacles, more control should be given to the computer. However, when the user is performing well again, more control should be given back to the user. A shared control system that can vary the control allocation is called an adaptive shared control system.

An adaptive shared control framework is proposed in this chapter. The adaptive shared control algorithm allocates control between the human and the computer based on the demonstrated performance of the user. In this chapter, the basic algorithm is first presented with some simulation results. Then, the implementation of the algorithm on PAMM SmartWalker is presented along with results from the field experiments with elderly users.

6.2 An Adaptive Shared Control Framework

The proposed adaptive shared control framework is shown in Figure 6.1. This approach has a similar structure to a classical adaptive controller [Narendra and Annaswamy, 1989]. The framework integrates the system planner and the human machine interaction control.

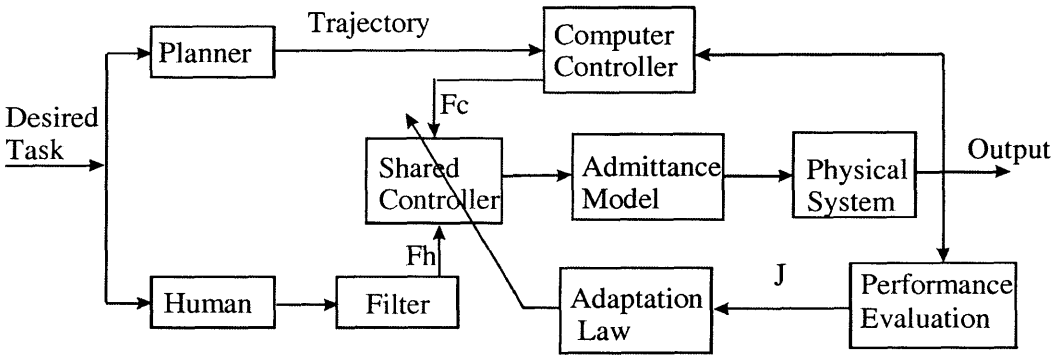

Figure 6.1 – Adaptive Shared Control Framework

The system has a planner that generates an ideal path based on the task and its knowledge of the environment. PAMM determines its location in the environment by identifying the sign posts with a CCD camera [Dubowsky, 2000]. The computer controller generates a virtual force input based on the preplanned and the actual trajectories. The user gives inputs to the system through a force/torque sensor. The two

control inputs to the shared controller have an associated gain, $K_{computer}$ and K_{human}, respectively. These gains reflect the control authority of the computer and the human. These gains are changed by the adaptation law. The adaptation law first computes a performance index J based on a metric δ, which is a measure of how well the user is performing. It then adjusts the two gains to minimize J. The output of the shared controller is fed to the admittance-based control, which in turn generates the low-level control commands for the physical system. The different parts of the algorithm are discussed below.

6.2.1 Path Planning and Computer Control

The first step in this part of the control algorithm is to determine an ideal path and the velocity and acceleration profiles of the system along that path. The preplanned trajectory needs to take into account that the system has limited sensing capabilities and cannot know the entire environment explicitly. This introduces the fundamental problem of optimizing a system in a semi-known, dynamic environment. Here the system would reevaluate its trajectory when new information entered the range of its sensors. Exact knowledge of the environment can only be found inside one loop of the evaluation, and thus path optimization can only be calculated for that section of the total environment. This part of the work would likely require some extension of the previous work already done on planning in dynamic environments. Significant research has been done on path planning algorithms for autonomous mobile robots; it is not the focus of this thesis.

The main function of the computer controller is to guide the user back to the preplanned trajectory when the user deviates from it and when the shared controller deems it necessary based on the performance evaluation. However, one important issue

is that the controller should not force the human to the trajectory and upset the balance of the elderly person. The computer limits the control forces based on the capability of the user. Another function of the computer controller is to act as a safety watchdog, even when there is no preplanned path. For example, when PAMM is under free driving by its user, the computer is also monitoring the user's speed, location, stability, and even health conditions. When there is an imminent danger, the computer should act by limiting the speed or guiding the user to a safe path.

6.2.2 Performance Metrics

The performance metric is based on the task and how well the user performs the task. The user's performance metric needs to include such factors such as proximity to obstacles, deviation from the trajectory, excessive or high frequency oscillation about a path, and tip over margins [Papadopoulos and Rey, 1996]. The chosen metric here is a quadratic function combining all the factors considered and is given as:

$$\delta = k_1(x)^2 + k_2(\dot{x})^2 + k_3(\ddot{x})^2 + k_4(dis)^2 + k_5(S)^2 + \ldots$$

where k_i = weighting factors

$$x = \text{position}_{ideal} - \text{position}_{actual}$$

$$\dot{x} = \text{velocity}_{ideal} - \text{velocity}_{actual} \qquad (6.1)$$

$$\ddot{x} = \text{acceleration}_{ideal} - \text{acceleration}_{actual}$$

$$dis = \text{disance to obstacles}$$

$$S = f(\text{stability criteria})$$

The exact formulation of the performance metric depends on the specific application. The value of the weighting factors needs to be adjusted to some degree for a given population and environment

6.2.3 Adaptive Shared Control Structure

The proposed adaptive shared control algorithm has the control law:

$$F = F_c K_{computer} + F_h K_{human} \tag{6.2}$$

where:

$$K_{computer} + K_{human} = 1 \tag{6.3}$$

The adaptation law adjusts the gain $K_{computer}$, using the following method. First, at time t_i, a performance index J(i) is calculated, which is an integral of the performance metric δ as follows:

$$J(i) = \sum_{k=1}^{i} \delta(k) e^{-\lambda(i-k)\Delta t} \tag{6.4}$$

where λ is the forgetting factor and Δt is the sampling time of the controller.

In this method, to avoid an abrupt change, the control authority is adjusted based on the demonstrated performance history of the user. However, past data should carry less weight on the adaptation, thus an exponential forgetting factor λ is introduced. The parameter λ has units of 1/s. With a smaller λ (or longer forgetting term), the control authority is changed more gradually.

With the performance index J(i), the gains for the computer control and the human are calculated using the following adaptation law:

$$K_{computer}(i) = 1 - e^{-\beta J(i)} \tag{6.5}$$

$$K_{human}(i) = 1 - K_{computer}(i) \tag{6.6}$$

With this law, the computer control gain $K_{computer}$ will increase when the performance index increases. The increase of the computer control will help the user perform the task better and reduce the performance index. It also ensures that the control gain will not exceed 1.

The parameter β in Equation (6.5) is used to adjust the behavior of the adaptation. The value of β affects the rate of change of the computer control gain to the performance index J. The effect of β on the change of the computer control gain as a function of the performance index shown in Figure 6.2. The smaller β is, the smaller the computer control gain will be for the same J. This parameter is always considered together with the forgetting factor λ. For a smaller forgetting factor, the performance index J will be large as past data accumulate, β should also be smaller so as to prevent the computer gain from becoming equal to 1.

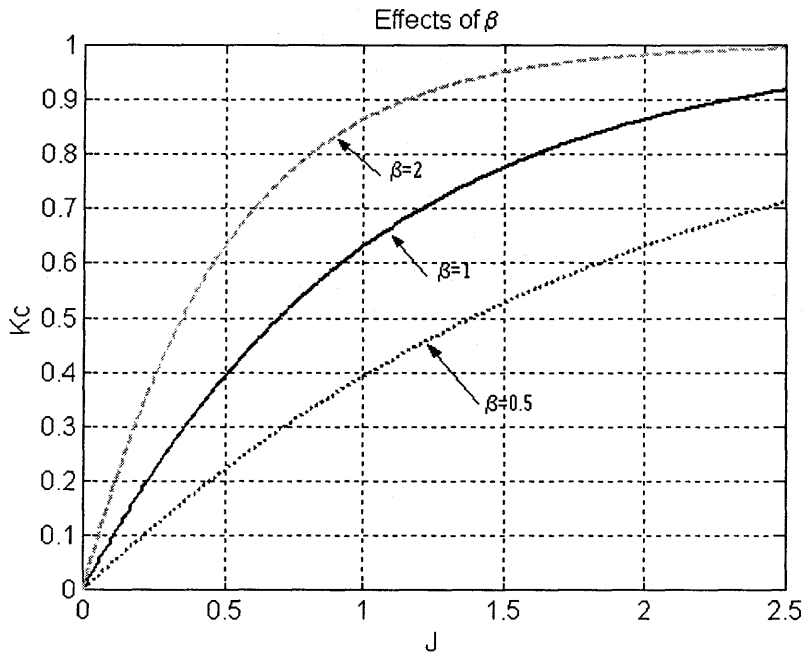

Figure 6.2 - Effect of Parameter β on Computer Control Gain

Under this adaptation law, the controller gains, $K_{computer}$ and K_{human}, are adapted to the user's capability measured by the performance metric. These gains determine the balance of the control authority that the human has compared to the preplanned trajectory, or how responsive the system will be to the user. Depending on the relative

control allocation, a system can be said to be in manual, shared, or autonomous control mode. However, these modes are continuous rather than discrete; the adjustment of control authority is automatic based user's performance.

6.3 Simulation Results

A simulation is performed to study the behavior and the effects of the gains of the adaptive shared control law. In the simulation, a vehicle modeled as a point mass is operated by a human operator to drive in the X direction. The input from the human is assumed to have a sinusoidal oscillation in the Y direction as shown in Figure 6.3. There are two obstacles on the side along the desired path. The performance metric used in the simulation is just the nearest distance to the obstacles. Figure 6.4 and Figure 6.5 show the path and the evolution of the control gains K_c and K_h. It can be seen that the adaptive controller can suppress the oscillation of the user input when it gets close the obstacles. When the vehicle is far from the obstacles, the user has full control despite the oscillations. Two different forgetting factors λ are simulated, each with an associated β. Figure 6.4 shows the results in the case λ is 10 and b is 0.5. Figure 6.5 shows the results in the case λ is 0.1 and b is 0.005. It is shown that with bigger λ, or short forgetting term, the control authority changes rapidly, which is undesirable. With a smaller λ, the control authority changes more gradually. However, it would also be undesirable if the control authority change were too slow, as it would penalize the human too much or it would help the user too little when trouble suddenly arises. The control should be given back the human if he or she has been doing fine for a certain period. The choice of the appropriate value for the forgetting factor depends on the specific implementation needs.

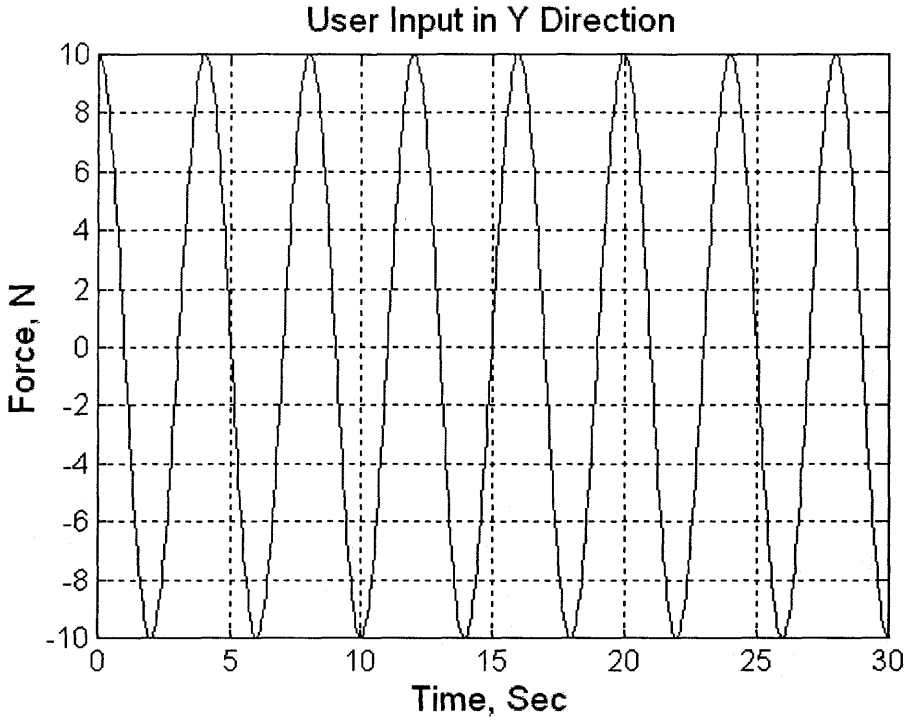

Figure 6.3 – User Input in Y Direction

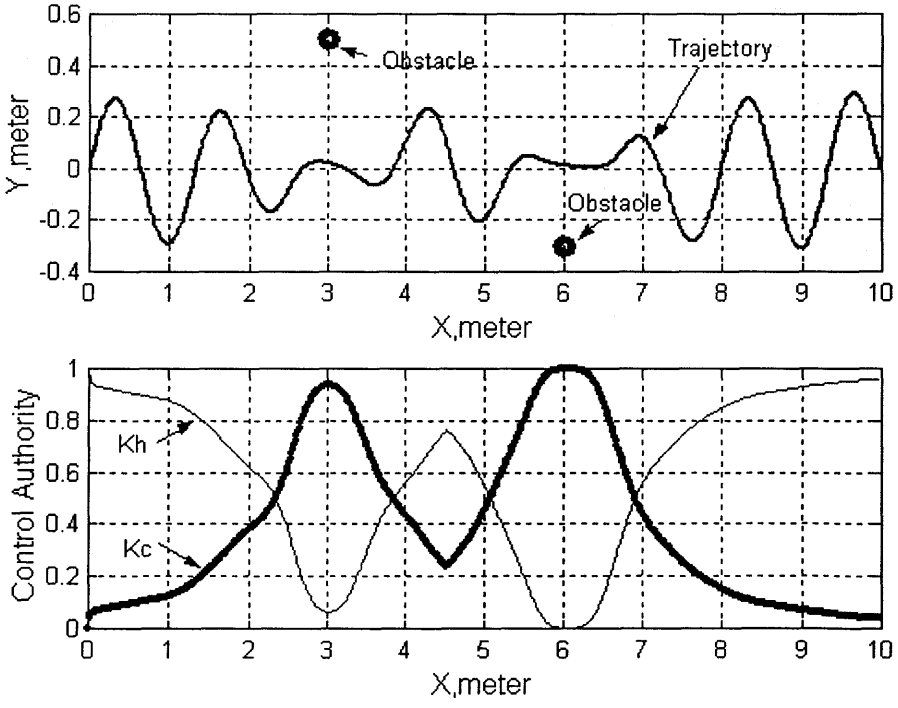

Figure 6.4 - Simulation of Adaptive Shared Control with λ=10, β=0.5

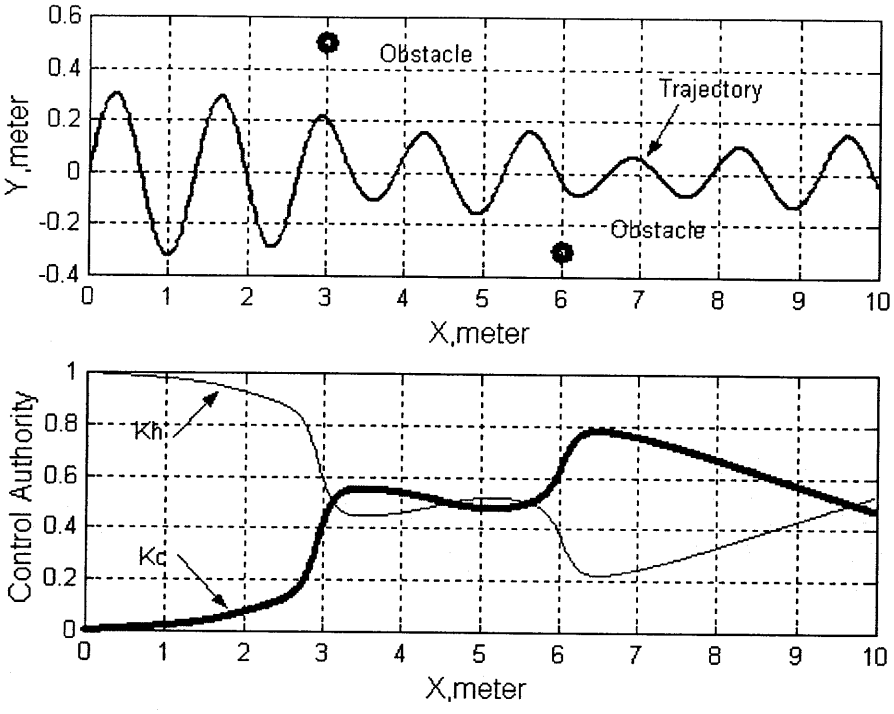

Figure 6.5 - Simulation of Adaptive Shared Control with λ=0.1, β=0.005

6.4 PAMM Implementation and Field Experiments

Obviously, the above simulation is highly simplified. It is difficult to model the interactive behavior of a human user operating the PAMM system and thus the validation of the shared control design depends largely on experimental work with real users. The field trials were conducted at an eldercare facility for the adaptive shared control using PAMM SmartWalker.

6.4.1 Adaptive Shared Control of PAMM SmartWalker

During the experiments, the users control their walker speed along the path. However, the maximum speed is limited at 0.4 to 0.5 m/s based on individual user's usual walking speed, which is estimated by measuring the time the user spent traversing a path with a conventional walker. The paths that the users were asked to follow were

programmed offline. The computer controller only guides the users back to the path when they deviate from the path. The computer controller generates a force in the normal direction to the path, which is given by:

$$F_c = K_p(dev) \tag{6.7}$$

Where K_p is the controller gain that is determined based on the amount of deviation and the magnitude of force allowed. This force is integrated with the user input force via the shared control law expressed in Equation 6.2 and then fed into the admittance controller. The total force to the admittance controller is limited based on the speed allowed for the walker to move back to the path. In order not to upset the balance of the user or make the user feel that the computer has its own mind, if the computer control force is in the same direction of the user applied force, the computer control force is ignored and the walker moves at the speed desired by the user.

The performance metrics used in these tests are the deviation from the path and the distance to the wall, which is expressed as:

$$\delta = k_1(dev^2) + k_2(\frac{1}{dis^2}) \tag{6.7}$$

The values of k_1 and k_2 are set 10 and 0.05 respectively. These values are selected based on the consideration of how much the user is allowed to deviate and how close the user is allowed to get close to obstacles. Using these values, when the user deviates from the path by 0.5 meters, its effect will dominate and the computer control gain will be close to 1.0 even if when the walker is far from any obstacles. On the other hand, when the distance to obstacles is about 0.15 meters, its effect will dominate even when the walker is not far from the path. The deviation is the shortest distance calculated from the center of the walker to the path. The distance to obstacles is the shortest distance calculated

from the edge of walker to the nearest obstacles. The obstacles are the walls and the doorways, which are represented by lines and their exact positions are programmed in the system map.

The implementation of the adaptation law expressed by Equation 6.4 is rewritten in the more computationally efficient form where only the current metric and index are used in the computation of the current performance index:

$$J(i) = \delta(i) + J(i-1)e^{-\lambda\Delta t} \tag{6.8}$$

6.4.2 Test Environment and Path Design

The tests were conducted in the same assisted living facilities as the tests for the admittance control. The tests were conducted in the users' residence without modification other than the markers put on the ceiling for the vision-based localization purposes. Appendix A shows the floor plan of the first floor of the assisted living facility. The test path has a total length of 35 meters that runs from a multifunction room, passing through two standard doorways that are 3 feet wide, running the long corridor that is 6.5 feet wide, to a mail room at the reception area, see Figure 6.6.

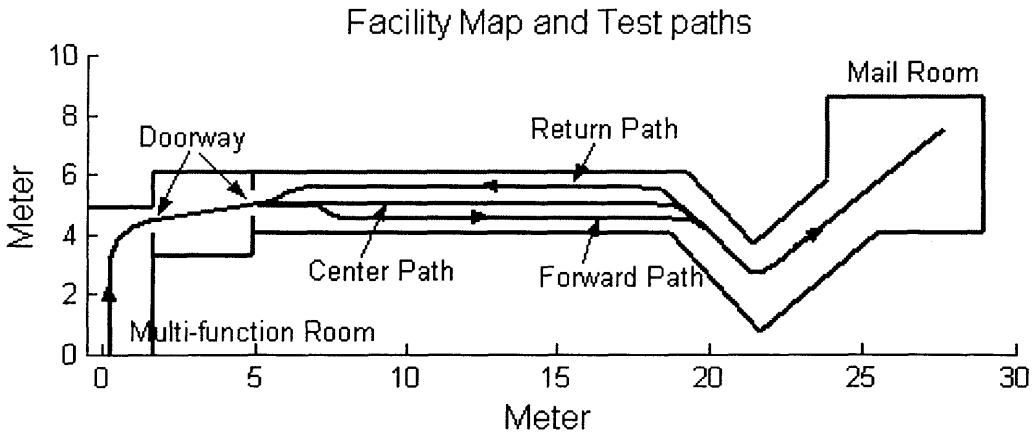

Figure 6.6 - Field Trial Path Design

The paths are the most frequently used routes in the daily activities of the residents. In the corridor, three different paths were selected, the one along the center is designed to make the task easier, the other two close to the wall are designed to make the task tougher as the user has walk to the right and not hit the wall. These paths were not marked on the floor during the tests. Users were just told where to go and where they should keep to the center or keep to the right during the tests.

6.4.3 User Profile and Practice Trials

A group of 5 female and 1 male residents participated in the experiments. The ages of these residents range from 84 to 95. Figure 6.7 shows a 94 years old female user and a 85 years old male user testing the PAMM SmartWalker. These participants were all volunteers and were chosen by the staff at the facility. None of them suffer from serious health problem, but they all use conventional walkers for their activities for physical support. One of the female users tends to forget the way to her own room from time to time.

Figure 6.7 - Elderly Users (94 and 85Years old) Testing PAMM SmartWalker

Before the formal tests for the adaptive shared control design, each user was asked to drive PAMM freely along the center path three to five times depending whether he or she had experience with the SmartWalker before. These tests were intended to get the user familiar with PAMM and to get all users at the same exposure to PAMM. Before they used the SmartWalker, they were explained how to operate PAMM and what they should do when they feel uncomfortable with PAMM during the trial. The users were given a few minutes rest between each trial or waited until they felt comfortable walking again. At least one person would follow the user during the tests to ensure safety of the user. The SmartWalker could be stopped immediately when needed. During these tests, all the users could drive the SmartWalker from the multifunction room to the library without any serious problem. Most of them said they like the PAMM SmartWalker as they did not have to lift and stop it as they did with the traditional walker, though most of them slowed down and look very carefully at the wheels when passing through the doorways in the first few trials. Each user was also asked to walk along the path with his or her conventional walker either before or after using the SmartWalker. It was found that they walked at about the same speed with PAMM.

6.4.4 Adaptive Shared Control Tests

For comparison, each user tested PAMM under three different control modes along the same path. Three users tested on the path that requires them to walk to the right. The first mode is the free-driving mode. The human control gain K_{human} is always set to 1 under this mode. The second mode is the adaptive shared control mode. The third mode is the full computer control. Under this mode, the computer control gain $K_{computer}$ is always set to 1, therefore the user would feel a force driving back to the path

whenever there is deviation from the path. The order of the control modes tested with each user was different. The users were not told which control mode they were going to test.

Figure 6.8 shows the results of user #1 driving the SmartWalker along the path under the adaptive shared control. In the figure, (a) shows the actual path of the user and the desired path. It can be seen that the user followed the desired path closely, with some deviations only at those places that require turning. (b) shows the performance index J and the computer control gain $K_{computer}$ plotted with the length of the trajectory S. It clearly shows that when the use passes the narrow doorway, the distance to obstacles is very small and the value of the performance index increased. The increase of the performance index makes the computer control gain increase so that the user is kept on the path. In other part the trajectory, the computer control gain decreases as long as the user is not getting too close to the wall. In the open area, the computer control gain reduces even if the user deviates from the path. The forgetting factor λ used in this trial is 10 and β is 0.5, therefore, past data is forgotten rapidly and the both the performance index and the shared control gains change quite fast.

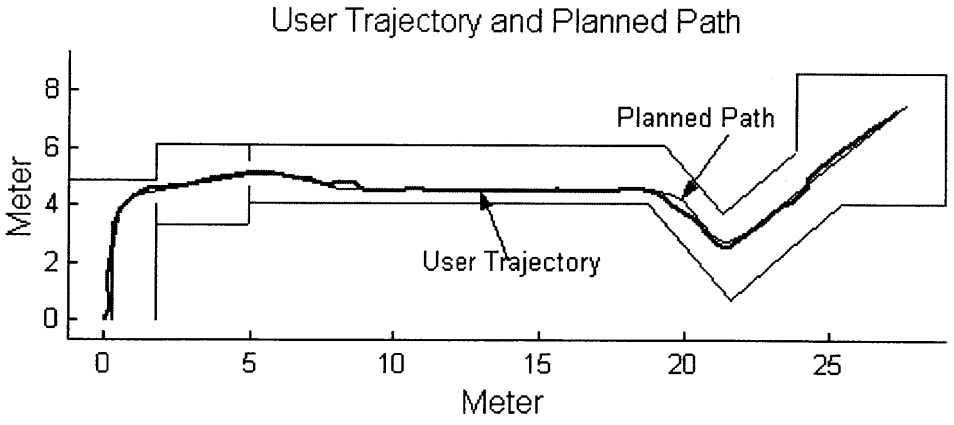

(a). User Path and the Desired Path

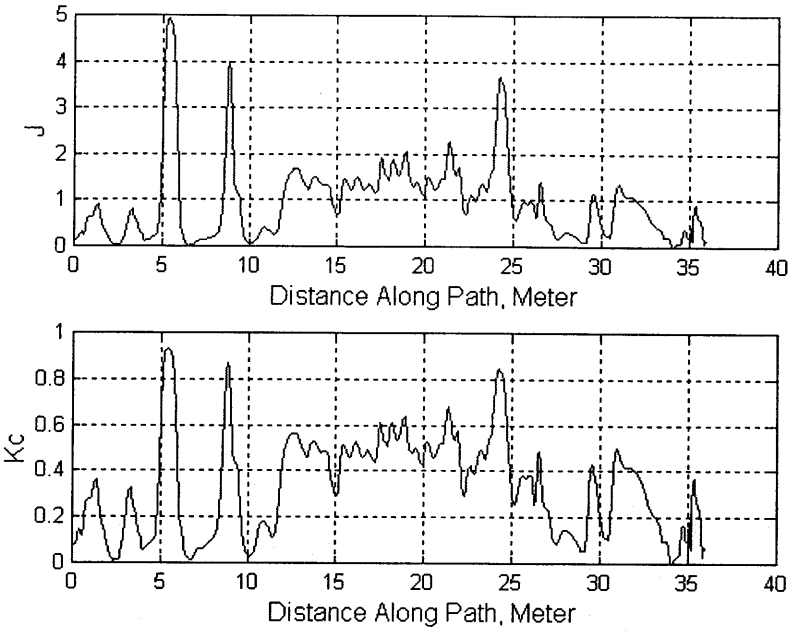

(b) Performance Index J and Computer Control Gain K_c

Figure 6.8 - Path and Control Gain under Adaptive Shared Control (User #1)

To compare the performance of the same user under different control modes, the distances to the walls and deviations from the path under the free driving, shared control and full computer control were plotted in Figure 6.9, Figure 6.10, and Figure 6.11 respectively. The user was instructed to follow the paths closest to the wall during these tests. Under free driving mode, the user deviated from the path as much as 0.38 meters with a RMS value of 0.114 meters. Under the adaptive shared control mode, the maximum deviation deviated of the user is about 0.3 meters with a RMS value of only 0.095 meter. It also should be noted that the maximum deviations happened in the open area where the path is far from any obstacles and the user should be given more freedom in this areas. The comparison of the RMS values shows that the user followed the path more closely in the rest of path under the adaptive shared control mode. What's more interesting is to look at the distance to the obstacles, especially in the section along the

corridor. Under free driving, the user got as close as 0.05 meters to the wall, the RMS value of the distance is 0.103 meters. Under adaptive shared control, the RMS value of the deviation is 0.1465 meters, meaning that the user could maintain a constant distance of about 0.15 meters from the wall along the corridor. Obviously, the performance of the user was improved under the adaptive shared control mode. However, the user could not notice the difference between the free driving and the adaptive shared control modes. It can be seen from Figure 6.11 that performance of the user under the full computer control is also good. However, the user did not like the full computer control and complained that PAMM had "a mind of its own". This is because the controller did not allow the user to deviate from the path even she was far from the wall. This tells us that users need to be given as much control as possible.

The performance improvements were consistent among the three users performing the same tests. Figure 6.12 shows the RMS value of the deviations from the path for all the three users under different control modes. Figure 6.13 shows the RMS value of the distances to the obstacles for all the users under the three different control modes. Although the performances are different for the three users, all the users have improved performance under the adaptive shared control mode.

Theses experiments demonstrated that the adaptive shared control can help users stay on path and prevent them from colliding to obstacles by changing the control gains adaptively based on the task situation and the performance demonstrated by the users. The change of the control gains does not affect the comfort of the user as observed during the experiments. This is because the use could always have some control on the system unless it is very close to the dangerous situations. By comparison, the full computer

control strategy could make the user uncomfortable by taking the control completely from the user.

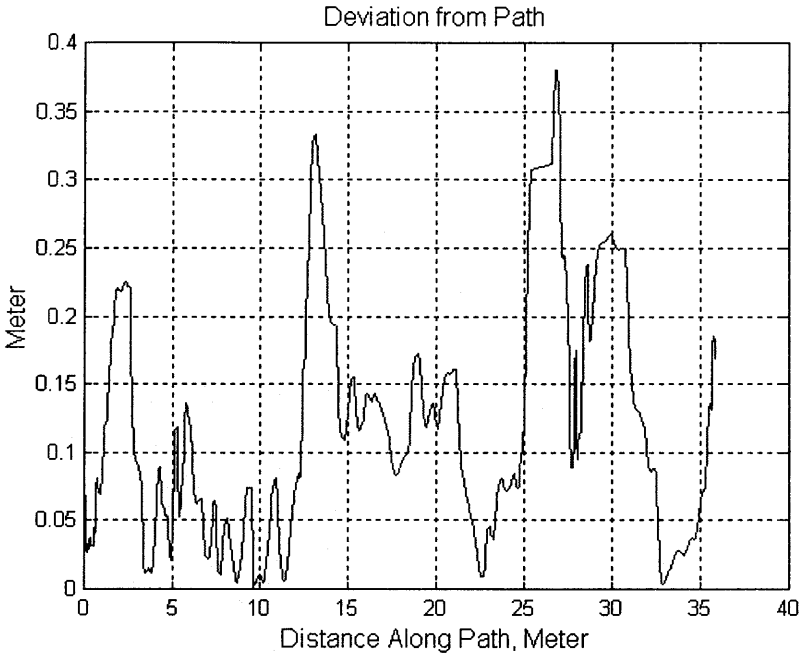

(a). Deviation from Planned Path

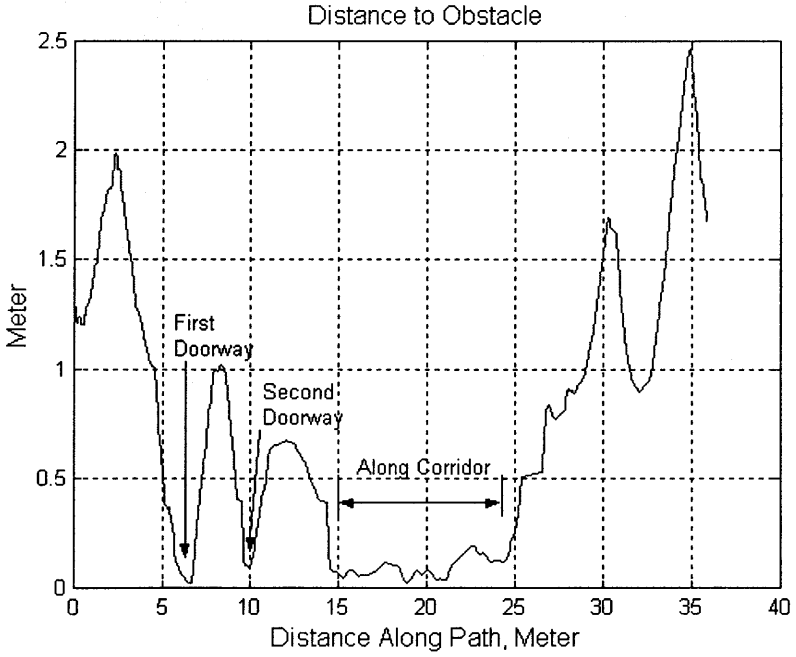

(b). Distance from Obstacles

Figure 6.9 – User #1 Performance under Free-Driving

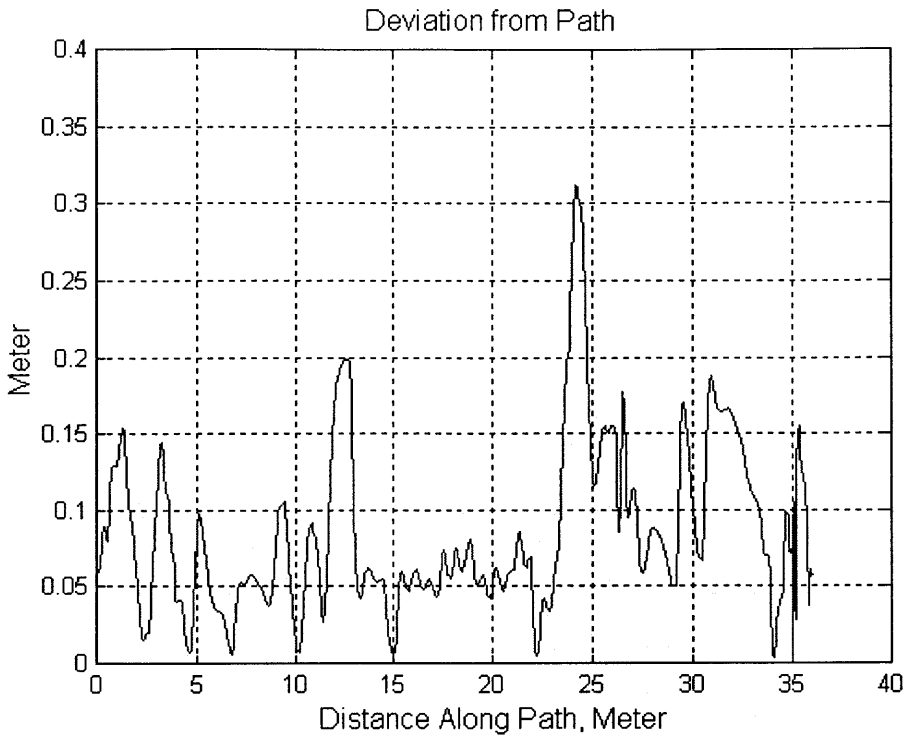

(a). Deviation from Planned Path

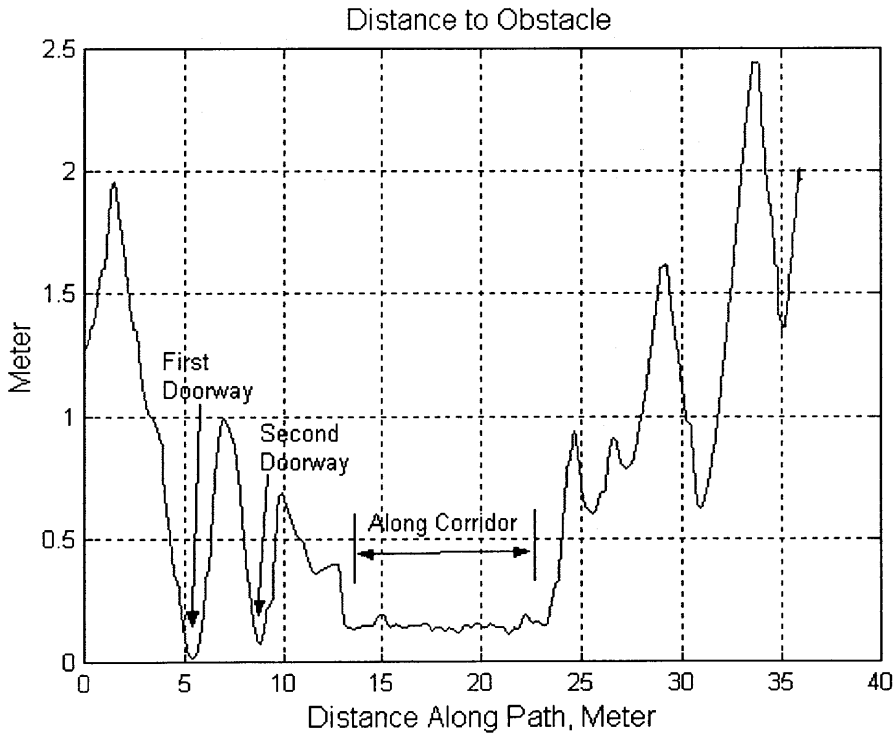

(b). Distance from Obstacles

Figure 6.10 – User #1 Performance under Adaptive Shared Control

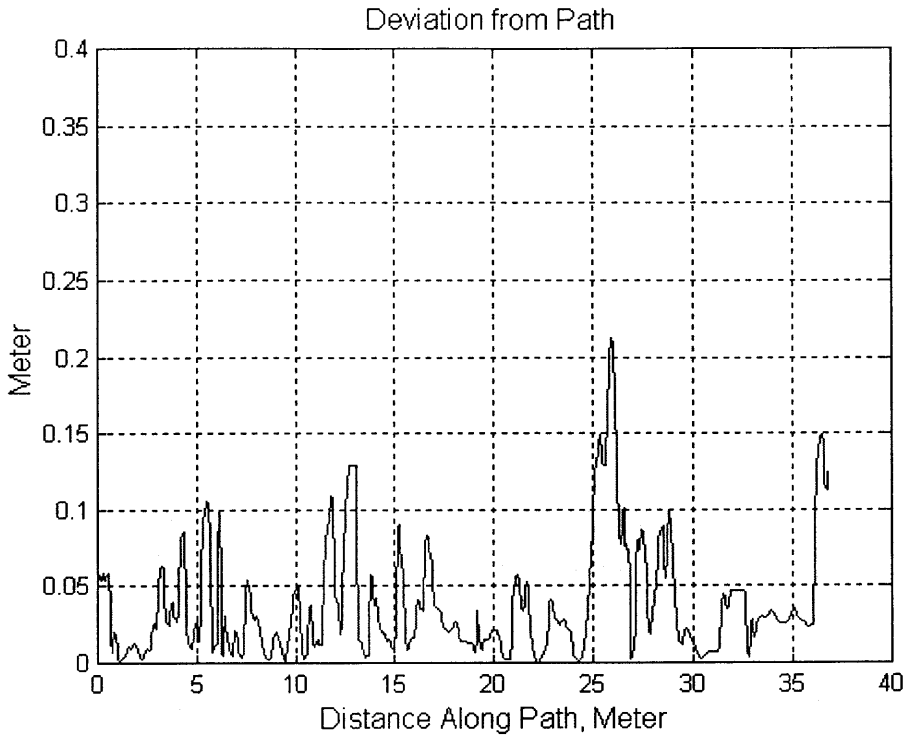

(a). Deviation from Planned Path

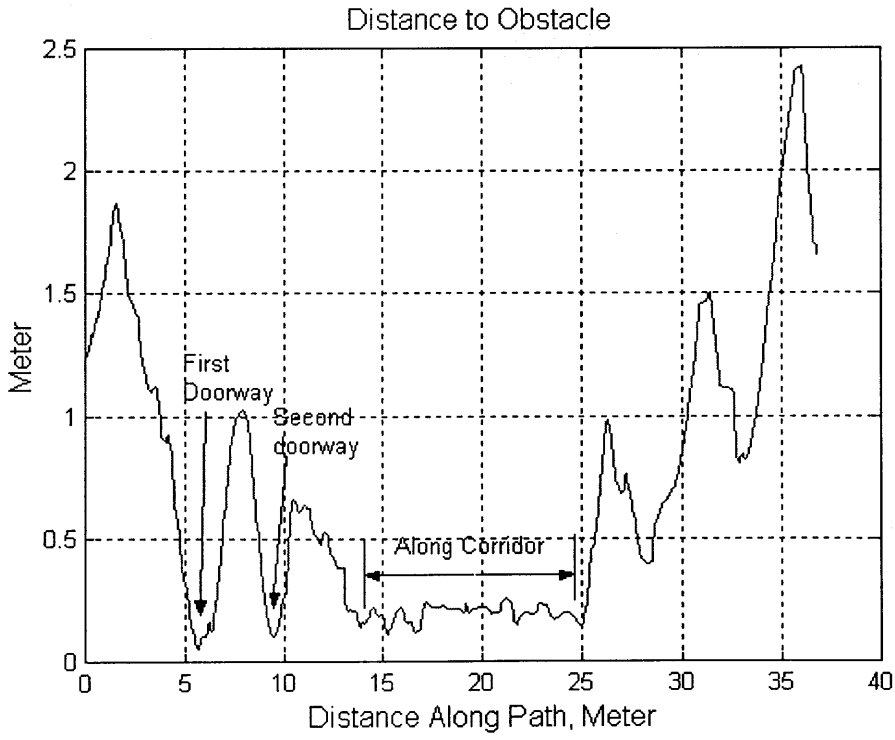

(b). Distance from Obstacles

Figure 6.11 – User #1 Performance under Full Computer Control

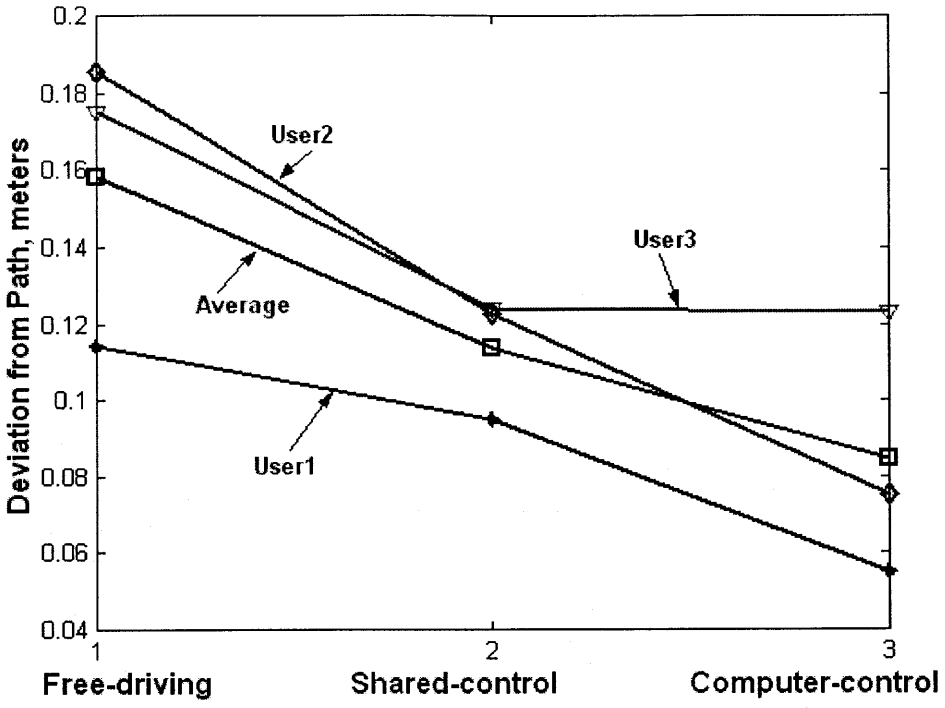

Figure 6.12 - RMS Values of Deviation from Path for all three Users

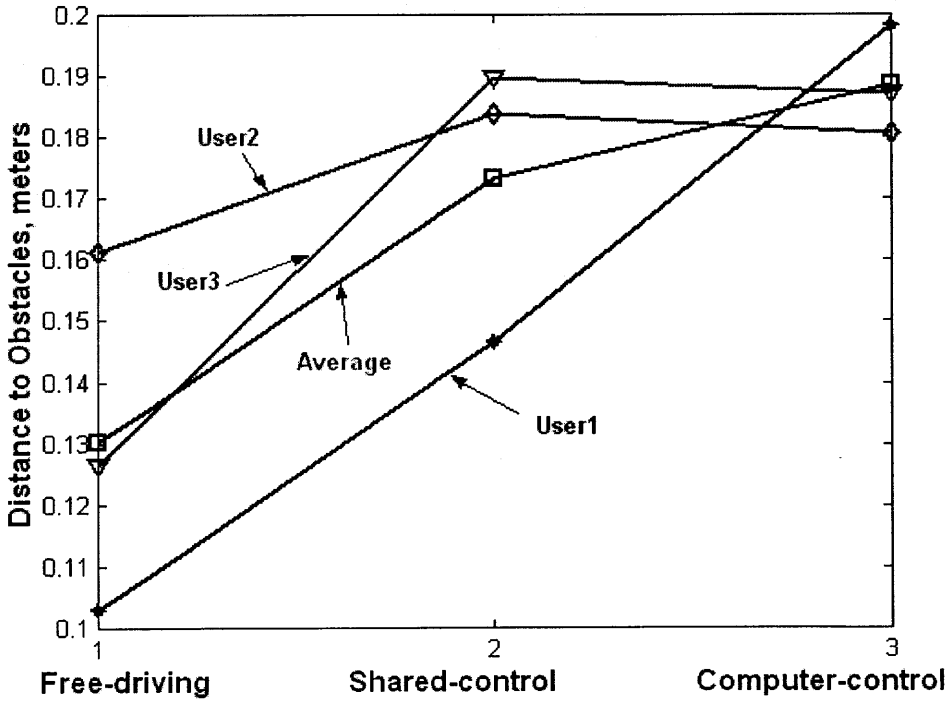

Figure 6.13 – RMS Values of Distance to Obstacles for all three Users

To show the effects of the forgetting factor, a user (#3) tested the adaptive shared control with different forgetting factors along the center path. Figure 6.14 shows the deviation and the computer control gain change for λ=10. Figure 6.15 shows deviation and the computer control gain change for λ=0.1. It can be seen from Figure 6.14 that, with short forgetting terms (bigger λ value), the computer control gain changes quickly. The controller behaves like a reactive obstacle avoidance algorithm. With longer forgetting terms, the control is not given back to the user immediately after the computer gains more control, as shown in Figure 6.15. It can be seen that the performance with the longer forgetting term is better. In general, rapid change of control gains should be avoided and the forgetting term should not be too short. However, the forgetting term should also not be too long so as not to avoid abridging the control of the user too much. If the forgetting factor is too long, the control will not be given back to the user even if there is no danger and the user is doing well, or it will be dangerous if the user has more control and the control gain could not be given to the computer when the user is not performing well enough. The value of the forgetting factor should different for different users. The appropriate forgetting factor should be determined based on the capability of the user.

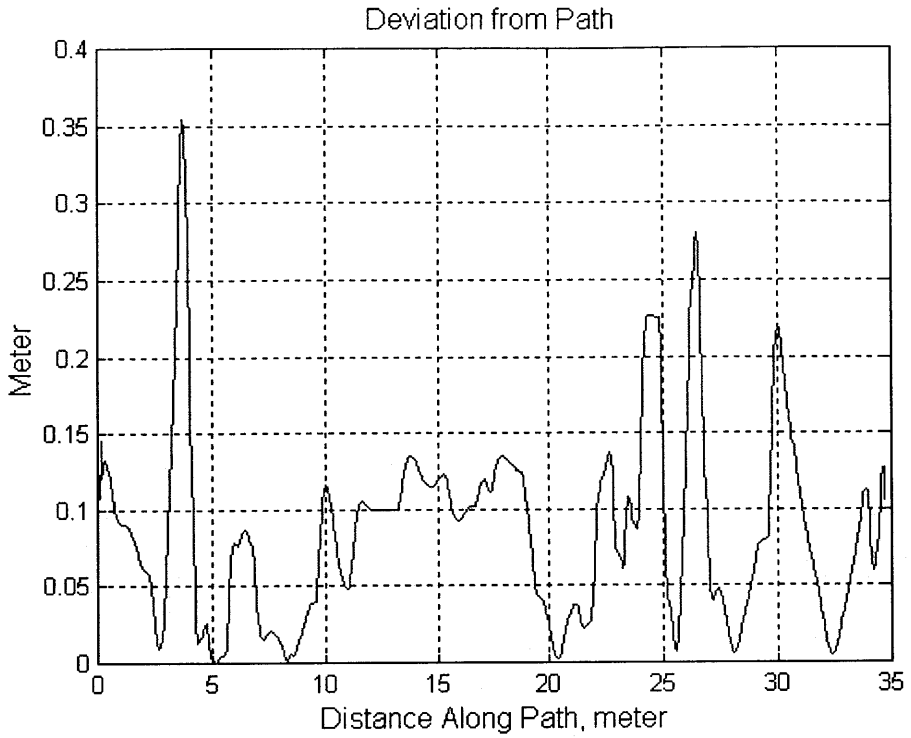

(a). Deviation from Planned Path

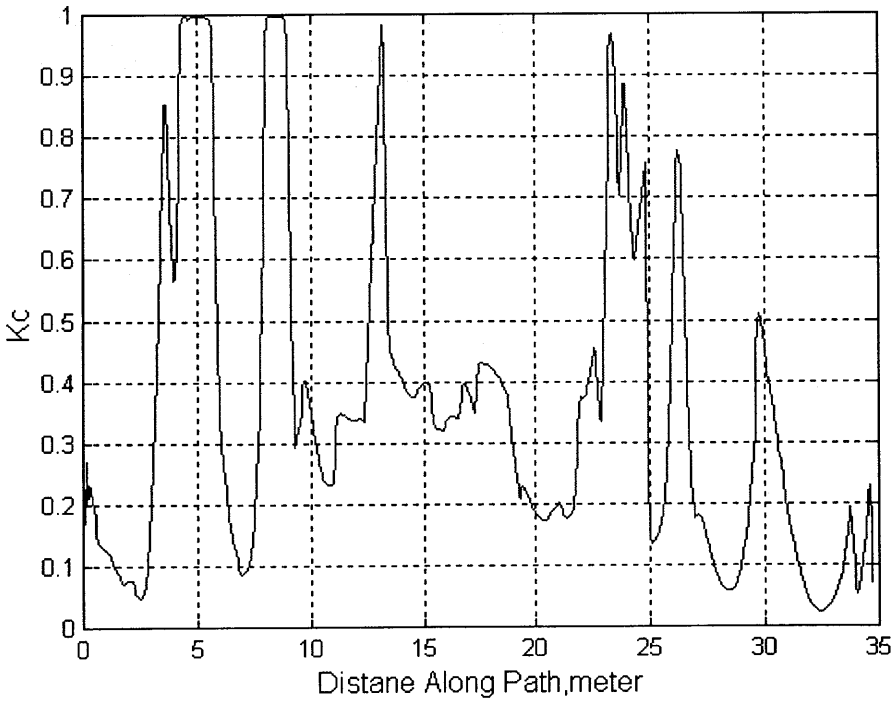

(b) Performance Index J and Computer Control Gain K_c

Figure 6.14 - User Performance with Shorter Forgetting Term (λ=10)

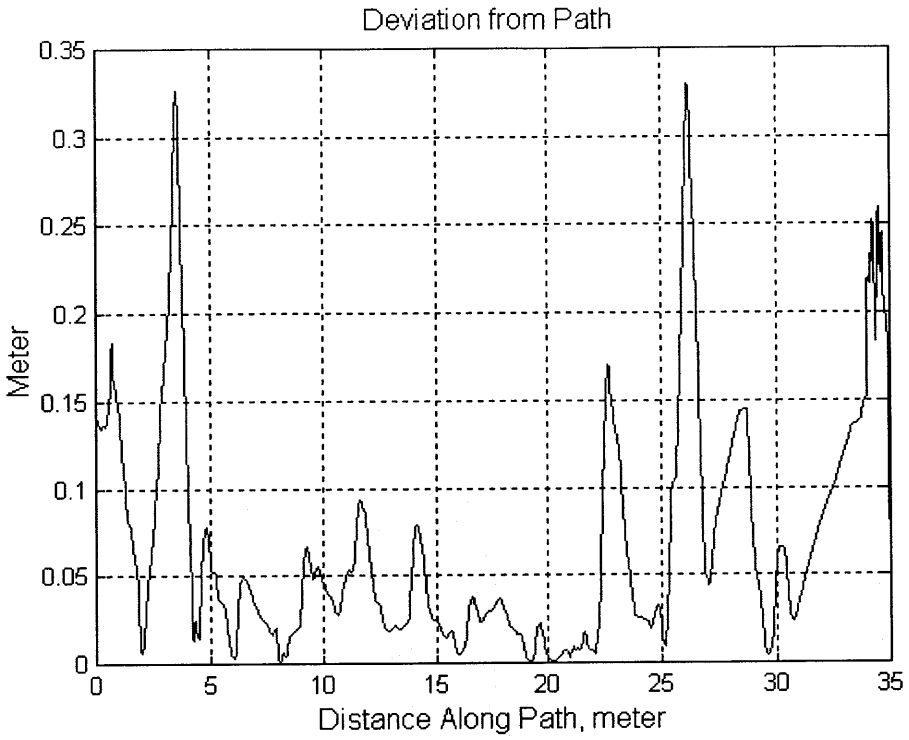

(a). Deviation from Planned Path

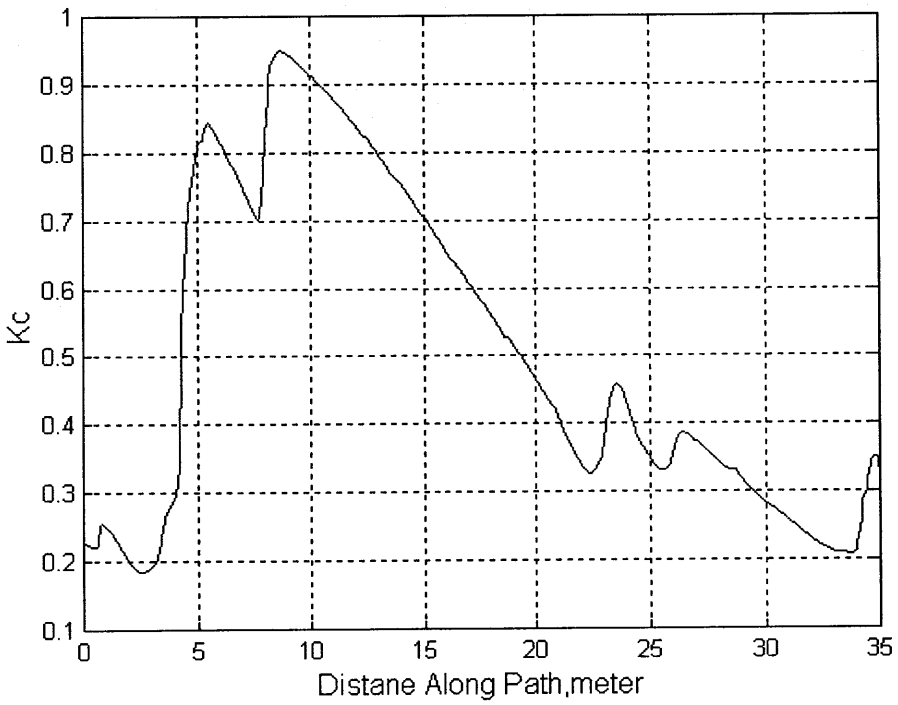

(b) Performance Index J and Computer Control Gain K_c

Figure 6.15 - User Performance with Longer Forgetting Term (λ=0.1)

6.5 Summary and Conclusions

An adaptive shared control framework is proposed in this chapter. The adaptive shared control algorithm allocates the control between the human and the computer based on the demonstrated capabilities of the human. The control authority change is continuous rather than discrete. By choosing different performance metrics and controller gains, the algorithm can be used in many different applications. The algorithm is implemented on PAMM SmartWalker and tested in an assisted living facility. These experiments demonstrated the effectiveness of the adaptive shared control. The adaptive shared control helps improve user performance.

Chapter

7

Conclusions and Suggestions for Future Work

7.1 Summary of the Thesis Contributions

When an elderly individual moves toward higher levels of care (i.e., from independent living to assisted living facilities to nursing homes), costs increase and quality of life decreases rapidly. The largest change occurs during the transition into a nursing home. Delaying the transition through the use of robotic assistive devices will be extremely beneficial for the individuals and economically favorable for society. A research program has been conducted at the Field and Space Robotics Lab to develop the fundamental technology for a Personal Aid for Mobility and Monitoring (PAMM) that meets the needs of elderly people living independently or in senior assisted-living facilities. There are a number of major technical challenges in the development of such devices. The objectives of this thesis are to address two of the most important issues: mobility design and control.

An omni-directional mobility design concept using conventional wheels has been independently developed. The design has been implemented and tested on the PAMM SmartWalker, where it has demonstrated excellent omni-directional capability. This

design is simple, lightweight, and robust to floor irregularities. Important issues for effective implementation and control have been analyzed. This design is also energy efficient because of its dual-wheel construction. An analytical method for studying the wheel scrubbing, an important issue for wheeled robotic systems, has been developed.

An admittance-based control methodology has been developed for effective human-machine interaction. Together with the force/torque sensor, this provides a natural and intuitive human machine interface that can be tuned to individual characteristics. An adaptive shared control framework has been proposed to allocate control authority between the user and the machine based on the demonstrated performance of the user. As an integral part of this research, a series of field experiments were conducted with the PAMM SmartCane and SmartWalker at an assisted living facility in Cambridge Massachusetts. In these field trials, overall user acceptance of PAMM and the effectiveness of the control were evaluated. Both the admittance based control and the adaptive shared control were proven effective in field trials.

7.2 Suggestions for Future Work

Although initially implemented for and tested on the PAMM SmartWalker, both the mobility design and control method can be used for many other applications. Example applications could include heavy material handling devices for factories, ammunition handling devices for soldiers. These devices would augment human power by taking or sharing the physical load. The mobility design developed in this research can help improve the maneuverability in congested environments for these applications. The

control strategy can help improve safety, while reducing physical and mental workload for the operators.

Clinical trials are crucial for the development of assistive devices like PAMM. More formally structured clinical trials should be conducted before PAMM can be commercialized.

Another application to be explored for PAMM is rehabilitation. PAMM provide an excellent platform for patients to improve their mobility functions. In this application, algorithms need to be developed to detect and prevent balance loss of individuals from a variety of causes, including peripheral neuropathy, Parkinson's disease, certain types of stroke, vestibular disorders, certain MS patients, and cerebellar ataxia.

Appendix A

Floor Plan of the Assisted Living Facility

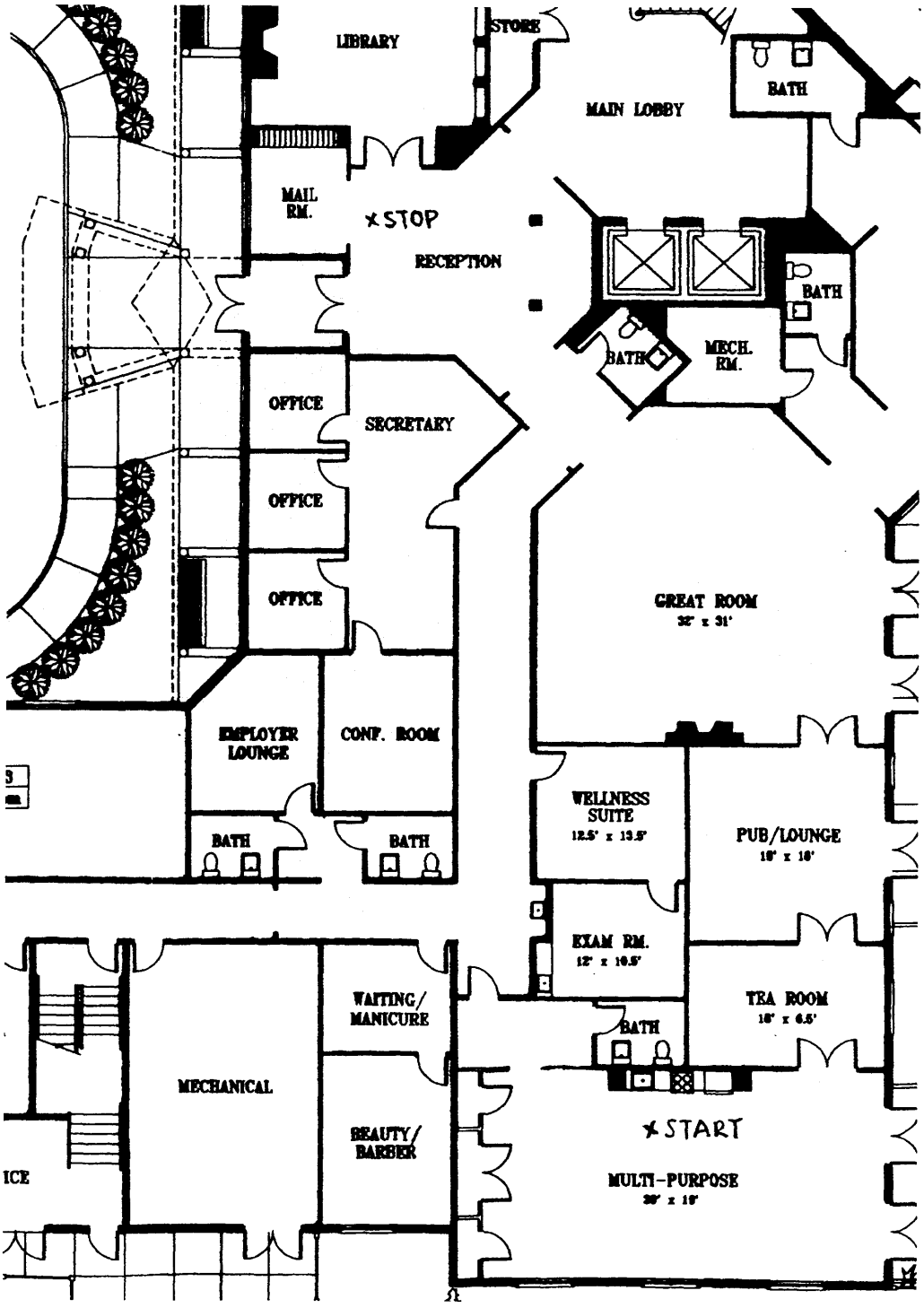

Appendix B.

SmartWalker Evaluation Questionnaire

I. Personal Information

(a) Name: _____

(b) Age:_____

(c) Weight:_____

(d) Height:_____

(e) Gender: Circle one – Male/ Female

(f) Do you have any disabilities or health problems that affect your mobility?

(Examples include stroke, arthritis, Parkinson's disease, etc.)

_____

_____

(g) What kind of mobility aid are you currently using? (For example, cane, four-point cane, walker?)

_____

(h) Have you ever tested the SmartWalker before? Circle one – Yes/No.

If yes, how many times? _____

II. Evaluation of the SmartWalker (Please circle a number)

1. Overall how did you find it to operate the SmartWalker?

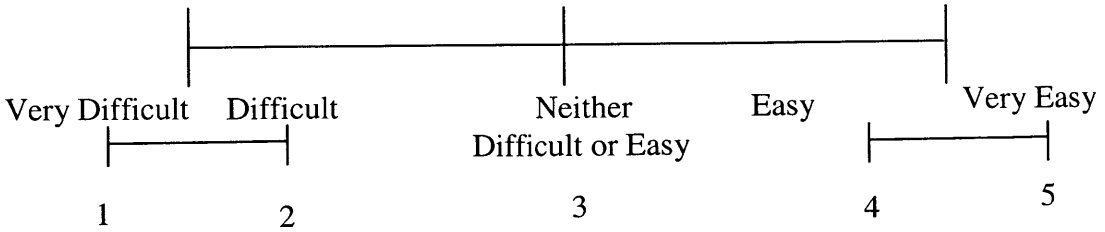

2. Is it easy to control the SmartWalker to go straight?

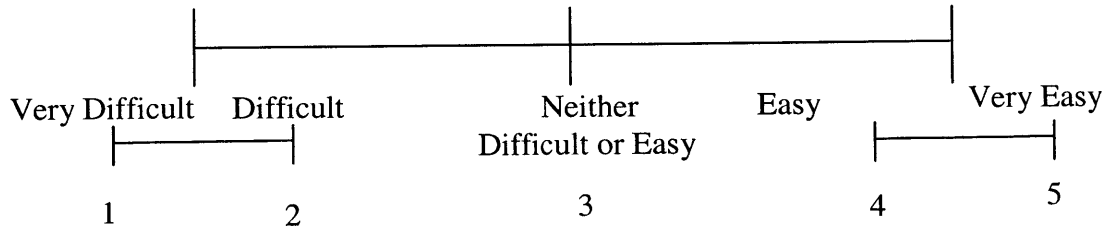

3. Is it easy to control the SmartWalker to turn?

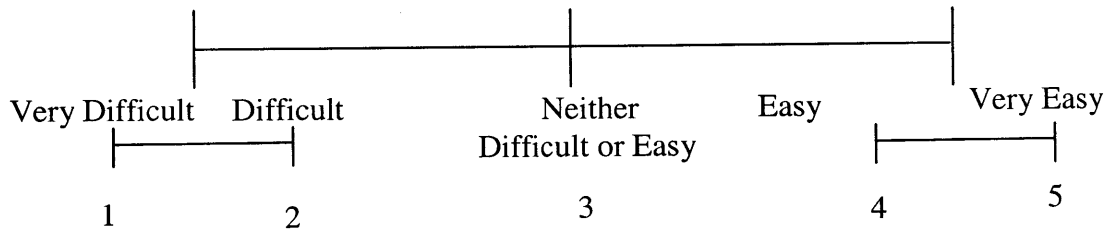

4. Is it heavy to push the SmartWalker?

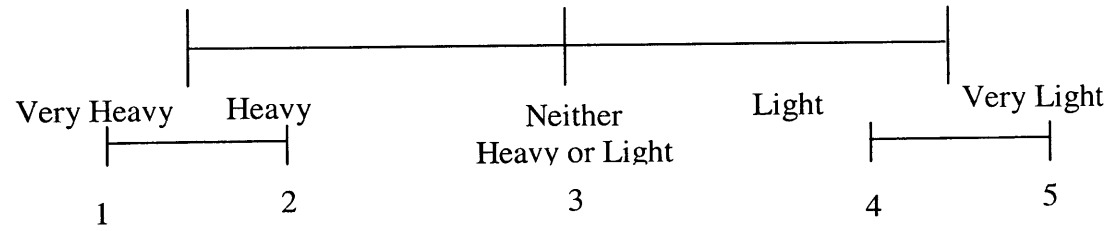

5. Is it easy to learn to use the SmartWalker?

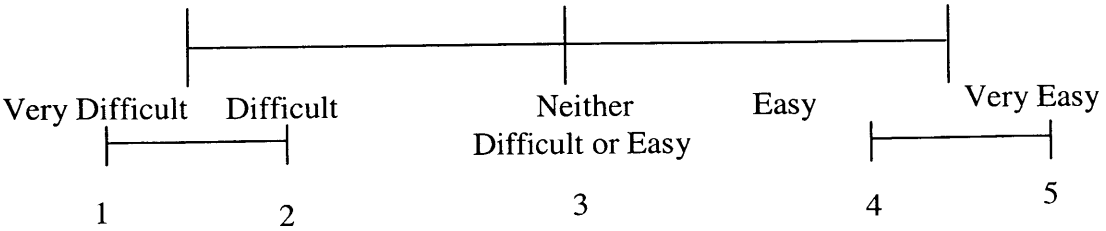

6. Do you get sufficient support from the SmartWalker?

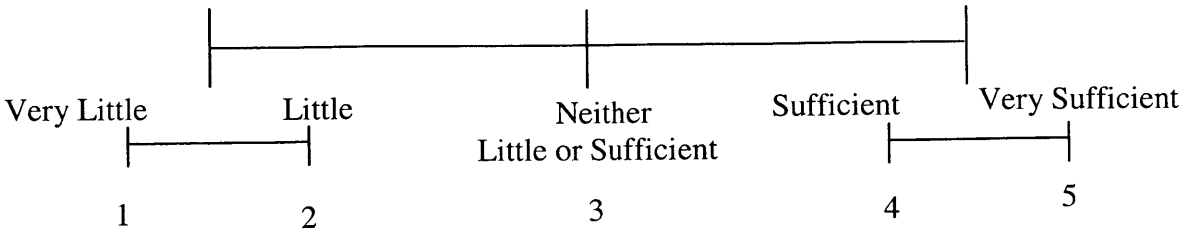

7. Are you satisfied with the SmartWalker as a mobility aid?

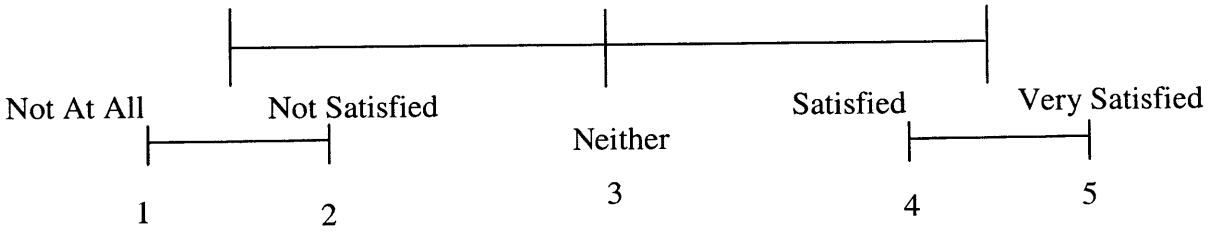

8. How satisfied are you with your current walker?

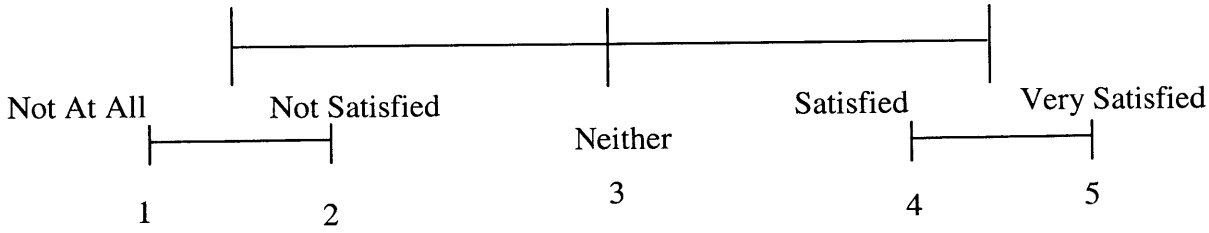

9. How does the SmartWalker compare to your current walker?

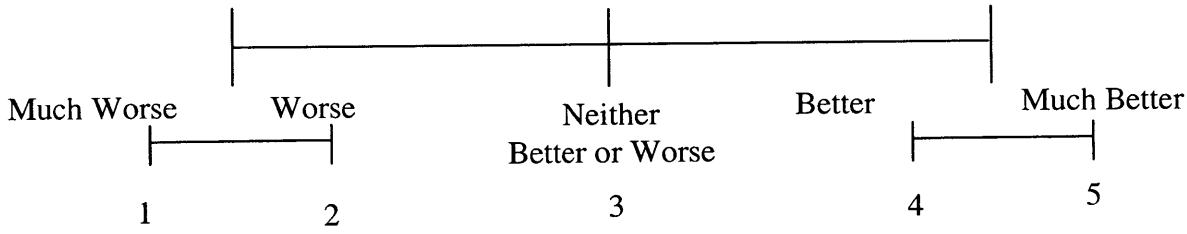

References:

[1] Akella, P., Peshkin, M., Colgate, E., Wannasuphoprasit, W., Nagesh, N., Wells, J., Holland, S.,Pearson, T., Peacock, B. "Cobots for the Automobile Assembly Line," Proceedings of 1999 IEEE International Conference on Robotics and Automation, Vol.1, pp. 728 –733, Detroit, May 10-15, 1999.

[2] ALFA Advisor (New Letter), "New Report Offers Draft Regulations for Assisted Living for People with Dementia," *ALFA* (The Assisted Living Federation of America) Advisor, pp. 1-2, July, 1995.

[3] Al-Jarrah, O.M.; Zheng, Y.F., "Arm-manipulator coordination for load sharing using variable compliance control," Proceedings of 1997 IEEE International Conference on Robotics and Automation. Vol. 1, pp. 895-900, Albuquerque, New Mexico, April 20-25, 1997.

[4] AOA (Administration on Aging, U.S. Department of Health and Human Services), "A Profile of Older Americans: 2001," 2001. http://www.aoa.gov/aoa/stats/profile/default.htm.

[5] Baltus, G., et al. "Towards personal service robots for the elderly," Proceeding of the 2000 Workshop on Interactive Robotics and Entertainment (WIRE-2000), Pittsburgh, April 30 - May 1, 2000.

[6] Barber J. R., *Elasticity*. Kluwer Academic Publishers, P.O. Box 17, 3300 AA Dordrecht, the Netherlands, 1992.

[7] Betourne A., Fournier A., "Kinematics, dynamics and control of a conventional wheeled omnidirectional mobile robot," Proceedings of IEEE International Conference Systems, Man, and Cybernetics, Vol.2, pp. 276 -281, 1993.

[8] Boreinstein, J., Everett, H.R., Feng, L., Navigating Mobile Robot. AK Peters, Wellesley, Massachusetts, 1996.

[9] Burton, L. J. "A Shoulder to Lean on: Assisted Living in the U.S," American Demographics, pp. 45-51, July 1997.

[10] Cooper, R., "Intelligent Control of Power Wheelchairs," IEEE Engineering in Medicine and Biology, pp. 423-431, July/August 1995.

[11] D'Arrigo, C. "Health Monitoring Sensors for a Personal Mobility Aid for the Elderly," Master Thesis. Department of Mechanical Engineering. Massachusetts Institute of Technology, 2001.

[12] Dubowsky, S., "Personal Aid for Mobility and Monitoring: A Helping Hand for the Elderly," PAMM Concept Study, MIT Home Automation and Healthcare Consortium, August 1997.

[13] Dubowsky, S., "Personal Aid for Mobility and Monitoring: A Helping Hand for the Elderly," Progress Report No.2-5: Oct. 1, 2000, MIT Home Automation and Healthcare Consortium.

[14] Dubowsky, S., Genot, F., Godding S., Kozono, H., Skwersky, A., Yu, L., Yu, H., "PAMM - A Robotic Aid to the Elderly for Mobility Assistance and Monitoring: A Helping-Hand for the Elderly," Proceedings of the 2000 IEEE International Conference on Robotics and Automation, San Francisco, CA, April 22-28, 2000.

[15] Durfee, W.K., Idris, H.R. and Dubowsky, S., "Real-Time Control of the MIT Vehicle Emulation System," Proceedings of the 1991 American Control Conference, Boston, MA, June 26-28, 1991.

[16] Ferriere L., Raucent B., "ROLLMOBS, a New Universal Wheel Concept," Proceedings of 1998 IEEE International Conference on Robotics and Automation, pp.1877-1882, Leuven, Belgium, May 1998.

[17] Fujisawa S., Ohkubo K., Yoshida T., Satonaka N., Shidama Y., Yamaura H., "Improved Moving Properties of An Omnidirectional Vehicle Using Stepping Motor," Proceedings of the 36th Conference on Decision & Control, pp.3654-3657, San Diego, California, December, 1997.

[18] Fujisawa Y, et al, "Manipulator for Man-Robot Cooperation (Control Method of Manipulator/Vehicle System with Fuzzy Logic Inference)," Proceedings of the IEEE.1992 International Conference on Power Electronics and Motion Control, Vol.2, pp. 630 – 635, San Diego, CA, USA, Nov. 9-13, 1992.

[19] Gillespie, T.D, Fundamentals of vehicle Dynamics. Society of Automotive Engineers, Inc, 400 Commonwealth Drive, Warrendale, PA 15096, 1992.

[20] Godding, S. "Field Tests on a Personal Mobility Aid for the Elderly," Bachelor Thesis. Department of Mechanical Engineering. Massachusetts Institute of Technology, 1999.

[21] Graf, B. "Reactive Navigation of an Intelligent Robot Walking Aid," Proceedings. of the IEEE International Workshop on Robot and Human Interaction, RO-MAN 2001, pp. 353-358, Bordeaux-Paris, France, September 18-21, 2001.

[22] Graf, B. Hägele, M. "Dependable Interaction with an Intelligent Home Care Robot," Proceedings of the 2001 IEEE International Conference on Robotics and Automation, Seoul, Korea, May21-26, 2001.

[23] Hertz, H. Gesammelte Werke, Vol. I, Leigzig, 1895.

[24] Hoeniger, T. "Dynamically shared control in human-robot teams through physical interactions," Proceedings of 1998 IEEE/RSJ International Conference on intelligent Robots and Systems, Vol. 2 , pp. 744 –749, Victoria, BC, Canada, Oct. 13-17, 1998.

[25] Holmberg R., Khatib O., "Development of a Holonomic Mobile Robot for Mobile Manipulation Tasks," Proceedings of the Conference on Field and Service Robotics, pp. 268-273, Pittsburgh, PA, August, 1999.

[26] Kazerooni, H. "Human power extender: an example of human-machine interaction via the transfer of power and information signals," 5th International Workshop on Advanced Motion Control, AMC '98-Coimbra, pp. 565 –572, Coimbra University, Coimbra, Portugal, June 29-July 1, 1998.

[27] Killough S.M., Pin F.G., "A New Family of Omnidirectional and Holonomic wheeled platforms for mobile robots," IEEE Transactions on Robotics and Automation, Vol.10, No.4, pp. 480-489, 1994.

[28] Kosuge, K.; Kazamura, N. "Control of a Robot Handling an Object in Cooperation with a Human," Proceedings of 6th IEEE International Workshop on Robot and Human Communication, 1997. RO-MAN '97, pp. 142 –147, Sendai, Japan, Sept. 29 - Oct. 1, 1997.

[29] Kozono, H. "PAMM SmartWalker Electronics and Computer Manual," Field and Space Robotics Laboratory, Department of Mechanical Engineering. Massachusetts Institute of Technology, 2000.

[30] Lacey, G., Dawson-Howe, K. M., "The Application of Robotics to a Mobility Aid for the Elderly Blind," Robotics and Automation Systems, Volume 23, Issue 4, pp. 245-252, July 30, 1998.

[31] Lacey, G, MacNamara, S., "User involvement in the design and evaluation of a smart mobility aid," Journal of Rehabilitation Research and Development, Vol. 37 No. 6, November/December 2000.

[32] Levine, S.P.; Bell, D.A.; Jaros, L.A.; Simpson, R.C.; Koren, Y.; Borenstein, J. "The NavChair Assistive Wheelchair Navigation System," IEEE Transactions on Rehabilitation Engineering, Vol. 7 4, pp.443-451, December, 1999.

[33] Moore D. F., *The friction of pneumatic tires.* Elsevier Scientific Publishing Company, New York, 1975.

[34] Mori, H., and Kotani, S., "A Robotic Travel Aid for the Blind – Attention and Custom for Safe Behavior," International Symposium of Robotics Research, Springer-Verlag, pp.237-245, 1998.

[35] Muir P.F., Neuman C.P., "Kinematic Modeling for Feedback Control of an Omni-directional Wheeled Mobile Robot," Proceedings of IEEE International Conference on Robotics and Automation, pp. 1772-1778, Raleigh, North Carolina, USA, March 31- April 3, 1987.

[36] Narendra, K. S., Annaswamy, A. M., *Stable adaptive systems.* Prentice Hall, Englewood Cliffs, N.J., 1989

[37] Nemoto et al., "Power Assist Control for Walking Support System," Proceedings of the Ninth International Conference on Advanced Robotics, pp 15-18, October 25-27, Tokyo, Japan, 1999.

[38] Nemoto, Y., et al. "Power-Assisted Walking Support System for Elderly," Proceedings of the 20th Annual International Conference of the IEEE Engineering in Medicine and Biology Society, Vol.5, pp. 2693 – 2695, Hong Kong, China, 29 Oct.-1 Nov. 1998.

[39] Papadopoulos, E. G., Rey, D. A., "A New Measure of Tipover Stability Margin for Mobile Manipulators," Proceedings of the 1996 IEEE International Conference on Robotics and Automation, pp. 3111-3116, Minneapolis, MN, April, 1996.

[40] Samson, C., Ait-Abderrahim, K. "Feedback control of a non-holonomic wheeled cart in cartesian space," Proceedings of the 1991 IEEE International Conference on Robotics and Automation, pp. 1136-1141, Sacramento, CA, April 9-11, 1991.

[41] Schneider, E.L., "Aging in the Third Millennium," *Science*, 1999, Vol. 283, No. 54003, pp. 796-797.

[42] Schraft, R.D., Schaeffer, C., and May, T., "Care-O-bot(tm): The Concept of a System for Assisting Elderly or Disabled Persons in Home Environments," IECON'98: Proceedings of the 24th Annual Conference of the IEEE Industrial Electronics Society, Vol.4, pp.2476-2481, Aachen, Germany, August 31-September 4, 1998.

[43] Sheridan, T. B, William R. F., Man-machine systems; information, control, and decision models of human performance. The MIT press, Cambridge MA, 1974.

[44] Sheridan, T. B, *Telerobotics, automation, and human supervisory control.* The MIT press, Cambridge MA, 1992.

[45] Shiller, Z., and Dubowsky, S. "On Computing the Global Time Optimal Motions of Robotic Manipulators in the Presence of Obstacles," IEEE Journal of Robotics and Automation, Vol. 7, No. 6,1991

[46] Simpson, R.C.; Levine, S.P. "Automatic adaptation in the NavChair Assistive Wheelchair Navigation System," IEEE Transactions on Rehabilitation Engineering, Vol. 7 4, pp. 452–463, December, 1999.

[47] Slocum A., Precision machine Design. Prentice Hall, Englewood Cliffs, New Jersey, 1992.

[48] Snyder, T.J.; Kazerooni, H, "A Novel Material Handling System," Proceedings of Proceedings of the 1996 IEEE International Conference on Robotics and Automation (ICRA-96), Vol.2, pp. 1147–1152, Minneapolis, MN, USA, April 22-28, 1996.

[49] Spenko, M. "Design and Analysis of the SmartWalker, a Mobility Aid for the Elderly," Master Thesis. Department of Mechanical Engineering. Massachusetts Institute of Technology, 2001.

[50] Spenko, M., Yu, H., Dubowsky, S., "Analysis and Design of an Omni Directional Platform for Operation on Non-Ideal Floors," Proceedings of 2002 IEEE International Conference on Robotics and Automation, Washington D.C, May 11-May 15, 2002.

[51] Stelman, N. M., "Design and control of a six-degree-of-freedom platform with variable admittance," Master Thesis. Department of Mechanical Engineering. Massachusetts Institute of Technology, 1988.

[52] Wada M., Mori S., "Holonomic and Omnidirectional Vehicle with Conventional Tires," Proceedings of IEEE International Conference on Robotics and Automation. pp. 3671-3676, Minneapolis, MN, USA, April 22-28 1996.

[53] Wada M., "Omnidirectioanl Vehicle and Method of Controlling the Same," US Patent No. 5924512, July 20, 1999.

[54] Wasson, G., Gunderson, J., Graves, S. and Felder, R. "An Assistive Robotic Agent for Pedestrian Mobility," International Conference on Autonomous Agents: AGENTS'01, pp. 169-173, Montreal, Quebec, Canada, May 28-June 1, 2001.

[55] Wasson, G., Gunderson, J., Graves, S. and Felder, R. Effective Shared Control in Cooperative Mobility Aids. FLAIRS '01: 509-513, 2001.

[56] West M., Asada H., "Design of Ball wheel Mechanisms for Omnidirectional Vehicles with Full Mobility and Invariant Kinematics," Journal of Mechanical Design, Vol.119, pp153-161, June 1997.

[57] Wong J. Y., *Theory of Ground Vehicles.* Second edition. Wiley Interscience, 1993.

[58] Yamamoto, Y., et al. "Coordinated task execution of a human and a mobile manipulator," Proceedings of IEEE International Conference on Robotics and AutomationVol.2, pp. 1006 - 1011, Minneapolis, MN, USA, April 22-281996.

[59] Yu, H., Dubowsky, S., and Skwersky, A., "Omni-directional Mobility Using Active Split Offset Castors," Proceedings of 2000 ASME IDETC/CIE 26th Biennial Mechanics and Robotics Conference, Baltimore, Maryland, September 10-13, 2000.